AGU PUBLICATIONS

Tectonics

RESEARCH ARTICLE

10.1002/2017TC004599

Key Points:

- Sikhote-Alin terranes were supplied by the Bureya-Jiamusi-Khanka Block and the North China Craton
- The Sikhote-Alin terranes were transported northward after depostion during Jurassic to Cretaceous

Correspondence to:
J. Zhang,
zhjj@pku.edu.cn

Citation:
Liu, K., Zhang, J., Wilde, S. A., Liu, S., Guo, F., Kasatkin, S. A., … Wang, J. (2017). U-Pb dating and Lu-Hf isotopes of detrital zircons from the southern Sikhote-Alin orogenic belt, Russian Far East: Tectonic implications for the Early Cretaceous evolution of the Northwest Pacific margin. *Tectonics*, *36*, 2555–2598. https://doi.org/10.1002/2017TC004599

Received 7 APR 2017
Accepted 27 SEP 2017
Accepted article online 5 OCT 2017
Published online 17 NOV 2017

U-Pb Dating and Lu-Hf Isotopes of Detrital Zircons From the Southern Sikhote-Alin Orogenic Belt, Russian Far East: Tectonic Implications for the Early Cretaceous Evolution of the Northwest Pacific Margin

Kai Liu[1,2], Jinjiang Zhang[1], Simon A. Wilde[2], Shiran Liu[1], Feng Guo[3], Sergey A. Kasatkin[4], Vladimir V. Golozoubov[4], Maohui Ge[1], Meng Wang[5], and Jiamin Wang[6]

[1]Key Laboratory of Orogen and Crustal Evolution, Ministry of Education, Peking University, Beijing, China, [2]The Institute for Geoscience Research, Department of Applied Geology, Curtin University, Perth, Western Australia, Australia, [3]Key Laboratory of Marginal Sea Geology, Guangzhou Institute of Geochemistry, Chinese Academy of Sciences, Guangzhou, China, [4]Far East Geological Institute, Far East Branch, Russian Academy of Sciences, Vladivostok, Russia, [5]Key Laboratory for the study of Focused Magmatism and Giant Ore Deposits, School of Earth Science and Resources, Chang'an University, Xi'an, China, [6]State Key Laboratory of Lithospheric Evolution, Institute of Geology and Geophysics, Chinese Academy of Sciences, Beijing, China

Abstract The Sikhote-Alin orogenic belt in Russian Far East is comprised of several N-S trending belts, including the Late Jurassic to Early Cretaceous accretionary prisms and turbidite basin which are now separated by thrusts and strike-slip faults. The origin and collage of the belts have been studied for decades. However, the provenance of the belts remains unclear. Six sandstone samples were collected along a 200 km long east-west traverse across the major belts in the southern Sikhote-Alin for U-Pb dating and Lu-Hf isotope analysis to constrain the provenance and evaluate the evolution of the northwest Pacific margin at this time. The result reveals that the sediments from the main Samarka belt was mainly from the adjacent Bureya-Jiamusi-Khanka Block (BJKB); the eastern Samarka belt and the Zhuravlevka turbidite basin were supplied by detritus from both the North China Craton (NCC) and the BJKB; the Taukha belt was mainly fed by sediments from the NCC; whereas the data from the Sergeevka nappes are insufficient to resolve their provenance. In the Late Jurassic to Early Cretaceous, collision and subduction was important in the initial collage of most belts in Sikhote-Alin. However, merely E-W trending collage cannot explain the increasing importance of the NCC provenance from west to east. It is proposed that the main Samarka belt was located adjacent to the BJKB when deposited, whereas the other belts were farther south to accept the materials from the NCC. Sinistral strike-slip faulting transported the eastern belts northward after their initial collage by thrusting.

1. Introduction

The East Asian continent consists of three major cratons which are, from north to south, the Siberia Craton, North China Craton, and South China Craton (Figure 1). Several orogenic belts/suture zones welded the cratons to form the tectonic framework of northeastern Asian continent.

The Central Asian Orogenic Belt (CAOB) is located between the Siberia and North China cratons. This gigantic orogenic belt is composed of many arcs, basins, and continental blocks within the Paleo-Asian Ocean which was closed in the Late Paleozoic (Chen et al., 2016; Rowley et al., 1985; Şengör, 1984; Şengör et al., 1993; Sengör & Natal'In, 1996; Song et al., 2015; Wilde, 2015; Windley et al., 2007; Xiao et al., 2003; Xu et al., 2015; Zhao et al., 2013; Zonenshain, 1973). The eastern segment of the Mongol-Okhotsk Ocean between the CAOB and Siberia Craton did not close until the Early Cretaceous (Donskaya et al., 2013; Khanchuk, Didenko, Popeko, et al., 2015; Kravchinsky et al., 2002). The South China Craton (SCC) collided with and was subducted beneath the North China Craton (NCC) along the Dabie-Sulu Orogen between ca. 240–225 Ma, resulting in high-pressure and ultrahigh-pressure metamorphism (Liu & Liou, 2011; Wu & Zheng, 2013; R. Zhang et al., 2009), whereas the orogenic belt along the East Asian margin belongs to the Pacific tectonic realm or the Pacific orogenic belt, which was active after the collage of the three major cratons (Zhou & Li, 2017). There are numerous Mesozoic to Cenozoic accretionary complexes, arcs, and continental blocks in the Pacific tectonic realm, extending from Taiwan to Kamchatka for ~3,000 km. The Pacific orogenic belt is named as "Nipponides" by Sengör and Natal'In (1996).

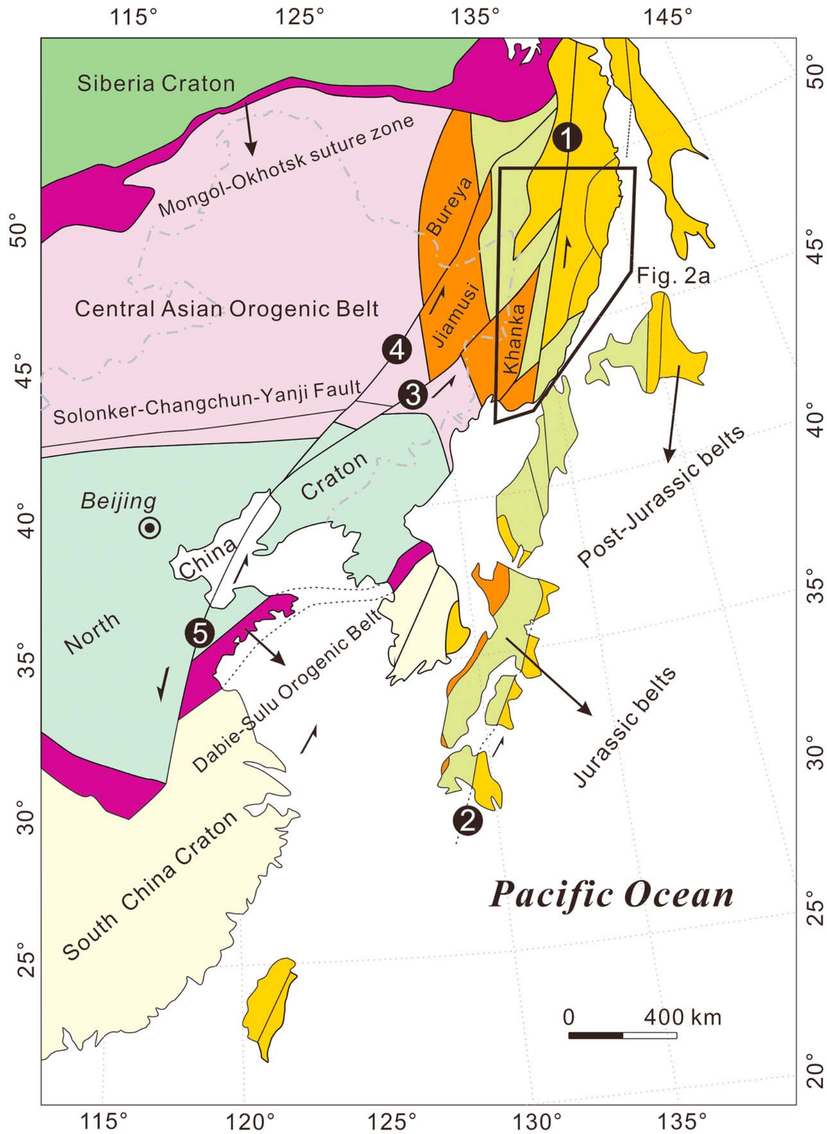

Figure 1. Tectonic framework of East Asia at the end of the Early Cretaceous after termination of northward transport. Modified after Sun, Xu, Wilde, & Chen (2015) and Xu et al. (1987). Japanese Islands are moved back to the Asian continental margin before the opening of the Sea of Japan (Khanchuk, 2001; Kojima, 1989; Taira, 2001). The main strike-slip faults in East Asia are (numbers in black circles): 1. Central Sikhote-Alin Fault; 2. Median Tectonic Line; 3. Dun-Mi Fault; 4. Jia-Yi Fault; and 5. Tan-Lu Fault.

The Sikhote-Alin orogenic belt is part of the Pacific orogenic belt and is located along the eastern margin of the CAOB (Figures 1 and 2). Over the past 30 years, many studies on paleontology, stratigraphy, and paleomagnetism were carried out to reveal the geological history of the NNE trending belts of the Sikhote-Alin orogenic belt and adjacent areas. The lithology and structural features of belts in Sikhote-Alin were compared and associated with the Japanese Islands, especially SW Japan. However, the origin and tectonic evolution of these belts are still very controversial. Based on the “terrane tectonics” theory, many late Mesozoic “tectonostratigraphic terranes” were identified in NE China, Sikhote-Alin, and Japanese Islands (Figure 1; Howell et al., 1985; Khanchuk, 2001; Kojima, 1989; Kojima et al., 2000; Mizutani, 1987; Shao & Tang, 1995). Most boundaries between these terranes/belts are thrusts or strike-slip faults. The terranes were believed to be transported from south to north by the strike-slip faults, and the displacement was estimated from hundreds to thousands of kilometers (Gilder et al., 1999; Khanchuk, 2001, 2016; Lee, 1999; Xu et al., 1987; Xu & Zhu, 1994; Yin & Nie, 1993). However, collisional orgeny was recognized in SW Japan and some other places in

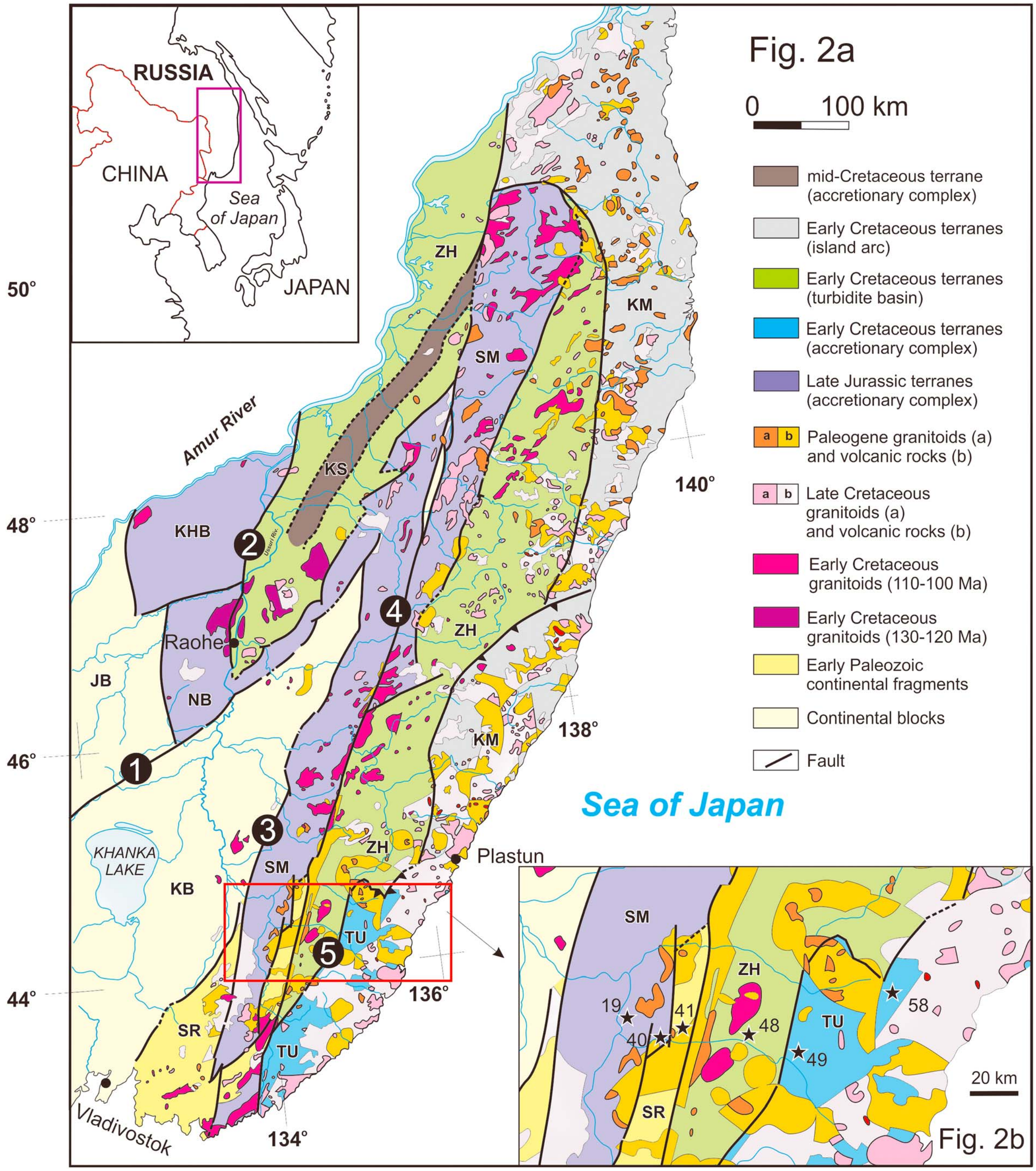

Figure 2. (a) Geological map of the southern Sikhote-Alin. Modified after Grebennikov et al. (2016). Abbreviations: JB = Jiamusi Block; KB = Khanka Block; SR = Sergeevka nappes; KHB = Khabarovsk belt; NB = Nadanhada-Bikin belt; SM = Samarka belt; KS: Kisilevsky belt; ZH = Zhuravlevka turbidite basin; TU = Taukha accretionary complex; KM = Kema arc. Faults (numbers in black circles): (1) Dun-Mi Fault, (2) Koukansky Fault, (3) Arsen'evsky Fault, (4) Central Sikhote-Alin Fault, and (5) Fourmanovsky Fault. (b) Sample locations in the southern Sikhote-Alin belts. Numbers are abbreviated from samples SAL-19, SAL-40, SAL-41, SAL-48, SAL-49, and SAL-58.

the continental margin (Charvet et al., 1985; Faure et al., 1986; Natal'in, 1993; Otsuki, 1992). The collision of buoyant blocks (mature arcs or continental blocks) onto the hinterland is considered to be very important to shape the tectonics of the East Asia, such as the large thrust sheet/nappe tectonics. There are some other studies suggesting that the Pacific tectonic realm is a typical "accretionary orogen," especially for the Japanese Islands. In their models, Japanese Islands were basically an accretionary complex built in long-term subduction of the Paleo-Pacific Ocean. High-pressure metamorphism and ridge subduction were important for the deformation and magmatism in the SW Japan according to their models (Isozaki et al., 2010; Maruyama, 1997).

In Sikhote-Alin, detailed research has been implemented on structural geology, micropaleontology, and magmatism (Golozoubov et al., 1999; Jahn et al., 2015; Khanchuk, 2001; Khanchuk et al., 1996; Kemkin & Kemkina, 2000; Kojima, 1989; Kojima et al., 2008; Tang et al., 2016). However, the provenance issue, which is very significant to understand the origin and tectonic history of the belts, remains unclear. U-Pb dating and Lu-Hf isotopes of detrital zircons are an effective means for determining the provenance of sediments (Bingen et al., 2001; Cawood et al., 2012; Fernández et al., 2010; Fernandez-Suarez et al., 2002; Gehrels, 2014; Grasse et al., 2001; Gutiérrez-Alonso et al., 2003; Wyld & Wright, 2001). Here we present U-Pb dating and Lu-Hf isotopic data for detrital zircons from the southern Sikhote-Alin orogenic belt in order to ascertain their maximum depositional age, their provenance, and to better understand the tectonic processes operating along the eastern Asian continental margin during the Late Jurassic to Early Cretaceous.

2. Geological Outline of the Southern Sikhote-Alin Orogenic Belt

The southern Sikhote-Alin orogenic belt is located to the east of the Bureya-Jiamusi-Khanka block (BJKB), which has a Neoproterozoic basement ca. 850–960 Ma in age and records late Pan-African granulite-facies metamorphism at ~500 Ma (Figure 1; Wilde et al., 1997; Wilde et al., 2003; Yang et al., 2017). After Jurassic, the BJKB became the easternmost part of the CAOB. However, the location of the BJKB prior to the Jurassic is controversial, with some authors considering it to be part of the CAOB that underwent rifting in the Triassic (Zhou et al., 2009), whereas others have considered it is an exotic block that was accreted to the CAOB in the Jurassic (Wu, Han, et al., 2007), possibly being derived from Gondwana (Wilde et al., 1999) or Siberia (Zhou et al., 2009). New detrital zircon data show that the Jiamusi Block may have affinity of the Tarim Craton (Luan et al., 2017). These various hypotheses have been invoked to explain the origin of the Heilongjiang Complex, developed along the western margin of the Jiamusi Block, which is an accretionary complex that welded the Jiamusi Block to the Songliao Block of the CAOB in the Early Jurassic (Wu, Han, et al., 2007; Zhou et al., 2009). Significantly, terrigenous rocks in the Sikhote-Alin orogenic belt along the eastern margin of the BJKB were mainly deposited after the Early Jurassic. The N-S trending belts/zones investigated in this study are, from west to east, the Samarka accretionary complex (Jurassic), the Zhuravlevka turbidite basin (Early Cretaceous), and the Taukha accretionary complex (Early Cretaceous). In addition, the Sergeevka nappes are thrust over the southern Samarka accretionary complex. The northwestern boundary of the Taukha belt and the boundary between the Kema and Zhuravlevka belts are likely thrusts. However, the western boundary of the Taukha belt is sinistral strike-slip fault. Likewise, the Central Sikhote-Alin Fault, the boundary between the Samarka belt and the Zhuravlevka basin, is a famous sinistral strike-slip fault in the Russian Far East (Figures 2a and 2b).

The oldest units in the Sikhote-Alin are the Sergeevka nappes (SR on Figure 2a), which include several separate early Paleozoic continental fragments that were thrust over the Samarka belt (SM on Figure 2a). These nappes are also known as the Sergeevka Terrane in the Russian literatures (Khanchuk et al., 2016), although it is inappropriate to refer to these as a terrane because they are present in several areas and do not form a coherent geological unit (Figure 2a). The Sergeevka nappes contain Early Ordovician granitoids with a biotite Ar-Ar age of 491 Ma (Figure 2a; Khanchuk et al., 1996). The fragments mainly comprise gabbro, diorite, migmatite, and amphibolite and are themselves overlain by Jurassic conglomerate and sandstone (Figures 3, 4, and 5c and 5d). Some blueschist-facies metamorphic rocks are present between the Jurassic sedimentary rocks and Early Paleozoic continental fragments, representing a pre-Cretaceous orogeny (Khanchuk, 2006; Khanchuk et al., 2016).

The Samarka belt is a Late Jurassic accretionary complex (SM on Figure 2a) that consists of several deformed tectonic slices or thrust sheets (Figure 4). The boundaries between slices are reverse faults/thrusts. In each slice, the depositional sequence changes from chert and siltstone upward into sandstone. At the top of some slices, sedimentary rocks were faulted and folded into mélange that is characterized by strong deformation and contains blocks of various sizes (Figures 3 and 5a and 5b; Kemkin, 2008). The chert varies in age from Late Permian to Early Jurassic and represents pelagic sediments. In contrast, the clastic rocks are mainly terrigenous and Late Jurassic in age (Kemkin et al., 2006). The mélange contains blocks of limestone, chert, and

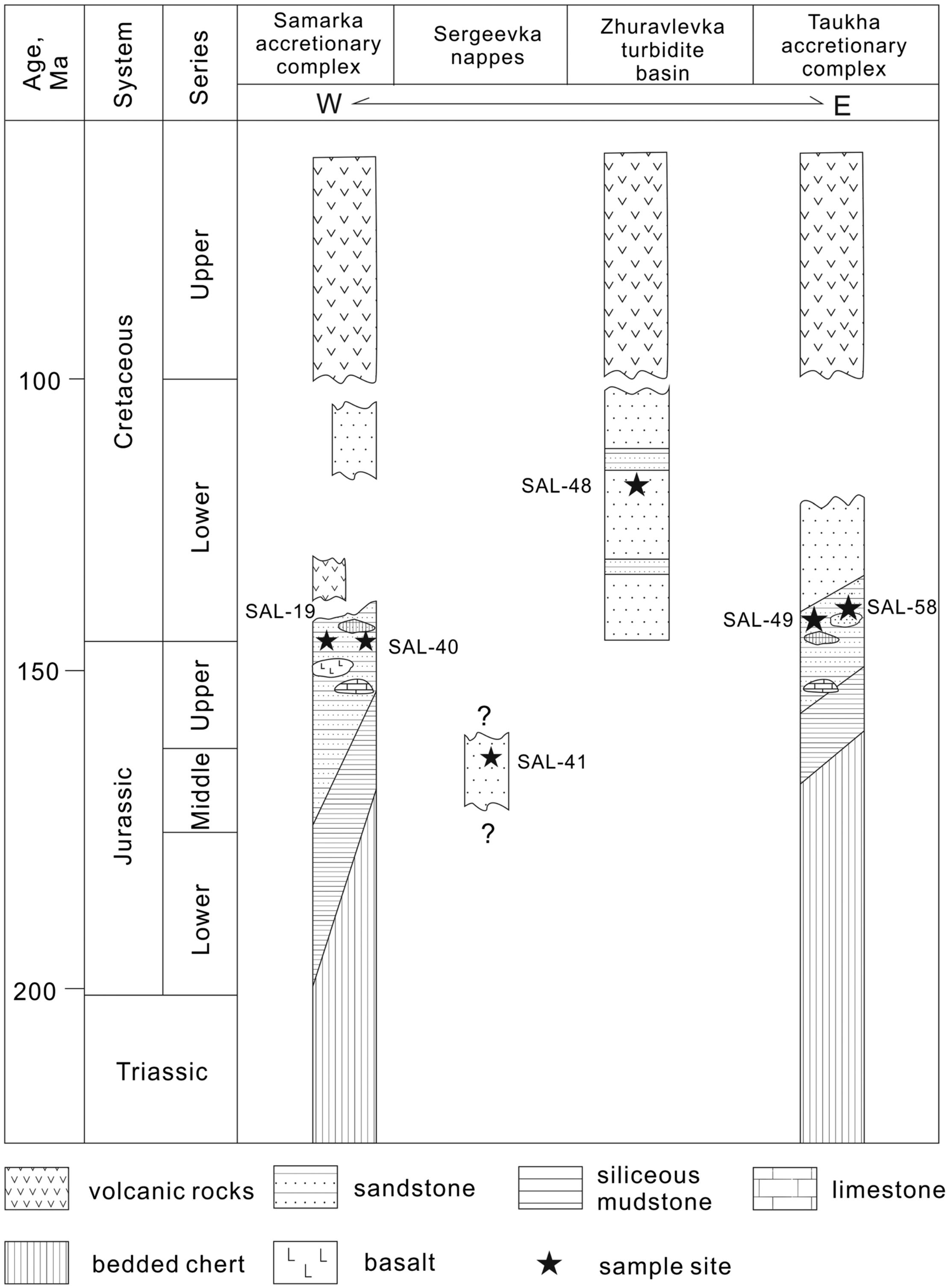

Figure 3. Tectonostratigraphic column of the southern Sikhote-Alin belts, modified after Kemkin (2008), Kemkin and Kemkina (2015), Khanchuk et al. (2016), and Malinovsky and Golozubov (2011). Only part of the Sergeevka nappes is shown on this figure because the stratigraphic information is incomplete.

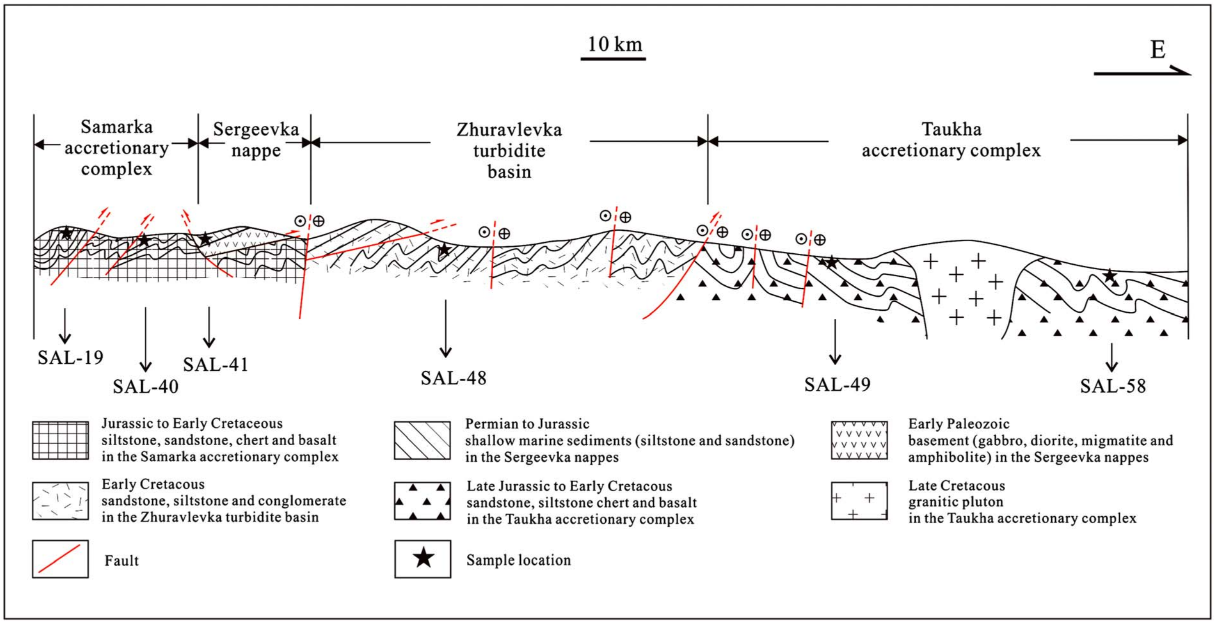

Figure 4. Cross section along the sampling traverse in the southern Sikhote-Alin orogenic belt.

basalt within a siltstone matrix. Another feature of the Samarka accretionary complex is that it contains fragments of Paleozoic ophiolites, including peridotite, gabbro, and basalt pillows, interpreted as components from an oceanic plateau but now outcropped as nappe/klippe in the Samarka accretionary complex (Khanchuk & Vysotskiy, 2016). The age of ophiolite was estimated as Late Devonian to Early Carboniferous based on the conodont and foraminifera research in the sedimentary rocks contacting the pillow basalts (Khanchuk & Vysotskiy, 2016).

To the east, the Zhuravlevka turbidite basin (ZH on Figure 2a) is truncated by the Central Sikhote-Alin Fault (Figure 2a). The basin was mainly filled by turbidites showing well-developed Bouma sequences (Figure 5e), with some chert and conglomerates cropping out locally. Faults accompanied by vertically dipping strata are present near the boundaries of the basin, whereas deformation in the interior is represented by broad folds, less steeply inclined strata and several NNE trending strike-slip faults and thrusts (Figure 4). Heavy mineral studies and paleontological evidence suggest that depositional age spans the whole of the Early Cretaceous (from the late Berriasian to late Albian) and that these sediments were mainly derived from mature continental crust (Malinovsky & Golozubov, 2011).

Along the margin of the Sea of Japan, the Taukha belt (TU on Figure 2a) is a Late Jurassic to Early Cretaceous accretionary complex lying to the east of the Zhuravlevka turbidite basin and to the south of the Kema belt, an Early Cretaceous island arc (KM on Figure 2a). The boundary between the Taukha belt and the Zhuravlevka basin is mainly sinistral strike slip with thrust characteristic in the north segment (Figure 4; Golozoubov, 2006; Kemkin & Kemkina, 2000). The rock types in the Taukha accretionary complex are similar to those in the Samarka accretionary complex although the age is younger. For example, in some areas where the original stratigraphic sequence has survived, the chert that has been dated from Late Triassic to Late Jurassic in age, changes upward to chert-mudstone, siltstone, turbidite, and olistostromes, which are latest Jurassic to Early Cretaceous in age (Figures 3 and 5f; Kemkin & Kemkina, 2000). This chert-siltstone-sandstone sequence is considered to represent oceanic plate stratigraphy (Berger & Winterer, 1974; Isozaki et al., 1990). Some mélange zones crop out where the siltstone and sandstone are strongly deformed by folds and faults in the northern Taukha belt. Jurassic basalts overlain by Late Jurassic chert are found locally in the northwest Taukha belt (Kemkin & Kemkina, 2000; Kemkin et al., 2016). Radiolarian research suggests that the limestone and chert blocks in the mélange could be as old as Late Devonian or Permian (Figure 2b; Kemkin & Kemkina, 2000, 2015).

The Jurassic to Cretaceous belts in the southern Sikhote-Alin are separated by a series of faults which are, from west to east, the Arsen'evsky Fault, the Central Sikhote-Alin Fault, and the Fourmanovsky Fault (Faults 3, 4, and 5, respectively, on Figure 2a). The Central Sikhote-Alin Fault is a sinistral strike-slip fault which is

Figure 5. Outcrop photographs of the southern Sikhote-Alin belts. (a) Foliated siltstone in the Samarka accretionary complex, (b) folded chert in the Samarka accretionary complex. Red curves mark the folds, (c) conglomerate in the Sergeevka nappes, including clasts of gabbro, sandstone, chert and quartzite, (d) cumulate gabbro in the Sergeevka nappes, (e) turbidite in the Zhuravlevka turbidite basin; (f) mélange in the Taukha accretionary complex, involving different-size sandstone lenses in foliated siltstone.

traceable for over 1,000 km in length (Utkin, 2013), and the offset on this fault may be greater than 200 km, based on the dislocated Samarka and Zhuravlevka belts (Figures 1 and 2a; Utkin, 1993). Deep seismic sounding shows that the Arsen'evsky and Central Sikhote-Alin faults cut the Moho at a depth of ~40 km (Argentov et al., 1976). The Fourmanovsky Fault is characterized by sinistral strike slip in the western part with thrusting in the north part (Figure 2).

During the Early Cretaceous to Paleogene, felsic magmatic rocks were emplaced extensively into the belts of the southern Sikhote-Alin (Figure 2a). The earliest granitoids are 131 to 124 Ma in age and are rare, only being found in the Nadanhada-Bikin accretionary complex and the adjacent part of the Zhuravlevka turbidite basin (Figure 2a; Cheng et al., 2006; Grebennikov et al., 2016; Jahn et al., 2015). However, magmatism was interrupted between 130 and 110 Ma in the other belts, after which it was reactivated by rapid oblique Paleo-Pacific subduction (the Izanagi Plate) and became quasi-continuous from 110 Ma to 56 Ma (Jahn et al., 2015; Kruk et al., 2014; Tang et al., 2016).

The correlation between the Jurassic to Cretaceous belts in NE China, Sikhote-Alin, and SW Japan has been discussed for decades. Based on paleontological and paleomagnetic data, Kojima (1989) proposed that the Late Jurassic Nadanhada-Bikin accretionary complex in NE China and Sikhote-Alin are the northern extension of the Tanba-Mino belt in SW Japan (Figure 1). Khanchuk (2001) also connected the arc magmatism and accretionary complexes in the Sikhote-Alin with equivalents in SW Japan. The correlation between the Taukha belt and the Northern Kitakami belt was supported by the paleontological research and stratigraphic characteristic (Kojima et al., 2008).

3. Sample Locations and Petrology

Six sandstone samples were collected along a 200 km traverse, extending from west to east in the southern Sikhote-Alin orogenic belt, in order to evaluate any changes in provenance within the belts, especially across the Central Sikhote-Alin Fault (Figures 2b, 3, and 4).

Sample SAL-19 was collected in the central part of the Samarka belt. It is a sandstone within a fine- to medium-grained Bouma sequence. However, the chert-siltstone-sandstone stratigraphic sequence is disrupted because of faults and folds (Figure 5a). Some basalt blocks are present near the contact between the sandstone and the underlying folded and thinly bedded chert. Sample SAL-19 is a dark grey, fine-grained sandstone that is poorly sorted with angular quartz grains that are 15–30 μm in length (Figure 6a) and composed mainly of quartz (25%) and plagioclase (30%), with minor muscovite (1%). The space between the grains is filled by lithic fragments (45%), which are mainly felsic volcanic fragments.

Sample SAL-40 was collected from the eastern Samarka belt, separated from sample SAL-19 by an unnamed fault (Figure 2b). This fault cuts Paleogene granitoids, indicating movement after granitoid emplacement, although the precise timing of movement is unknown. Sample SAL-40 is a dark grey, coarse-grained sandstone that is poorly sorted or rounded (Figure 6b). The main minerals are quartz (45%), plagioclase (25%), K-feldspar (10%), sericite (3%), and clay minerals (2%), with felsic lithic fragments (15%). The clastic grains are mainly 70–100 μm in length. Subgrained quartz and local quartz veins are observed in thin section (Figure 6c). Adjacent to these areas, K-feldspar and quartz are weakly oriented and reduced in grain size (15–40 μm) due to granulation (Figure 6c).

Sample SAL-41 was collected from a Jurassic sandstone interbedded with conglomerate from one of the Sergeevka nappes. The conglomerate contains fragments of gabbro, chert, sandstone, and quartzite (Figure 5c). Because the sample is small in size and was used to obtain zircons as a whole, no thin section was made of this sample. However, based on the outcrop, it is a grey, medium- to coarse-grained sandstone that is poorly sorted or rounded. Some small angular fragments of chert and gabbro, 0.5–2 cm in diameter, were observed.

Sample SAL-48 was obtained from the Zhuravlevka turbidite basin, located 50 km to the east of sample SAL-41. Sample SAL-48 is separated from samples SAL-40 and SAL-41 by the Central Sikhote-Alin Fault (Fault 4 on Figure 2a). The outcrop consists of turbidite with interbedded mudstone and siltstone defining a Bouma sequence. Grains in sample SAL-41 are angular and poorly sorted and 30–150 μm in length (Figure 6d). It mainly comprises quartz (60%), plagioclase (25%), opaque minerals (10%), and lithic fragments (5%).

Two samples (SAL-49 and SAL-58) were collected from the Taukha accretionary belt (Figure 2b). The former was located 40 km to the east of sample SAL-48 and the latter 110 km northeast of SAL-48. Both samples from the Taukha accretionary complex are separated from sample SAL-48 (in the Zhuravlevka basin) by the Fourmanovsky Fault (Fault 5 on Figure 2a). Sample SAL-49 is a coarse sandstone that contains minor subangular chert fragments (0.5–3 cm), and it is moderately well sorted and with poorly rounded grains that range in length from 100–200 μm. The main minerals are quartz (55%), K-feldspar (35%), and muscovite (5%),

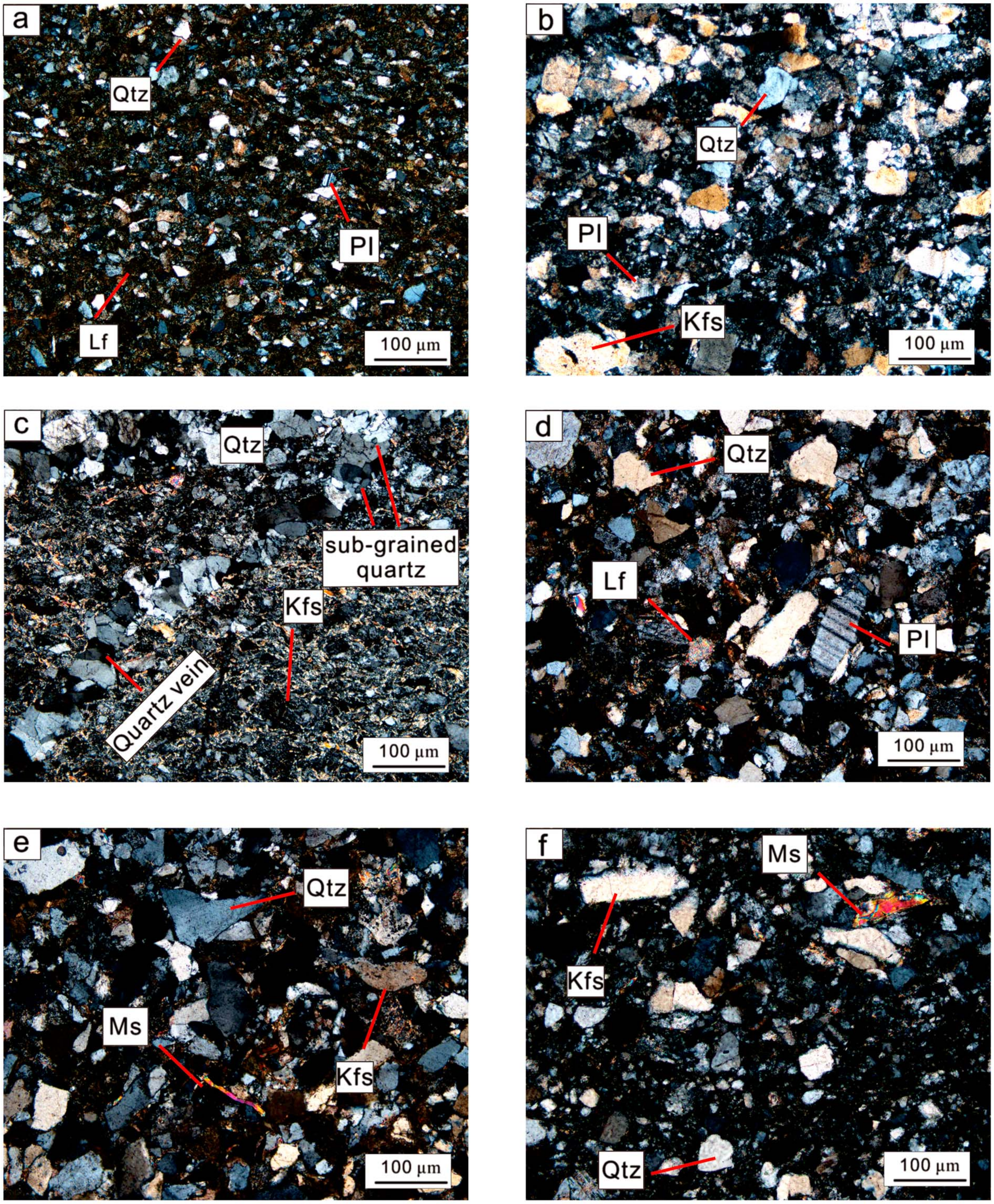

Figure 6. Photomicrographs of sandstone samples. (a) Sample SAL-19, (b) sample SAL-40, (c) deformed zone of sample SAL-40, in which weak deformation and sub-grained quartz can be observed, (d) sample SAL-48, (e) sample SAL-49; and (f) sample SAL-58. Abbreviation: Qtz = quartz; Pl = plagioclase; Kfs = K-feldspar; Lf = lithic fragments; Ms = muscovite.

with lithic fragments (5%; Figure 6e). Sample SAL-58 was collected from a mélange that occurs in the northern Taukha belt, 60 km to the southwest of Plastun (Figure 2a). There are numerous sandstone blocks within a matrix of siltstone (Figure 5f), with the size of blocks varying from 5 to 150 cm in diameter. Sample SAL-58 shows no sign of deformation and the mineralogy consists of quartz (70%), K-feldspar (15%), and muscovite (5%), with lithic fragments (10%). The grains are poorly sorted with lengths from 20 to 150 μm (Figure 6f).

Overall, in the southern Sikhote-Alin orogenic belt, sandstones are always interbedded with mudstones and underlain by folded and/or faulted chert, showing a change from a typical pelagic marine sequence to terrigenous sedimentation. Some sandstones include angular fragments of chert and/or mudstone and show graded bedding (including Bouma sequences), suggesting strong hydrodynamic conditions related to turbidity currents. The quartz and feldspar grains are all poorly sorted and angular, with lithic fragments and feldspar collectively greater than quartz in some units. All these features are typical of sediments deposited on a continental slope and trench, resulting from erosion of an adjacent continental margin or an arc, with deposition by turbidity currents after short-distance transport.

4. Methodology

Zircons were separated from the six samples by standard heavy-liquid and magnetic techniques and hand-picked under a binocular microscope. About 200 zircon grains from each sample were embedded in a 25 mm epoxy resin disk and polished to approximately half of the grain's thickness. Cathodoluminescence (CL) imaging was obtained using a Quanta 200 FEG Scanning Electron Microscope at the Key Laboratory of Orogenic Belts and Crustal Evolution of the Education Ministry of China, Peking University in order to observe the internal structure of the zircons.

Zircon U-Pb isotopic analyses were carried out using laser ablation inductively coupled plasma mass spectrometry (LA-ICP-MS) at the Key Laboratory of Continental Collision and Plateau Uplift, Chinese Academy of Sciences, Beijing. Laser sampling was performed using a NewWave and ATL 193 nm ArF excimer laser ablation system (UP193FX), with short pulses (<4 ns) and a spot size of 35 μm. Element and isotope ion-signal intensities were acquired by an Agilent 7500a ICP-MS. Both high-purity helium and argon were used as carrier gases, which were mixed via a T-connector before entering the MS. Helium was adjusted by a mass flow controller installed in the laser system, whereas argon was controlled by the ICP-MS. Helium and argon carrier gas flows were optimized by ablating National Institute of Standards and Technology (NIST) Standard Reference Material (SRM) 612 reference glass to obtain maximum signal intensity for ^{238}U and ^{208}Pb, minimum oxide, and double-charge interference, minimum gas blank, and most stable signal intensity. The analytical procedure was 15–20 s gas blank acquisition (warm up), 40 s data acquisition from the sample aerosol (ablation), and 45–55 s washout time in the spot sampling mode and TRF data acquisition mode of the Agilent ChemStation. Zircon 91500 was used as an external standard for the matrix-matched calibration. NIST SRM 612 reference glass was analyzed as an external standard for the trace element content calibration. The 91500 zircon and NIST SRM 612 standards were analyzed after each 5 to 10 analyses. Off-line isotope ratios and trace element concentrations were calculated using the GLITTER_Ver4.0 program (Van Achterbergh et al., 2001); U-Pb concordia diagrams, weighted mean calculations, and probability density plots of U-Pb ages were made using Isoplot/Ex_ver 3 (Ludwig, 2001).

The zircon Lu-Hf isotopes were analyzed at the State Key Laboratory of Geological Processes and Mineral Resources of the China University of Geosciences, Wuhan. Based on the in-house instrumentation and data acquisition protocols (Hu et al., 2012), the analyses were conducted with a beam of 44 μm, using the ICPMSDataCal program to conduct the off-line signal selection and integration and mass bias calibrations (Liu et al., 2010). The Lu-Hf isotopes of zircons were obtained from the same LA-LCP-MS sites or adjacent domains of same CL structure when insufficient material was available. Data were acquired using a Neptune MC-ICP-MS (Thermo Fisher Scientific, Germany) in combination with a Geolas 2005 excimer ArF laser ablation system (Lambda Physik, Göttingen, Germany). In order to correct for isobaric interferences, the mass bias of Hf (β_{Hf}) and Yb (β_{Yb}) were calculated using ^{179}Hf/^{177}Hf = 0.7325 and ^{173}Yb/^{171}Yb = 1.13017, which were normalized by an exponential correction for mass bias (Segal et al., 2003). By measuring the interference-free ^{173}Yb isotope and using ^{176}Yb/^{173}Yb = 0.79381, the interference of ^{176}Yb on ^{176}Hf was corrected (Segal et al., 2003). Similarly, the interference of ^{176}Lu on ^{176}Hf was corrected by measuring the interference-free ^{175}Lu and using ^{176}Lu/^{175}Lu = 0.02656 (Blichert-Toft & Albarède, 1997). Because of the similarity between Yb and Lu,

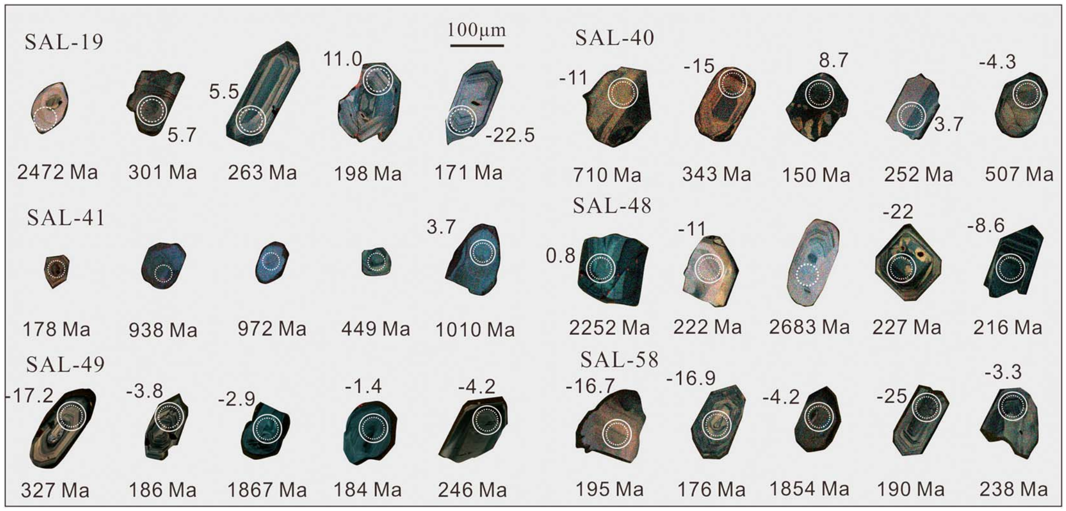

Figure 7. Representative CL images of detrital zircons. Dashed and solid circles represent analytical spots of U-Pb and Lu-Hf isotopes, respectively. The numbers beside the circles are U-Pb ages and $\varepsilon_{Hf}(t)$ values.

the mass bias of Yb (β_{Yb}) was used to calculate the mass fractionation of Lu (Hu et al., 2012). Other parameters used to calculate the isotopes were as follows: $^{176}Hf/^{177}Hf$ ratios were 0.282793 (chondrite) and 0.28325 (depleted mantle), $^{176}Lu/^{177}Hf$ ratios were 0.0338 (chondrite) and 0.0384 (depleted mantle), the radioactive decay coefficient of ^{176}Lu to ^{176}Hf was 1.867×10^{-11} a^{-1}, and the $^{176}Lu/^{177}Hf$ ratio of bulk continental crust was 0.015 (Griffin et al., 2004; Iizuka et al., 2015; Söderlund et al., 2004).

5. Results

Representative CL images of the analyzed detrital zircons are shown in Figure 7. The results of U-Pb dating and Lu-Hf isotopic analysis are shown in Figures 8 and 9, respectively, with detailed analytical data presented in Tables 1 and 2, respectively. The ages of young zircons (<1,000 Ma) are shown by $^{206}Pb/^{238}U$ ages in Figures 8 and 9, whereas the old ones (>1,000 Ma) use $^{207}Pb/^{206}Pb$ ages. Zircon U-Pb ages with high discordance (>10%) were excluded from the calculations.

When the age$^{206Pb/238U}$ of zircon is younger than 1,000 Ma,

$$\text{Discordance} = \left(\text{Age}^{206Pb/238U}/\text{Age}^{207Pb/235U} - 1\right) \times 100\%;$$

When the age$^{206Pb/238U}$ of zircon is older than 1,000 Ma,

$$\text{Discordance} = \left(\text{Age}^{207Pb/235U}/\text{Age}^{207Pb/206Pb} - 1\right) \times 100\%.$$

Discordance is expressed by absolute value.

Because of their sizes (<50 μm), not all the zircons could be analysed for Lu-Hf isotopes. Most detrital zircons are from felsic magmatic rocks which were melted from crust. Thus, $\varepsilon_{Hf}(t)$ and T_{DM2} are used here to evaluate the characteristics of the Lu-Hf isotopes, representing the isotopic feature of the crust in which the zircons were crystallized.

5.1. The Samarka Accretionary Complex

5.1.1. Sample SAL-19

Most zircons are 30–200 μm in length and show magmatic oscillatory zones (Figure 7), although a few zircons have core-rim structures. Seventy-three concordant ages were obtained from 95 analyses and define six age groups (Figure 8a): 162–227 Ma (33%), 236–268 Ma (19%), 275–434 Ma (12%), 452–579 Ma, 729–1,197 Ma (12%), and 1,580–2,756 Ma (11%). Three peak ages are shown in the spectrum, 181 Ma, 263 Ma, and 502 Ma (Figure 8a). The Th/U ratios of 72 of the concordant analyses vary from 0.19 to 2.38, indicating a magmatic origin, and only one zircon with an age of 503 Ma has a Th/U ratio of 0.07, possibly indicating a

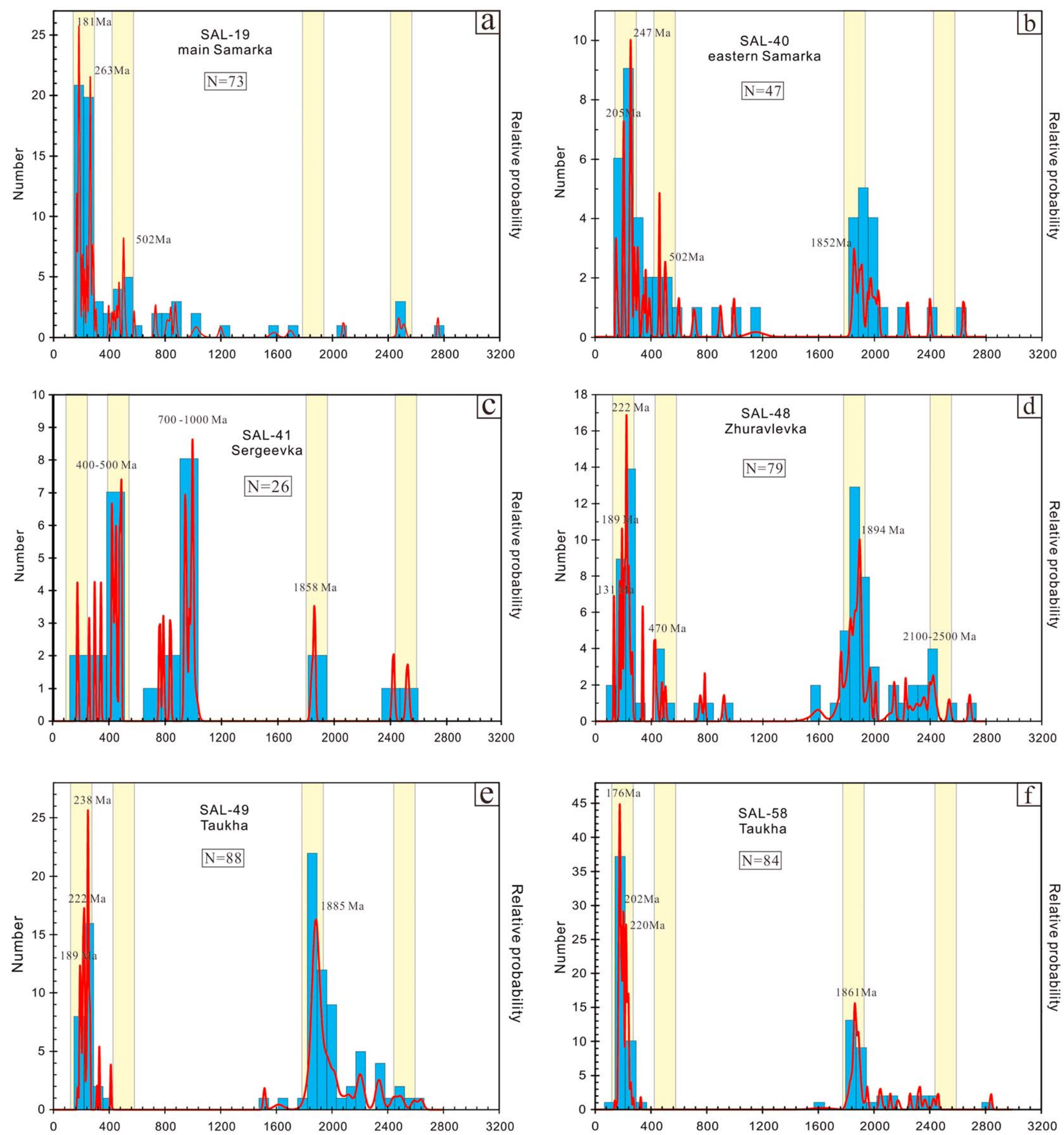

Figure 8. Age spectra of detrital zircons. The spectra diagram uses $^{206}Pb/^{238}U$ ages for young zircons (<1,000 Ma) and $^{207}Pb/^{206}Pb$ ages for old ones (>1,000 Ma). Zircons with high discordance (>10%) are excluded. (a) Sample SAL-19 from the central Samarka accretionary complex, (b) sample SAL-40 from the eastern Samarka accretionary complex, (c) sample SAL-41 from the Sergeevka nappes, (d) sample SAL-48 from the Zhuravlevka turbidite basin, (e) sample SAL-49 from the Taukha accretionary complex, and (f) sample SAL-58 from the Taukha accretionary complex. Four common age groups are marked by yellow bands, namely, 170–260 Ma, 450–550 Ma, 1.6–1.9 Ga, and 2.3–2.6 Ga. The late Pan-African age of 450–550 Ma is important in the BJKB, whereas the ~1.8 Ga and 2.5 Ga ages are dominant in the NCC.

metamorphic origin. Zircons from the Early Permian to Early Jurassic account for 59% of the analyses. Thirty zircons were analyzed for Lu-Hf isotopes and the $\varepsilon_{Hf}(t)$ values of 23 of these vary between −3 and 11 (Figure 9a), with T_{DM2} model ages from 494 to 1,456 Ma. However, four zircons with ages of 162–180 Ma show quite different $\varepsilon_{Hf}(t)$, ranging from −23 to −6, with T_{DM2} model ages of 3.8–2.1 Ga.

5.1.2. Sample SAL-40

Zircons from sample SAL-40 range from 40 to 150 μm in length and have a variety of structures and crystal forms. Some zircons show magmatic oscillatory zones, whereas some are sector zoned and others are only weakly zoned (Figure 7). Sixty-two zircons were analyzed, and 47 concordant ages were obtained with the Th/U ratios ranging from 0.1 to 7.1. In this sample, 36% of zircon ages range from 1.8 to 2.6 Ga with a peak age at 1.85 Ga, forming a major age group. There are five other age populations defined by Phanerozoic

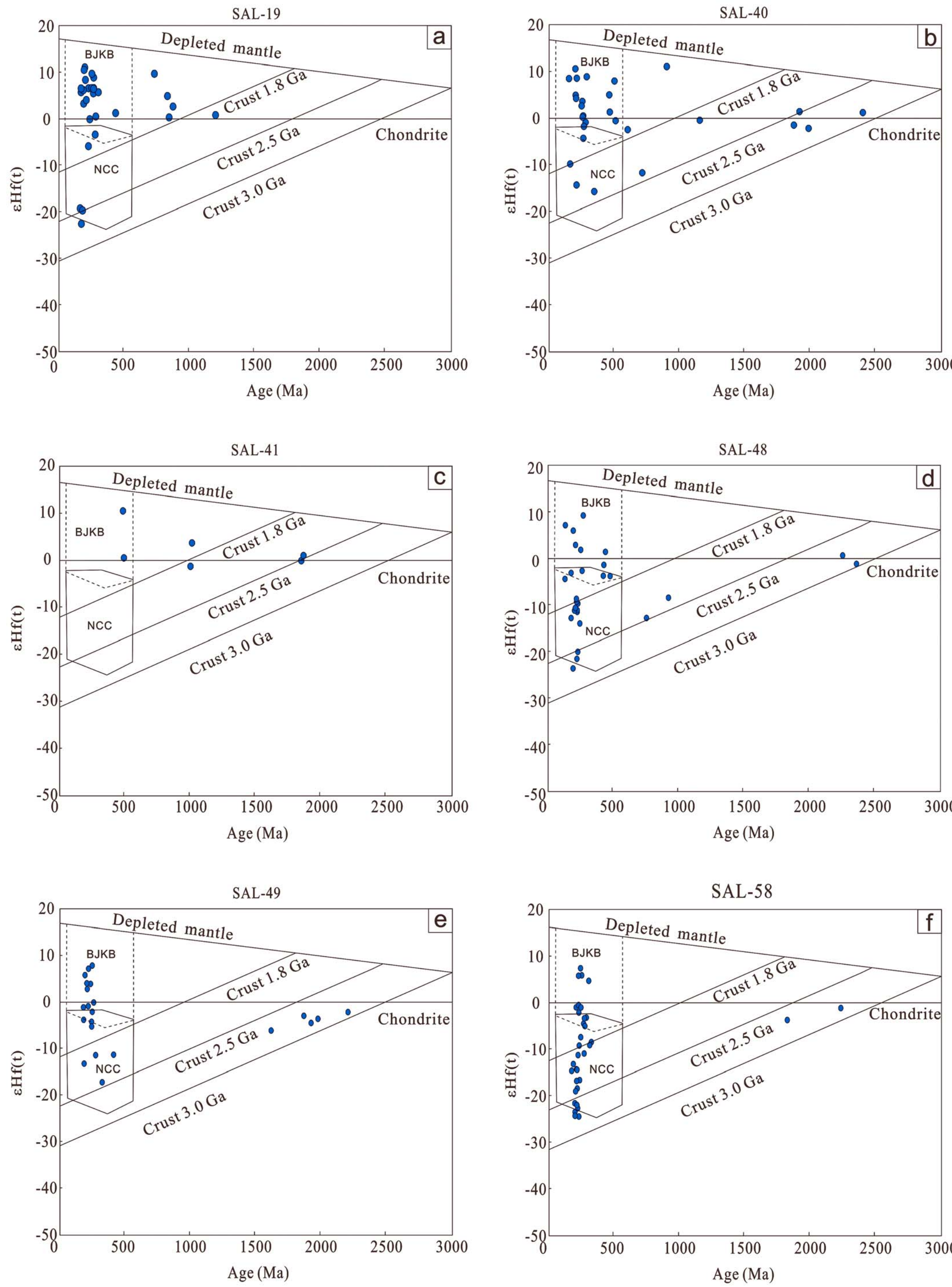

Figure 9. Zircon $\varepsilon_{Hf}(t)$ values versus $^{206}Pb/^{238}U$ ages. (a) Sample SAL-19 from the central Samarka accretionary complex, (b) sample SAL-40 from the eastern Samarka accretionary complex, (c) sample SAL-41 from the Sergeevka nappes, (d) sample SAL-48 from the Zhuravlevka turbidite basin, (e) sample SAL-49 from the Taukha accretionary complex, and (f) sample SAL-58 from the Taukha accretionary complex. The fields of zircon $\varepsilon_{Hf}(t)$ values of the BJKB and NCC are modified after Cheong et al. (2013) and Yang et al. (2006).

10.1002/2017TC004599

Table 1
Zircon U-Pb Isotope Test Results

Sample and analyses spot number	Th (ppm)	U (ppm)	Th/U	Isopotic ratios						Ages(Ma)						Discordance (%)
				$^{207}Pb/^{206}Pb$	1 s	$^{207}Pb/^{235}U$	1 s	$^{206}Pb/^{238}U$	1 s	$^{207}Pb/^{206}Pb$	1 s	$^{207}Pb/^{235}U$	1 s	$^{206}Pb/^{238}U$	1 s	
SAL-19-01	158.02	313.15	0.50	0.04928	0.00206	0.18038	0.00726	0.02656	0.00026	161	76	168	6	169	2	0.59
SAL-19-02	41.61	68.83	0.60	0.04469	0.00443	0.21967	0.02147	0.03566	0.00057	164	158	162	12	162	2	0.00
SAL-19-03	112.32	259.99	0.43	0.04951	0.00216	0.18388	0.00775	0.02694	0.00027	1098	54	241	8	162	2	48.77
SAL-19-04	98.53	181.19	0.54	0.06749	0.00281	0.29012	0.01158	0.03119	0.00034	178	131	165	11	164	2	0.61
SAL-19-05	108.37	244.24	0.44	0.16296	0.00214	10.0181	0.11246	0.44585	0.00302	481	161	189	12	166	2	13.86
SAL-19-06	106.51	157.26	0.68	0.16542	0.00204	10.23108	0.09232	0.44873	0.00304	172	43	168	4	167	1	0.60
SAL-19-07	94.8	225.29	0.42	0.06811	0.00132	1.35869	0.02339	0.14473	0.00105	167	118	167	10	167	3	0.00
SAL-19-08	206.69	553.16	0.37	0.04972	0.00142	0.20341	0.00544	0.02968	0.00024	647	198	204	20	168	4	21.43
SAL-19-09	134.13	168.02	0.80	0.06628	0.00247	1.22817	0.04368	0.13443	0.00154	163	105	168	9	169	2	0.59
SAL-19-10	110.98	155.09	0.72	0.05152	0.00238	0.29576	0.01318	0.04165	0.00046	173	68	170	6	170	2	0.00
SAL-19-11	61.47	148.56	0.41	0.05237	0.00238	0.34673	0.01526	0.04803	0.00051	172	80	171	7	171	2	0.00
SAL-19-12	320.37	1292.85	0.25	0.05712	0.0008	0.62949	0.00701	0.07996	0.00049	183	60	179	5	179	2	0.00
SAL-19-13	164.58	142.66	1.15	0.16576	0.0027	10.90764	0.15302	0.47743	0.00426	186	131	181	12	180	3	0.56
SAL-19-14	313.02	2,414.87	0.13	0.05699	0.00081	0.6347	0.00722	0.0808	0.0005	188	22	182	2	181	1	0.55
SAL-19-15	106.41	218.6	0.49	0.05076	0.00237	0.25066	0.01133	0.03582	0.00038	186	64	181	6	181	2	0.00
SAL-19-16	276.63	501.74	0.55	0.05003	0.00144	0.20861	0.00564	0.03025	0.00025	188	64	183	6	183	2	0.00
SAL-19-17	86.62	195.71	0.44	0.06363	0.00167	1.0524	0.02566	0.11999	0.00103	191	60	187	6	187	2	0.00
SAL-19-18	413.32	788.01	0.52	0.05091	0.00151	0.26114	0.0073	0.03721	0.00031	182	47	188	5	189	2	0.53
SAL-19-19	357.35	776.49	0.46	0.06718	0.00092	1.29342	0.01374	0.13969	0.00088	184	98	189	9	190	2	0.53
SAL-19-20	267.86	333.05	0.80	0.05142	0.00161	0.29848	0.00881	0.04212	0.00036	613	68	226	8	191	2	18.32
SAL-19-21	57.18	120.95	0.47	0.0533	0.00322	0.23435	0.01378	0.0319	0.00041	196	47	192	5	192	2	0.00
SAL-19-22	159.81	300.47	0.53	0.05194	0.00201	0.32055	0.01186	0.04478	0.00045	853	65	259	9	198	2	30.81
SAL-19-23	629.04	968.33	0.65	0.04951	0.00133	0.17944	0.00449	0.02629	0.00021	331	65	209	7	198	2	5.56
SAL-19-24	352.46	429.27	0.82	0.12861	0.00162	6.74037	0.06307	0.38024	0.00253	199	82	201	8	201	2	0.00
SAL-19-25	159.73	604.59	0.26	0.05028	0.00152	0.22739	0.00649	0.03281	0.00028	213	45	203	5	202	2	0.50
SAL-19-26	180.97	357.91	0.51	0.05601	0.00155	0.56013	0.01447	0.07256	0.00061	342	110	214	11	202	3	5.94
SAL-19-27	90.45	109.61	0.83	0.09764	0.00233	3.7379	0.08231	0.27773	0.00276	208	50	208	5	208	2	0.00
SAL-19-28	128.79	487.96	0.26	0.05304	0.00204	0.22805	0.00838	0.03119	0.00032	206	55	209	6	209	2	0.00
SAL-19-29	415.64	1465.27	0.28	0.05119	0.00122	0.27159	0.00594	0.03849	0.00029	212	149	211	15	211	4	0.00
SAL-19-30	60.25	104.51	0.58	0.04933	0.00416	0.17304	0.01433	0.02545	0.00039	219	74	222	8	222	2	0.00
SAL-19-31	251.45	541.73	0.46	0.04991	0.00172	0.20277	0.00664	0.02948	0.00026	1203	42	332	8	222	2	49.55
SAL-19-32	32.42	63.67	0.51	0.18933	0.00322	12.90089	0.18808	0.4942	0.00431	230	85	227	9	227	2	0.00
SAL-19-33	139.78	382.05	0.37	0.07316	0.00122	1.72665	0.02447	0.17124	0.00119	237	49	236	6	236	2	0.00
SAL-19-34	290.22	759.65	0.38	0.0547	0.00126	0.47403	0.00993	0.06287	0.00048	248	72	239	8	238	2	0.42
SAL-19-35	109.45	84.22	1.30	0.06682	0.00294	1.26649	0.05374	0.13751	0.00179	249	36	244	5	243	2	0.41
SAL-19-36	64.72	82.54	0.78	0.10947	0.00189	4.97196	0.07453	0.32952	0.00267	523	64	274	9	246	2	11.38
SAL-19-37	98.84	172.17	0.57	0.04976	0.00268	0.20515	0.01073	0.02991	0.00036	254	40	252	5	252	2	0.00
SAL-19-38	261.43	587.44	0.45	0.05211	0.00157	0.32834	0.00932	0.04571	0.00038	248	225	252	27	253	6	0.40
SAL-19-39	517.42	497.42	1.04	0.05129	0.00132	0.28141	0.00671	0.0398	0.00031	547	70	285	10	254	3	12.20
SAL-19-40	220.13	219.57	1.00	0.08592	0.00135	2.26157	0.02969	0.19098	0.00134	261	97	256	12	255	3	0.39
SAL-19-41	139.02	159.6	0.87	0.05845	0.00247	0.32352	0.01313	0.04015	0.00043	260	110	256	13	256	3	0.00
SAL-19-42	185.93	391.94	0.47	0.08006	0.00113	2.25176	0.02539	0.20406	0.00135	261	129	262	15	262	3	0.00
SAL-19-43	257.77	303.93	0.85	0.05641	0.00144	0.58641	0.01386	0.07542	0.00061	264	82	263	10	263	3	0.00
SAL-19-44	333.05	855.39	0.39	0.05116	0.00211	0.26521	0.01051	0.03761	0.00039	261	36	264	5	265	2	0.38
SAL-19-45	209.62	253.14	0.83	0.07612	0.00289	0.26728	0.00963	0.02547	0.00028	260	39	264	5	265	2	0.38
SAL-19-46	121.76	201.4	0.60	0.05783	0.00224	0.31011	0.01148	0.0389	0.00039	260	52	265	7	266	2	0.38
SAL-19-47	1,007.42	912.47	1.10	0.04941	0.00329	0.17857	0.01156	0.02622	0.0004	261	54	265	7	266	2	0.38

Table 1 *(continued)*

Sample and analyses spot number	Th (ppm)	U (ppm)	Th/U	Isopotic ratios $^{207}Pb/^{206}Pb$	1 s	$^{207}Pb/^{235}U$	1 s	$^{206}Pb/^{238}U$	1 s	Ages(Ma) $^{207}Pb/^{206}Pb$	1 s	$^{207}Pb/^{235}U$	1 s	$^{206}Pb/^{238}U$	1 s	Discordance (%)
SAL-19-48	231.79	308.58	0.75	0.04932	0.00288	0.18019	0.01022	0.02651	0.00034	270	85	268	11	268	3	0.00
SAL-19-49	343	783.2	0.44	0.05023	0.00162	0.22855	0.007	0.03301	0.00029	405	44	283	6	269	2	5.20
SAL-19-50	59.02	91.07	0.65	0.05115	0.00629	0.28189	0.03397	0.03998	0.00102	280	56	276	8	275	2	0.36
SAL-19-51	263.06	632.6	0.42	0.04986	0.00182	0.1979	0.0069	0.0288	0.00027	277	43	277	6	277	2	0.00
SAL-19-52	123.79	135.25	0.92	0.05143	0.00309	0.28733	0.01682	0.04053	0.00054	276	92	277	12	278	3	0.36
SAL-19-53	255.46	368.41	0.69	0.05179	0.00264	0.31418	0.01553	0.04401	0.00051	283	66	282	9	282	3	0.00
SAL-19-54	428.24	609.88	0.70	0.09248	0.00114	2.8689	0.02569	0.22507	0.00141	290	50	288	7	288	2	0.00
SAL-19-55	134.26	140.27	0.96	0.05559	0.00213	0.53309	0.01955	0.06957	0.00072	302	81	302	12	302	3	0.00
SAL-19-56	95.19	169.07	0.56	0.04963	0.00359	0.1763	0.01245	0.02577	0.00039	400	33	394	7	393	3	0.25
SAL-19-57	370.02	388.78	0.95	0.05483	0.00153	0.32192	0.0084	0.04259	0.00035	1,455	40	614	13	411	4	49.39
SAL-19-58	187.22	79.41	2.36	0.06372	0.00319	1.05195	0.05085	0.11978	0.00169	417	74	418	14	419	5	0.24
SAL-19-59	41.36	605.94	0.07	0.05743	0.00191	0.64287	0.02026	0.08121	0.00079	436	63	434	13	434	4	0.00
SAL-19-60	269.12	397.08	0.68	0.05008	0.00228	0.21834	0.00959	0.03163	0.00034	732	36	489	9	438	3	11.64
SAL-19-61	1,042.01	2,320.47	0.45	0.04985	0.00085	0.19598	0.00288	0.02852	0.00019	453	42	452	9	452	4	0.00
SAL-19-62	187.61	245.29	0.76	0.05053	0.00209	0.24389	0.00971	0.03502	0.00035	467	71	467	15	467	5	0.00
SAL-19-63	134.99	194.55	0.69	0.04981	0.0036	0.19477	0.01374	0.02837	0.00044	469	38	469	9	469	4	0.00
SAL-19-64	112.51	73.47	1.53	0.04383	0.00553	0.15673	0.01954	0.02594	0.00049	496	14	496	4	496	3	0.00
SAL-19-65	205.9	209.57	0.98	0.05637	0.00241	0.58363	0.024	0.07511	0.00087	491	14	499	4	501	3	0.40
SAL-19-66	308.45	414.64	0.74	0.05166	0.0025	0.30244	0.01413	0.04247	0.00051	508	52	504	13	503	5	0.20
SAL-19-67	237.26	282.47	0.84	0.05036	0.0042	0.23086	0.01878	0.03326	0.00062	505	45	504	11	504	4	0.00
SAL-19-68	147	251.51	0.58	0.19163	0.00224	14.09081	0.11721	0.53344	0.00359	513	31	513	8	513	4	0.00
SAL-19-69	602.25	539.27	1.12	0.05144	0.00122	0.29711	0.00649	0.0419	0.00032	580	18	579	6	579	4	0.00
SAL-19-70	509.89	839.48	0.61	0.05181	0.00136	0.31304	0.0077	0.04384	0.00032	670	80	612	22	596	7	2.68
SAL-19-71	602.92	933.96	0.65	0.04952	0.00193	0.18209	0.0068	0.02667	0.00027	732	78	730	25	729	10	0.14
SAL-19-72	49	57.43	0.85	0.06189	0.00305	0.82698	0.03943	0.09694	0.00126	729	37	730	13	731	6	0.14
SAL-19-73	121.84	128.92	0.95	0.05511	0.00241	0.50971	0.02142	0.0671	0.00076	815	55	814	20	813	9	0.12
SAL-19-74	431.89	567.51	0.76	0.05143	0.00128	0.29741	0.00684	0.04195	0.00032	832	67	831	24	831	10	0.00
SAL-19-75	474.78	652.51	0.73	0.05935	0.00096	0.76842	0.01054	0.09393	0.00063	843	12	843	6	843	5	0.00
SAL-19-76	250.45	146.76	1.71	0.07077	0.00143	1.72582	0.03132	0.17691	0.00138	872	24	871	10	871	6	0.00
SAL-19-77	322.87	266.95	1.21	0.06027	0.00254	0.24973	0.0101	0.03006	0.00033	879	44	878	17	877	8	0.11
SAL-19-78	511.84	298.05	1.72	0.05672	0.00402	0.20417	0.01428	0.02611	0.0003	1,018	18	1,019	9	1,019	7	0.10
SAL-19-79	368.31	279.38	1.32	0.06833	0.00215	1.37339	0.04084	0.14581	0.00151	1,037	31	1,037	15	1,037	9	0.00
SAL-19-80	205.41	207.85	0.99	0.07384	0.0018	1.7763	0.04006	0.17452	0.00156	951	24	1,018	12	1,050	8	9.43
SAL-19-81	414.23	592.89	0.70	0.0498	0.00181	0.19495	0.0068	0.0284	0.00026	1,336	15	1,200	9	1,127	7	18.54
SAL-19-82	158.55	125.59	1.26	0.05146	0.00346	0.29412	0.0194	0.04146	0.00051	1,198	12	1,197	8	1,197	7	0.08
SAL-19-83	258.74	285.23	0.91	0.05187	0.00172	0.31184	0.00984	0.04361	0.00039	1,477	8	1,374	7	1,309	7	12.83
SAL-19-84	114.61	130.63	0.88	0.05145	0.00274	0.2863	0.0148	0.04037	0.00049	1,580	26	1,580	18	1,580	14	0.00
SAL-19-85	233.91	231.9	1.01	0.16172	0.00206	10.41934	0.10115	0.46739	0.00332	1,698	18	1,696	14	1,695	13	0.18
SAL-19-86	290.3	350.67	0.83	0.05736	0.00169	0.64252	0.01785	0.08126	0.00072	1,791	16	1,815	13	1,836	13	2.45
SAL-19-87	269.39	251.22	1.07	0.06372	0.00162	0.61788	0.01453	0.07034	0.00058	2,079	8	2,078	8	2,077	12	0.10
SAL-19-88	89.02	54.9	1.62	0.06121	0.0067	0.22242	0.02389	0.02636	0.00056	2,487	23	2,436	10	2,377	13	4.63
SAL-19-89	259.19	272.42	0.95	0.08024	0.00251	0.3871	0.01135	0.03499	0.00034	2,512	7	2,456	8	2,390	14	5.10
SAL-19-90	155.94	815	0.19	0.05756	0.00127	0.65696	0.01318	0.08279	0.0006	2,474	8	2,473	9	2,472	15	0.08
SAL-19-91	592.02	473.22	1.25	0.04974	0.00171	0.19255	0.00629	0.02808	0.00025	2,515	12	2,515	13	2,516	19	0.04
SAL-19-92	247.46	153.66	1.61	0.10409	0.00197	4.31563	0.07243	0.30076	0.00258	2,736	29	2,672	14	2,589	19	5.68
SAL-19-93	193.35	127.66	1.51	0.09142	0.00286	0.82995	0.02428	0.06586	0.00068	2,756	6	2,756	8	2,756	15	0.00
SAL-40-01	74.27	229.53	0.32	0.0689	0.00243	1.42	0.04764	0.14956	0.00157	896	52	897	20	898	9	0.11

Table 1 *(continued)*

Sample and analyses spot number	Th (ppm)	U (ppm)	Th/U	Isopotic ratios $^{207}Pb/^{206}Pb$	1 s	$^{207}Pb/^{235}U$	1 s	$^{206}Pb/^{238}U$	1 s	Ages(Ma) $^{207}Pb/^{206}Pb$	1 s	$^{207}Pb/^{235}U$	1 s	$^{206}Pb/^{238}U$	1 s	Discordance (%)
SAL-40-02	101.41	104.65	0.97	0.05344	0.00439	0.40254	0.03224	0.05466	0.00103	348	148	343	23	343	6	0.00
SAL-40-03	51.09	48	1.06	0.06309	0.00366	1.01145	0.05695	0.11635	0.00179	711	94	710	29	710	10	0.00
SAL-40-04	59.59	134.85	0.44	0.11719	0.00193	5.58062	0.07771	0.34556	0.00269	1,914	14	1,913	12	1,913	13	0.05
SAL-40-05	218.83	242.17	0.90	0.05248	0.00289	0.34671	0.01851	0.04794	0.00063	306	98	302	14	302	4	0.00
SAL-40-06	392.41	915.79	0.43	0.05156	0.00127	0.29054	0.00657	0.04089	0.00029	266	39	259	5	258	2	0.39
SAL-40-07	42.33	122.18	0.35	0.05723	0.00231	0.63398	0.02458	0.08038	0.00085	500	67	499	15	498	5	0.20
SAL-40-08	297.21	631.01	0.47	0.13692	0.00159	5.40527	0.05306	0.28631	0.00178	2,189	21	1,886	8	1,623	9	34.87
SAL-40-09	215.5	236.54	0.91	0.1218	0.00194	6.03896	0.08029	0.35979	0.00277	1,983	13	1,981	12	1,981	13	0.10
SAL-40-10	133.87	544.08	0.25	0.05175	0.0024	0.31364	0.01401	0.04398	0.00051	274	81	277	11	277	3	0.00
SAL-40-11	272.37	292.6	0.93	0.04905	0.00243	0.15884	0.00762	0.0235	0.00026	150	90	150	7	150	2	0.00
SAL-40-12	216.51	467.66	0.46	0.05031	0.00278	0.22977	0.01231	0.03314	0.00043	209	100	210	10	210	3	0.00
SAL-40-13	106.45	296.79	0.36	0.15473	0.0019	9.59963	0.08397	0.45017	0.00293	2,399	7	2,397	8	2,396	13	0.13
SAL-40-14	346.75	379.76	0.91	0.10425	0.00179	4.05114	0.0638	0.28183	0.00192	1,701	32	1,645	13	1,601	10	6.25
SAL-40-15	69.82	497.37	0.14	0.11965	0.00144	5.82794	0.04869	0.35342	0.00218	1,951	7	1,951	7	1,951	10	0.00
SAL-40-16	98.46	501.92	0.20	0.12353	0.00186	6.21511	0.07587	0.36505	0.00269	2,008	12	2,007	11	2,006	13	0.10
SAL-40-17	170.31	392.37	0.43	0.04996	0.00211	0.21552	0.00875	0.0313	0.00031	193	76	198	7	199	2	0.50
SAL-40-18	61.66	81.91	0.75	0.05025	0.00477	0.22614	0.02119	0.03265	0.00045	207	186	207	18	207	3	0.00
SAL-40-19	303.86	458.91	0.66	0.05922	0.00125	0.4255	0.00799	0.05214	0.00037	575	28	360	6	328	2	9.76
SAL-40-20	142.07	707.85	0.20	0.12098	0.00147	5.96301	0.05056	0.35763	0.00223	1,971	7	1,970	7	1,971	11	0.05
SAL-40-21	56.46	28.62	1.97	0.05432	0.00519	0.46594	0.04379	0.06223	0.00112	384	180	388	30	389	7	0.26
SAL-40-22	0.134	0.175	0.77	0.28231	0.21924	11.87605	9.02021	0.30521	0.0743	3,376	1,509	2,595	711	1,717	367	96.62
SAL-40-23	139.66	192.32	0.73	0.16336	0.00199	9.85077	0.08475	0.43752	0.00285	2,491	7	2,421	8	2,340	13	6.45
SAL-40-24	152.06	246.69	0.62	0.05225	0.00309	0.32586	0.01869	0.04525	0.00063	296	106	286	14	285	4	0.35
SAL-40-25	145.9	164.17	0.89	0.16344	0.00206	11.23926	0.10376	0.49892	0.00339	2,492	7	2,543	9	2,609	15	2.53
SAL-40-26	585.98	814.38	0.72	0.05	0.0011	0.21802	0.00433	0.03163	0.00022	195	33	200	4	201	1	0.50
SAL-40-27	20.78	51.03	0.41	0.12084	0.00477	5.76806	0.22009	0.34631	0.006	1,969	43	1,942	33	1,917	29	2.71
SAL-40-28	251.86	441.64	0.57	0.05622	0.00112	0.57079	0.01009	0.07366	0.00051	461	27	459	7	458	3	0.22
SAL-40-29	115.77	151.63	0.76	0.04952	0.00658	0.17062	0.02222	0.025	0.00067	173	240	160	19	159	4	0.63
SAL-40-30	358.49	589.81	0.61	0.05627	0.00138	0.57668	0.01297	0.07435	0.00058	463	36	462	8	462	3	0.00
SAL-40-31	29.08	39.07	0.74	0.05132	0.0054	0.28149	0.02914	0.03979	0.00077	255	198	252	23	252	5	0.00
SAL-40-32	59.57	88.91	0.67	0.07817	0.00227	2.01625	0.05606	0.18707	0.0016	1,151	59	1,121	19	1,105	9	4.16
SAL-40-33	457.11	617.3	0.74	0.05122	0.00153	0.28344	0.00796	0.04015	0.00033	251	49	253	6	254	2	0.39
SAL-40-34	264.71	364.16	0.73	0.10616	0.00157	3.91483	0.05176	0.26744	0.00176	1,735	28	1,617	11	1,528	9	13.55
SAL-40-35	362.05	475.84	0.76	0.05139	0.00146	0.2888	0.00769	0.04077	0.00033	258	46	258	6	258	2	0.00
SAL-40-36	53.84	83.29	0.65	0.05995	0.00261	0.80457	0.03377	0.09736	0.00112	602	71	599	19	599	7	0.00
SAL-40-37	249.15	515.59	0.48	0.05743	0.00213	0.6479	0.02299	0.08184	0.00082	508	60	507	14	507	5	0.00
SAL-40-38	315.07	397.78	0.79	0.117	0.00136	5.56714	0.04364	0.34518	0.0021	1,911	7	1,911	7	1,912	10	0.05
SAL-40-39	389.75	596.57	0.65	0.12259	0.00153	5.89309	0.06321	0.34865	0.00222	1,994	23	1,960	9	1,928	11	1.66
SAL-40-40	196.13	658.62	0.30	0.0514	0.00116	0.29013	0.00594	0.04095	0.00029	259	34	259	5	259	2	0.00
SAL-40-41	71.95	225.49	0.32	0.16724	0.0018	10.39578	0.08997	0.45084	0.00287	2,530	18	2,471	8	2,399	13	5.46
SAL-40-42	1,057.66	1,142.16	0.93	0.05027	0.00245	0.22311	0.01049	0.0322	0.00037	207	88	204	9	204	2	0.00
SAL-40-43	136.75	174.78	0.78	0.17852	0.00222	12.44782	0.11278	0.50583	0.00346	2,639	7	2,639	9	2,639	15	0.00
SAL-40-44	61.14	301.22	0.20	0.11442	0.00139	5.30522	0.04513	0.33635	0.0021	1,871	7	1,870	7	1,869	10	0.11
SAL-40-45	310.45	701.88	0.44	0.05113	0.00111	0.27373	0.00535	0.03883	0.00027	247	32	246	4	246	2	0.00
SAL-40-46	138.9	88.64	1.57	0.12138	0.00201	5.68761	0.08003	0.33994	0.00269	1,977	14	1,929	12	1,886	13	4.83
SAL-40-47	91.4	141.48	0.65	0.11606	0.00165	5.47075	0.06141	0.34195	0.00239	1,896	11	1,896	10	1,896	11	0.00
SAL-40-48	194.97	475.26	0.41	0.11574	0.00147	5.44533	0.05097	0.3413	0.00221	1,891	8	1,892	8	1,893	11	0.11
SAL-40-49	233.86	219.58	1.07	0.11331	0.00149	5.20028	0.05178	0.33293	0.0022	1,853	9	1,853	8	1,853	11	0.00

Table 1 *(continued)*

Sample and analyses spot number	Th (ppm)	U (ppm)	Th/U	Isopotic ratios $^{207}Pb/^{206}Pb$	1 s	$^{207}Pb/^{235}U$	1 s	$^{206}Pb/^{238}U$	1 s	Ages(Ma) $^{207}Pb/^{206}Pb$	1 s	$^{207}Pb/^{235}U$	1 s	$^{206}Pb/^{238}U$	1 s	Discordance (%)
SAL-40-50	160.25	430.61	0.37	0.11351	0.00136	5.22268	0.04365	0.33376	0.00207	1,856	7	1,856	7	1,857	10	0.05
SAL-40-51	55.3	400.98	0.14	0.1097	0.00136	3.97297	0.03551	0.26272	0.00165	1,794	8	1,629	7	1,504	8	19.28
SAL-40-52	188.56	324.44	0.58	0.11289	0.00185	5.15892	0.07131	0.33151	0.00256	1,846	14	1,846	12	1,846	12	0.00
SAL-40-53	182.44	406.95	0.45	0.12509	0.00151	6.38351	0.05419	0.37019	0.00234	2,030	7	2,030	7	2,030	11	0.00
SAL-40-54	369.57	479.7	0.77	0.05254	0.00153	0.35535	0.00967	0.04907	0.00041	309	47	309	7	309	3	0.00
SAL-40-55	680.79	1,258.78	0.54	0.05372	0.00091	0.27566	0.00397	0.03722	0.00024	359	21	247	3	236	1	4.66
SAL-40-56	465.54	640.84	0.73	0.05173	0.0018	0.29815	0.00984	0.04181	0.00039	273	58	265	8	264	2	0.38
SAL-40-57	169.85	248.24	0.68	0.14071	0.00166	8.03907	0.06522	0.41445	0.00261	2,236	7	2,235	7	2,235	12	0.04
SAL-40-58	62.38	86.95	0.72	0.05382	0.00257	0.42746	0.01976	0.05761	0.00066	364	84	361	14	361	4	0.00
SAL-40-59	133.46	325.26	0.41	0.12071	0.00258	0.79292	0.01489	0.04765	0.0004	1,967	22	593	8	300	2	97.67
SAL-40-60	583.84	362.4	1.61	0.07231	0.00147	1.66135	0.03006	0.16666	0.00129	995	24	994	11	994	7	0.00
SAL-40-61	278.34	364.25	0.76	0.16056	0.00206	8.88319	0.09713	0.40127	0.0027	2,462	22	2,326	10	2,175	12	13.20
SAL-41-01	179.78	231.05	0.78	0.04966	0.00499	0.19174	0.01884	0.02801	0.00059	179	181	178	16	178	4	0.00
SAL-41-02	366.34	429.58	0.85	0.07037	0.00137	1.52032	0.02631	0.15671	0.00116	939	23	939	11	938	6	0.11
SAL-41-03	239.32	343.11	0.70	0.07162	0.00115	1.60711	0.02163	0.16276	0.00111	975	16	973	8	972	6	0.10
SAL-41-04	43.61	487.19	0.09	0.07086	0.00226	0.21172	0.00633	0.02167	0.0002	953	46	195	5	138	1	41.30
SAL-41-05	215.56	274.04	0.79	0.10996	0.00152	3.57864	0.03865	0.23608	0.00159	1,799	10	1,545	9	1,366	8	31.70
SAL-41-06	322.18	292.3	1.10	0.0786	0.0014	1.48157	0.02284	0.13674	0.00099	1,162	19	923	9	826	6	11.74
SAL-41-07	106.59	94.8	1.12	0.07894	0.00351	1.37064	0.05926	0.12593	0.00132	1,171	90	876	25	765	8	14.51
SAL-41-08	300.85	242.41	1.24	0.07058	0.00126	1.53321	0.02364	0.15759	0.00111	945	20	944	9	943	6	0.11
SAL-41-09	380.87	558.71	0.68	0.07219	0.00115	1.65654	0.022	0.16646	0.00113	991	16	992	8	993	6	0.10
SAL-41-10	202.05	372.62	0.54	0.09747	0.00152	3.21955	0.0453	0.23956	0.00162	1,576	30	1,462	11	1,384	8	13.87
SAL-41-11	278.87	204.95	1.36	0.07285	0.00129	1.70412	0.02605	0.16968	0.00122	1,010	19	1,010	10	1,010	7	0.00
SAL-41-12	221.03	447.25	0.49	0.05899	0.00142	0.38233	0.00844	0.04701	0.00036	567	35	329	6	296	2	11.15
SAL-41-13	159.9	203.61	0.79	0.07217	0.00131	1.65204	0.02611	0.16606	0.00121	991	20	990	10	990	7	0.00
SAL-41-14	279.55	267.02	1.05	0.08965	0.00221	1.46267	0.03293	0.11836	0.00108	1,418	29	915	14	721	6	26.91
SAL-41-15	147.63	338.51	0.44	0.09677	0.00149	3.07086	0.03893	0.23019	0.00163	1,563	13	1,425	10	1,335	9	6.74
SAL-41-16	995.61	591.24	1.68	0.06644	0.00106	0.93383	0.01235	0.10196	0.00068	820	17	670	6	626	4	7.03
SAL-41-17	146.51	160.68	0.91	0.06666	0.00206	1.11289	0.03249	0.12111	0.00119	827	44	760	16	737	7	3.12
SAL-41-18	382.37	579.88	0.66	0.05661	0.00137	0.59636	0.0133	0.07641	0.0006	476	35	475	8	475	4	0.00
SAL-41-19	1,6618.6	1,398.49	11.88	0.46764	0.01177	0.58792	0.01179	0.00912	0.00013	4,142	14	470	8	58.5	0.8	703.42
SAL-41-20	137.54	441.57	0.31	0.11281	0.00164	5.15253	0.06081	0.33134	0.00239	1,845	11	1,845	10	1,845	12	0.00
SAL-41-21	225.76	436.61	0.52	0.06451	0.00098	1.23238	0.01536	0.13859	0.00091	758	15	815	7	837	5	2.63
SAL-41-22	364.7	740.96	0.49	0.05142	0.00173	0.28859	0.00921	0.04071	0.00037	260	57	257	7	257	2	0.00
SAL-41-23	38.37	71.8	0.53	0.05577	0.00491	0.54935	0.04729	0.07146	0.00147	443	156	445	31	445	9	0.00
SAL-41-24	322.41	297.65	1.08	0.07227	0.00133	1.66747	0.02685	0.16738	0.00123	994	21	996	10	998	7	0.20
SAL-41-25	213.42	309.13	0.69	0.05527	0.0014	0.51373	0.01205	0.06743	0.00054	423	38	421	8	421	3	0.00
SAL-41-26	277.12	728.53	0.38	0.11639	0.00138	3.57075	0.0295	0.22256	0.00139	1,902	7	1,543	7	1,295	7	46.87
SAL-41-27	244.81	320.9	0.76	0.07067	0.0014	0.77162	0.01355	0.0792	0.00058	948	24	581	8	491	3	18.33
SAL-41-28	499.6	722.95	0.69	0.07378	0.00137	1.23978	0.02146	0.12187	0.00082	1,035	38	819	10	741	5	10.53
SAL-41-29	225.79	254.44	0.89	0.08498	0.00207	1.44158	0.03214	0.12306	0.0011	1,315	29	906	13	748	6	21.12
SAL-41-30	55.98	96.27	0.58	0.07736	0.00259	1.40911	0.04537	0.13211	0.00124	1,130	68	893	19	800	7	11.63
SAL-41-31	193.5	271.02	0.71	0.05672	0.00219	0.49461	0.01864	0.06324	0.00054	481	88	408	13	395	3	3.29
SAL-41-32	85.97	209.25	0.41	0.06457	0.0014	0.88671	0.01744	0.09962	0.00076	760	29	645	9	612	4	5.39
SAL-41-33	89.44	102.67	0.87	0.07405	0.00467	1.12589	0.06941	0.11027	0.00145	1,043	131	766	33	674	8	13.65
SAL-41-34	208.46	405	0.51	0.12613	0.00148	5.44049	0.04446	0.31291	0.00197	2,045	7	1,891	7	1,755	10	16.52
SAL-41-35	791.08	1,022.98	0.77	0.07687	0.001	1.0567	0.01031	0.09973	0.00062	1,118	10	732	5	613	4	19.41

Table 1 *(continued)*

Sample and analyses spot number	Th (ppm)	U (ppm)	Th/U	Isopotic ratios $^{207}Pb/^{206}Pb$	1 s	$^{207}Pb/^{235}U$	1 s	$^{206}Pb/^{238}U$	1 s	Ages(Ma) $^{207}Pb/^{206}Pb$	1 s	$^{207}Pb/^{235}U$	1 s	$^{206}Pb/^{238}U$	1 s	Discordance (%)
SAL-41-36	730.88	369.32	1.98	0.06543	0.00138	1.17165	0.02222	0.1299	0.001	788	27	787	10	787	6	0.00
SAL-41-37	437.73	748.26	0.58	0.07077	0.00126	1.54866	0.02391	0.15876	0.00115	951	20	950	10	950	6	0.00
SAL-41-38	192.82	205.62	0.94	0.16628	0.00253	10.97629	0.14021	0.4789	0.00402	2,521	11	2,521	12	2,522	18	0.04
SAL-41-39	344.04	1,077.67	0.32	0.05558	0.00094	0.52959	0.00771	0.06912	0.00046	436	21	432	5	431	3	0.23
SAL-41-40	1,196.36	715.81	1.67	0.06457	0.00089	1.11553	0.01208	0.12535	0.0008	760	13	761	6	761	5	0.00
SAL-41-41	156.81	164.15	0.96	0.05238	0.00223	0.34535	0.01415	0.04783	0.00051	302	74	301	11	301	3	0.00
SAL-41-42	209.6	247.88	0.85	0.15673	0.00211	9.84666	0.10463	0.45581	0.00337	2421	9	2,421	10	2,421	15	0.00
SAL-41-43	259.98	244.09	1.07	0.07812	0.00246	1.00189	0.03043	0.09302	0.00079	1150	64	705	15	573	5	23.04
SAL-41-44	173.42	320.81	0.54	0.05599	0.00155	0.55688	0.01442	0.07216	0.00061	452	42	449	9	449	4	0.00
SAL-41-45	631.51	904.96	0.70	0.07361	0.00097	1.24608	0.01258	0.12281	0.00078	1,031	11	822	6	747	4	10.04
SAL-41-47	336.3	676.82	0.50	0.05694	0.00096	0.61912	0.00886	0.07888	0.00053	489	20	489	6	489	3	0.00
SAL-41-48	198.74	299.02	0.66	0.05676	0.0013	0.60719	0.01271	0.07761	0.00059	482	33	482	8	482	4	0.00
SAL-41-49	206.35	684.47	0.30	0.11387	0.00128	5.25575	0.03937	0.33487	0.00206	1862	6	1,862	6	1,862	10	0.00
SAL-48-01	5	3.78	1.32	0.0505	0.00441	0.24372	0.0209	0.03501	0.00061	218	161	221	17	222	4	0.45
SAL-48-02	2.47	11.76	0.21	0.11258	0.0014	5.62975	0.05167	0.36274	0.00239	127	80	129	5	129	1	0.00
SAL-48-03	3	5.34	0.56	0.1511	0.00264	9.21233	0.14501	0.44225	0.00436	125	158	132	11	132	2	0.00
SAL-48-04	3.95	4.44	0.89	0.14203	0.00267	8.18223	0.14076	0.4179	0.00429	802	32	210	3	161	1	30.43
SAL-48-05	2.92	7.44	0.39	0.11417	0.00155	5.63191	0.05985	0.35784	0.00252	170	81	175	7	175	2	0.00
SAL-48-06	3.23	15.77	0.20	0.11661	0.00156	5.52103	0.05759	0.34346	0.0024	184	321	177	33	176	7	0.57
SAL-48-07	5.79	111.19	0.05	0.10759	0.00115	4.17791	0.02733	0.28168	0.00165	187	82	177	7	176	2	0.57
SAL-48-08	3.52	9	0.39	0.11589	0.00152	5.45068	0.05487	0.34117	0.00234	199	124	191	12	190	3	0.53
SAL-48-09	7.55	21.5	0.35	0.1397	0.00155	7.92537	0.05704	0.41153	0.00251	206	85	193	8	192	2	0.52
SAL-48-10	7.03	13.06	0.54	0.13984	0.0018	7.25574	0.07932	0.37631	0.00254	197	141	192	13	192	3	0.00
SAL-48-11	6.58	6.96	0.95	0.11564	0.00211	5.41653	0.08811	0.33978	0.00307	210	212	203	20	202	4	0.50
SAL-48-12	8.67	7.06	1.23	0.05931	0.0021	0.42895	0.01443	0.05247	0.00052	218	158	209	16	208	3	0.48
SAL-48-13	1.41	3.14	0.45	0.24047	0.00333	18.08537	0.20226	0.54547	0.00446	223	99	210	10	209	3	0.48
SAL-48-14	2.36	3.09	0.76	0.11115	0.00186	5.62601	0.08176	0.3672	0.00306	476	104	237	12	214	3	10.75
SAL-48-15	3.24	17.95	0.18	0.11368	0.00152	5.23451	0.05411	0.33402	0.00231	229	100	217	10	216	3	0.46
SAL-48-16	1.54	14.32	0.11	0.11128	0.00234	5.01391	0.09708	0.32685	0.0033	234	42	218	5	217	2	0.46
SAL-48-17	7.74	9.83	0.79	0.14592	0.00284	8.61755	0.15911	0.4284	0.00501	529	36	249	5	220	2	13.18
SAL-48-18	61.43	199	0.31	0.06587	0.00098	0.22978	0.0031	0.0253	0.00016	231	95	221	10	220	3	0.45
SAL-48-19	0.91	0.83	1.10	0.15713	0.00366	9.89126	0.22097	0.45665	0.0057	234	207	223	21	222	3	0.45
SAL-48-20	10.14	12.95	0.78	0.15448	0.00195	9.60012	0.09186	0.45083	0.0032		239	204	22	222	5	8.11
SAL-48-21	2.92	7.62	0.38	0.12037	0.00172	5.89109	0.06829	0.35503	0.00264	1,200	78	333	14	223	3	49.33
SAL-48-22	14.33	28.27	0.51	0.05534	0.0011	0.51609	0.0091	0.06765	0.00048	518	284	252	27	224	5	12.50
SAL-48-23	8.14	10.69	0.76	0.11912	0.00184	5.77939	0.07542	0.35196	0.00279	226	120	226	13	226	3	0.00
SAL-48-24	4.27	30.9	0.14	0.12085	0.00151	5.96075	0.05513	0.35781	0.00238	237	64	228	7	227	2	0.44
SAL-48-25	3.87	22.96	0.17	0.10807	0.00159	3.98012	0.05109	0.26711	0.00191	225	96	228	10	228	2	0.00
SAL-48-26	4.09	4.07	1.00	0.11136	0.00204	5.00771	0.08164	0.32621	0.00286	246	41	241	5	240	2	0.42
SAL-48-27	5.05	26.16	0.19	0.11169	0.00136	5.03848	0.04419	0.32726	0.00211	246	164	242	19	242	4	0.00
SAL-48-28	4.51	15.17	0.30	0.11621	0.00163	5.48164	0.06174	0.34218	0.00248	266	163	250	20	248	5	0.81
SAL-48-29	3.71	10.61	0.35	0.11104	0.0024	4.97451	0.09924	0.325	0.00334	270	108	261	13	260	4	0.38
SAL-48-30	4.67	6.22	0.75	0.04852	0.00422	0.13827	0.01179	0.02068	0.00035	282	52	269	7	267	2	0.75
SAL-48-31	7.13	7.24	0.98	0.1678	0.0025	11.16359	0.14192	0.48264	0.00421	2,674	51	800	26	300	6	166.67
SAL-48-32	6.26	3.23	1.94	0.06988	0.00216	1.47688	0.04338	0.15332	0.00158	578	56	362	10	330	3	9.70
SAL-48-33	17.63	36.62	0.48	0.05798	0.00144	0.27742	0.00634	0.03471	0.00027	340	22	337	4	337	2	0.00
SAL-48-34	25.29	23.52	1.08	0.06521	0.00109	1.16085	0.01647	0.12914	0.00089	617	343	394	49	357	8	10.36

Table 1 *(continued)*

Sample and analyses spot number	Th (ppm)	U (ppm)	Th/U	Isopotic ratios $^{207}Pb/^{206}Pb$	1 s	$^{207}Pb/^{235}U$	1 s	$^{206}Pb/^{238}U$	1 s	Ages(Ma) $^{207}Pb/^{206}Pb$	1 s	$^{207}Pb/^{235}U$	1 s	$^{206}Pb/^{238}U$	1 s	Discordance (%)
SAL-48-35	34.98	38.21	0.92	0.14642	0.00168	3.8914	0.02996	0.19281	0.00119	426	27	423	6	422	3	0.24
SAL-48-36	3.3	6.29	0.52	0.1314	0.00218	5.98502	0.08814	0.33035	0.00253	422	50	426	10	427	4	0.23
SAL-48-37	2.47	5.6	0.44	0.18335	0.00247	13.03044	0.14127	0.51557	0.00411	451	135	440	27	438	8	0.46
SAL-48-38	2.39	3.48	0.69	0.09701	0.00299	3.38532	0.09872	0.2531	0.00252	478	29	475	7	474	3	0.21
SAL-48-39	10.24	14.62	0.70	0.05066	0.0026	0.25192	0.01258	0.03607	0.00038	501	89	499	20	499	6	0.00
SAL-48-40	8.55	17.59	0.49	0.11655	0.00193	5.51181	0.07881	0.34309	0.00286	755	66	752	22	752	9	0.00
SAL-48-41	10.87	12.82	0.85	0.04947	0.0022	0.18784	0.00808	0.02755	0.00029	781	18	782	8	783	5	0.13
SAL-48-42	13.07	26.67	0.49	0.05666	0.00121	0.59625	0.01152	0.07635	0.00057	925	43	921	18	920	9	0.11
SAL-48-43	9.26	8.64	1.07	0.05086	0.00538	0.24539	0.02566	0.035	0.00056	2,305	6	1,612	6	1,137	6	102.73
SAL-48-44	12.58	1.85	6.80	0.18236	0.00913	1.19856	0.05597	0.04768	0.00093	1,567	59	1,501	23	1,454	13	7.77
SAL-48-45	4.57	10.71	0.43	0.10613	0.00178	4.58889	0.06926	0.31361	0.00229	1,767	27	1,630	10	1,526	10	15.79
SAL-48-46	17.37	21.57	0.81	0.05111	0.00134	0.26726	0.0065	0.03793	0.0003	1,857	19	1,690	7	1,559	9	19.11
SAL-48-47	3.87	14.55	0.27	0.11579	0.00143	5.44206	0.04897	0.34096	0.00223	1,598	31	1,576	12	1,561	9	2.37
SAL-48-48	8.45	11.78	0.72	0.05068	0.00325	0.24877	0.01562	0.03561	0.00046	1,759	5	1,670	5	1,600	8	9.94
SAL-48-49	7.23	41.25	0.18	0.05327	0.00094	0.39428	0.00603	0.0537	0.00036	1,828	25	1,763	10	1,709	10	6.96
SAL-48-50	6.09	20.81	0.29	0.12354	0.00142	6.22832	0.0484	0.36574	0.00228	1,942	35	1,840	15	1,751	11	10.91
SAL-48-51	3.95	17.63	0.22	0.1159	0.00144	5.45167	0.04962	0.34126	0.00224	1,734	31	1,747	13	1,758	11	1.37
SAL-48-52	24.56	30.75	0.80	0.05008	0.00346	0.20637	0.01389	0.0299	0.00047	1,766	24	1,762	18	1,758	17	0.46
SAL-48-53	2.67	16.06	0.17	0.11541	0.00217	5.40253	0.09151	0.33962	0.00316	1,876	13	1,815	11	1,763	12	6.41
SAL-48-54	1.8	4.65	0.39	0.13475	0.00223	6.70485	0.09721	0.36089	0.00286	1,805	39	1,800	28	1,795	23	0.56
SAL-48-55	17.47	13.89	1.26	0.11232	0.00168	5.10027	0.06344	0.32944	0.00247	1,817	22	1,815	17	1,814	16	0.17
SAL-48-56	4.52	6.56	0.69	0.05111	0.00457	0.26964	0.02364	0.03827	0.0007	1,820	26	1,817	20	1,816	19	0.22
SAL-48-57	4.41	3.71	1.19	0.15653	0.00224	9.8262	0.11618	0.45543	0.00368	1,822	17	1,821	14	1,820	14	0.11
SAL-48-58	11.16	16.43	0.68	0.11393	0.00262	5.25523	0.11319	0.33466	0.0037	1,820	21	1,822	16	1,823	16	0.16
SAL-48-59	6.32	16.24	0.39	0.11123	0.00281	4.98904	0.11927	0.32541	0.00388	1827	8	1,826	7	1,825	10	0.11
SAL-48-60	5.19	5.12	1.01	0.04977	0.01014	0.19013	0.0381	0.02772	0.00111	1,837	12	1,836	11	1,836	12	0.05
SAL-48-61	24.61	35.42	0.69	0.05085	0.00135	0.23943	0.00589	0.03416	0.00027	2,117	30	1,974	13	1,840	12	15.05
SAL-48-62	17.49	13.98	1.25	0.05092	0.00187	0.25134	0.00883	0.03581	0.00034	1,853	58	1,851	44	1,850	38	0.16
SAL-48-63	5.28	7	0.75	0.11353	0.00167	5.22172	0.06304	0.33369	0.00249	1,857	12	1,856	10	1,856	12	0.05
SAL-48-64	13.23	24.27	0.55	0.04856	0.00218	0.13545	0.00587	0.02023	0.00021	1,859	9	1,858	9	1,858	11	0.05
SAL-48-65	7.91	11.38	0.70	0.05024	0.00234	0.20938	0.00944	0.03023	0.00033	1,861	12	1,860	11	1,860	12	0.05
SAL-48-66	4.58	10.69	0.43	0.05725	0.00301	0.63471	0.03237	0.08044	0.00108	1,863	23	1,862	18	1,861	18	0.11
SAL-48-67	1.42	36.86	0.04	0.11353	0.00119	4.28137	0.03605	0.2735	0.00169	1,879	8	1,875	8	1,871	11	0.43
SAL-48-68	25.67	27.13	0.95	0.0506	0.0028	0.22986	0.01232	0.03296	0.00044	2,441	18	2,158	8	1,874	10	30.26
SAL-48-69	17.25	47.18	0.37	0.13341	0.0016	7.25624	0.06178	0.39461	0.00258	1,877	12	1,876	11	1,875	13	0.11
SAL-48-70	4.54	14.75	0.31	0.11494	0.00145	5.33606	0.04993	0.3368	0.00223	1,886	17	1,885	15	1,885	15	0.05
SAL-48-71	5.99	8.11	0.74	0.05078	0.00265	0.24289	0.01229	0.0347	0.00041	1,890	17	1,887	14	1,886	15	0.21
SAL-48-72	11.05	20.76	0.53	0.05193	0.00163	0.30301	0.00898	0.04233	0.00037	1,892	8	1,892	8	1,891	11	0.05
SAL-48-73	6.76	8.71	0.78	0.05661	0.00334	0.2632	0.01511	0.03373	0.00045	1,894	9	1,893	9	1,892	11	0.11
SAL-48-74	12.92	16.1	0.80	0.11904	0.00229	5.12328	0.0909	0.31214	0.00232	1,894	8	1,893	8	1,893	11	0.05
SAL-48-75	8.89	17.2	0.52	0.05524	0.00173	0.52083	0.01546	0.06841	0.00062	1,899	10	1,898	10	1,897	12	0.11
SAL-48-76	13.64	22.53	0.61	0.09858	0.00161	3.72345	0.05523	0.27393	0.00186	1,904	14	1,902	12	1,902	14	0.11
SAL-48-77	11.8	16.06	0.73	0.11378	0.00171	5.24627	0.06543	0.33453	0.00255	1,905	9	1,904	9	1,903	12	0.11
SAL-48-78	4.13	11.07	0.37	0.11033	0.00378	4.88429	0.16245	0.32118	0.0047	1,943	13	1,943	11	1,944	13	0.05
SAL-48-79	35.88	26.26	1.37	0.10801	0.00254	4.66854	0.103	0.31358	0.00344	1,962	11	1,960	10	1,959	13	0.15
SAL-48-80	3.1	14.4	0.22	0.11172	0.00152	4.67638	0.05485	0.30357	0.00209	1,867	10	1,921	9	1,972	12	5.32
SAL-48-81	10.58	37.92	0.28	0.15862	0.00167	7.37754	0.06253	0.33733	0.00212	1,969	8	1,970	8	1,972	11	0.15
SAL-48-82	6.34	7.18	0.88	0.11474	0.00181	4.97297	0.06615	0.31446	0.00247	2,161	29	2,073	13	1,986	14	8.81

Table 1 *(continued)*

Sample and analyses spot number	Th (ppm)	U (ppm)	Th/U	Isopotic ratios						Ages(Ma)						Discordance (%)
				$^{207}Pb/^{206}Pb$	1 s	$^{207}Pb/^{235}U$	1 s	$^{206}Pb/^{238}U$	1 s	$^{207}Pb/^{206}Pb$	1 s	$^{207}Pb/^{235}U$	1 s	$^{206}Pb/^{238}U$	1 s	
SAL-48-83	3.88	6.02	0.64	0.08013	0.00422	0.38824	0.01969	0.03515	0.00049	1,841	8	1,921	8	1,995	11	7.72
SAL-48-84	7.28	6.9	1.06	0.05033	0.00561	0.22088	0.02427	0.03184	0.00062	2,008	6	2,008	7	2,009	11	0.05
SAL-48-85	9.89	22.13	0.45	0.14908	0.00185	7.57485	0.07917	0.36852	0.00246	1,818	15	1,920	13	2,016	14	9.82
SAL-48-86	5.51	5.6	0.98	0.11328	0.00584	5.19024	0.26569	0.33242	0.00789	2,335	22	2,182	9	2,022	12	15.48
SAL-48-87	5.25	6.85	0.77	0.15787	0.00327	9.97047	0.19465	0.45822	0.00546	2,225	23	2,143	10	2,059	12	8.06
SAL-48-88	7.53	9.03	0.83	0.05005	0.00384	0.20861	0.01566	0.03024	0.00047	2,143	7	2,143	8	2,144	12	0.05
SAL-48-89	0.49	1.24	0.40	0.06038	0.00909	0.47425	0.07056	0.05696	0.00133	2,223	6	2,223	6	2,222	11	0.05
SAL-48-90	5.38	7.33	0.73	0.05155	0.00464	0.2791	0.02457	0.03928	0.00078	2,252	16	2,251	16	2,251	20	0.04
SAL-48-91	18.69	32.89	0.57	0.04982	0.00226	0.18999	0.00832	0.02767	0.0003	2,299	17	2,298	17	2,299	23	0.00
SAL-48-92	8.99	14.08	0.64	0.11484	0.00176	5.34346	0.06878	0.33757	0.00263	2,358	14	2,359	14	2,361	19	0.13
SAL-48-93	6.93	5.08	1.36	0.05049	0.00425	0.22826	0.01889	0.0328	0.00051	2,396	8	2,397	9	2,399	14	0.13
SAL-48-94	1.82	3.16	0.58	0.0577	0.0072	0.28148	0.03466	0.03538	0.00073	2,419	10	2,419	11	2,419	16	0.00
SAL-48-95	4.32	4.56	0.95	0.06441	0.00276	1.09822	0.04539	0.1237	0.00155	2,425	21	2,425	21	2,425	25	0.00
SAL-48-96	20.81	37.71	0.55	0.05164	0.00308	0.29342	0.01701	0.04122	0.00058	2,433	18	2,432	18	2,432	24	0.04
SAL-48-97	1.18	1.73	0.68	0.04605	0.00562	0.22254	0.02672	0.03505	0.00075	2,536	11	2,537	12	2,539	18	0.12
SAL-48-98	9.13	14.63	0.62	0.05074	0.00276	0.23797	0.01259	0.03403	0.00041	2,683	9	2,682	10	2,680	17	0.11
SAL-48-99	9.65	11.34	0.85	0.05597	0.00437	0.54178	0.04129	0.07024	0.00139	3,123	23	2,994	11	2,806	19	11.30
SAL-49-01	72.28	785.89	0.09	0.05288	0.00093	0.3802	0.00569	0.05215	0.00032	323.6	39.51	327.2	4.19	327.7	1.96	0.15
SAL-49-02	71.83	340.36	0.21	0.04978	0.00184	0.20105	0.00711	0.02929	0.00024	184.9	83.77	186	6.01	186.1	1.5	0.05
SAL-49-03	241.85	506.13	0.48	0.1124	0.00132	4.54698	0.03456	0.29341	0.00166	1,838.6	21.08	1,739.6	6.33	1,658.5	8.27	10.86
SAL-49-04	49.12	459.28	0.11	0.1326	0.00186	7.18262	0.07789	0.3929	0.00269	2,132.6	24.33	2,134.3	9.67	2,136.3	12.47	0.17
SAL-49-05	52.86	326.05	0.16	0.11445	0.00138	5.30053	0.04304	0.33593	0.00196	1,871.2	21.6	1,868.9	6.94	1,867.1	9.44	0.22
SAL-49-06	108.94	592.73	0.18	0.05148	0.00131	0.27627	0.00645	0.03892	0.00028	262.5	57.26	247.7	5.13	246.2	1.76	0.61
SAL-49-07	144.01	368.39	0.39	0.17854	0.00198	12.43542	0.08283	0.5052	0.00286	2,639.4	18.28	2,637.9	6.26	2,636.1	12.23	0.13
SAL-49-08	128.19	380.64	0.34	0.04977	0.00179	0.19933	0.00683	0.02905	0.00025	184.3	81.7	184.6	5.79	184.6	1.56	0.00
SAL-49-09	85.3	223.04	0.38	0.13109	0.00168	6.66398	0.06122	0.36875	0.00231	2,112.6	22.26	2,4067.9	8.11	2,023.5	10.87	4.40
SAL-49-10	273.7	455.71	0.60	0.11541	0.00137	5.40293	0.04249	0.3396	0.00196	1,886.2	21.24	1,885.3	6.74	1,884.7	9.43	0.08
SAL-49-11	40.14	1,199.21	0.03	0.11454	0.00125	5.31182	0.0335	0.3364	0.00182	1,872.6	19.53	1,870.8	5.39	1,869.3	8.77	0.18
SAL-49-12	238.15	396.53	0.60	0.14955	0.00168	9.02818	0.06274	0.43792	0.00249	2,340.7	19.17	2,340.9	6.35	2,341.3	11.15	0.03
SAL-49-13	42.95	161.76	0.27	0.12465	0.00187	6.3361	0.07616	0.36872	0.00264	2,023.9	26.28	2,023.5	10.54	2,023.4	12.43	0.02
SAL-49-14	51.58	242.18	0.21	0.11435	0.00151	5.29679	0.05128	0.336	0.00211	1,869.7	23.57	1,868.3	8.27	1,867.4	10.16	0.12
SAL-49-15	82.29	448.54	0.18	0.11502	0.00133	5.4514	0.04042	0.3438	0.00195	1,880.2	20.72	1,893	6.36	1,904.9	9.36	1.30
SAL-49-16	36.46	62.39	0.58	0.09964	0.00193	3.91756	0.06684	0.28522	0.00232	1,617.3	35.68	1,617.3	13.8	1,617.6	11.65	0.02
SAL-49-17	18.62	340.16	0.05	0.11284	0.0015	4.12109	0.04048	0.26494	0.00165	1,845.6	23.91	1,658.5	8.03	1,515.1	8.4	21.81
SAL-49-18	268.85	490.09	0.55	0.12242	0.00141	6.11207	0.04486	0.36218	0.00206	1,991.8	20.34	1,992	6.4	1,992.5	9.76	0.04
SAL-49-19	68.67	367.15	0.19	0.11515	0.00138	5.38357	0.04303	0.33915	0.00198	1,882.3	21.39	1,882.2	6.84	1,882.6	9.51	0.02
SAL-49-20	54.6	209.53	0.26	0.11777	0.00155	5.63161	0.05456	0.3469	0.00219	1,922.6	23.41	1,921	8.35	1,919.8	10.48	0.15
SAL-49-21	139.78	292.76	0.48	0.13821	0.00162	7.77019	0.0592	0.40784	0.00239	2,204.9	20.15	2,204.8	6.85	2205	10.94	0.00
SAL-49-22	222.61	275.05	0.81	0.05181	0.00222	0.29408	0.0121	0.04118	0.00043	277	95.21	261.8	9.5	260.1	2.68	0.65
SAL-49-23	49.05	346.12	0.14	0.11713	0.0015	5.57949	0.05148	0.34556	0.00214	1,912.9	22.84	1,912.9	7.94	1,913.4	10.24	0.03
SAL-49-24	181.65	405.88	0.45	0.07102	0.00189	0.30809	0.00752	0.03147	0.00025	958	53.37	272.7	5.83	199.7	1.59	36.55
SAL-49-25	103.99	157.42	0.66	0.04787	0.00252	0.24884	0.01273	0.03771	0.00043	91.6	121.32	225.6	10.35	238.6	2.64	5.45
SAL-49-26	26.98	578.17	0.05	0.11384	0.00131	5.25403	0.03813	0.33484	0.00189	1,861.5	20.57	1,861.4	6.19	1,861.8	9.15	0.02
SAL-49-27	97.69	403.79	0.24	0.12058	0.00144	5.90997	0.04727	0.35557	0.00209	1,964.9	21.14	1,962.7	6.95	1,961.1	9.94	0.19
SAL-49-28	110.44	252.07	0.44	0.05107	0.00187	0.24785	0.00863	0.03521	0.00031	243.9	81.99	224.8	7.03	223.1	1.93	0.76
SAL-49-29	45.2	690.68	0.07	0.11467	0.00129	5.33467	0.03716	0.33751	0.00189	1,874.6	20.2	1,874.4	5.96	1,874.7	9.11	0.01
SAL-49-30	45.55	252.32	0.18	0.11428	0.00147	5.29001	0.04881	0.33584	0.00207	1,868.5	22.96	1,867.3	7.88	1,866.6	10	0.10

10.1002/2017TC004599

Table 1 *(continued)*

Sample and analyses spot number	Th (ppm)	U (ppm)	Th/U	Isopotic ratios						Ages(Ma)						Discordance (%)
				$^{207}Pb/^{206}Pb$	1 s	$^{207}Pb/^{235}U$	1 s	$^{206}Pb/^{238}U$	1 s	$^{207}Pb/^{206}Pb$	1 s	$^{207}Pb/^{235}U$	1 s	$^{206}Pb/^{238}U$	1 s	
SAL-49-31	57.36	180.33	0.32	0.05131	0.00223	0.28148	0.01179	0.0398	0.0004	254.6	96.92	251.8	9.34	251.6	2.46	0.08
SAL-49-32	60.45	317.91	0.19	0.11805	0.00143	5.66368	0.04661	0.34808	0.00207	1,926.9	21.54	1,925.8	7.1	1925.4	9.89	0.08
SAL-49-33	110.19	175.49	0.63	0.05616	0.00236	0.26301	0.01057	0.03398	0.00035	458.2	90.79	237.1	8.5	215.4	2.18	10.07
SAL-49-34	39.37	262.75	0.15	0.11147	0.00151	5.00968	0.05095	0.32604	0.00209	1,823.6	24.34	1,821	8.61	1,819.2	10.16	0.24
SAL-49-35	34.45	1,206.35	0.03	0.1162	0.00127	5.49148	0.0352	0.34285	0.00188	1,898.6	19.53	1,899.3	5.51	1,900.4	9.05	0.09
SAL-49-36	66.18	485.96	0.14	0.13782	0.00159	7.71583	0.05671	0.40618	0.00236	2,199.9	19.84	2,198.4	6.61	2,197.4	10.81	0.11
SAL-49-37	178.37	455.32	0.39	0.12825	0.00153	6.70857	0.0534	0.3795	0.00225	2,074.1	20.83	2,073.8	7.03	2,074	10.53	0.00
SAL-49-38	141.51	230.5	0.61	0.05137	0.00185	0.29414	0.01008	0.04154	0.00037	257.7	80.61	261.8	7.91	262.4	2.31	0.23
SAL-49-39	139.44	220.94	0.63	0.04995	0.00326	0.20284	0.013	0.02946	0.00033	192.5	145.22	187.5	10.98	187.2	2.04	0.16
SAL-49-40	170.61	835.87	0.20	0.05232	0.00093	0.35499	0.00537	0.04922	0.00031	299.5	39.98	308.5	4.03	309.8	1.89	0.42
SAL-49-41	41.87	95.01	0.44	0.05124	0.0044	0.28146	0.02366	0.03985	0.00072	251.5	186.29	251.8	18.75	251.9	4.46	0.04
SAL-49-42	19.71	75.43	0.26	0.05037	0.00497	0.22836	0.02216	0.03289	0.00057	212	213.66	208.8	18.32	208.6	3.58	0.10
SAL-49-43	303.55	204.49	1.48	0.04953	0.00394	0.20362	0.01594	0.02982	0.00037	173.2	175.56	188.2	13.45	189.4	2.31	0.63
SAL-49-44	127.25	362.14	0.35	0.05132	0.00176	0.27652	0.00899	0.03909	0.00035	255.2	77.01	247.9	7.15	247.2	2.16	0.28
SAL-49-45	338.2	437.32	0.77	0.04989	0.00203	0.19023	0.00741	0.02766	0.00026	189.8	91.85	176.8	6.32	175.9	1.66	0.51
SAL-49-46	148.4	144.23	1.03	0.11083	0.00229	4.96446	0.09236	0.32498	0.00297	1,813.1	37.09	1,813.3	15.72	1,814	14.43	0.05
SAL-49-47	63.7	287.12	0.22	0.11535	0.00148	5.40053	0.05018	0.33969	0.00212	1,885.4	22.96	1,884.9	7.96	1,885.2	10.2	0.01
SAL-49-48	118.65	418.78	0.28	0.12075	0.00149	5.92558	0.05074	0.35604	0.00217	1,967.3	21.79	1,965	7.44	1,963.4	10.31	0.20
SAL-49-49	169.95	185.41	0.92	0.05054	0.00247	0.24887	0.01178	0.03572	0.00039	220	109.33	225.7	9.58	226.3	2.4	0.27
SAL-49-50	184.75	544.13	0.34	0.12396	0.00142	6.26298	0.04549	0.36657	0.00212	2,014	20.16	2,013.3	6.36	2013.2	9.98	0.04
SAL-49-51	138.32	226.61	0.61	0.05098	0.00262	0.28202	0.01405	0.04014	0.00044	239.7	114.13	252.3	11.13	253.7	2.74	0.55
SAL-49-52	108.41	540.01	0.20	0.11488	0.00136	5.35822	0.04225	0.33839	0.00199	1,878.1	21.21	1,878.2	6.75	1,878.9	9.6	0.04
SAL-49-53	99.08	311.56	0.32	0.12486	0.00171	6.35945	0.06661	0.36953	0.00248	2,026.9	24.09	2,026.7	9.19	2,027.2	11.68	0.01
SAL-49-54	182.83	717.74	0.25	0.11774	0.00134	5.64224	0.04062	0.34768	0.002	1,922.3	20.29	1,922.6	6.21	1,923.5	9.55	0.06
SAL-49-55	92.91	225.81	0.41	0.1732	0.00211	11.80944	0.10005	0.4947	0.00318	2,588.8	20.18	2,589.4	7.93	2,591	13.71	0.08
SAL-49-56	100.87	400.94	0.25	0.11493	0.00144	5.35977	0.04778	0.33835	0.00208	1,878.8	22.48	1,878.5	7.63	1,878.7	10.04	0.01
SAL-49-57	97.24	355.95	0.27	0.1492	0.00179	7.87235	0.06392	0.38283	0.00234	2,336.7	20.4	2,216.5	7.32	2,089.5	10.93	11.83
SAL-49-58	200.05	547.72	0.37	0.14018	0.00158	7.98032	0.05618	0.41305	0.00239	2,229.4	19.39	2,228.8	6.35	2,228.9	10.9	0.02
SAL-49-59	21.92	1,118.12	0.02	0.12007	0.00133	5.24391	0.03496	0.31687	0.00179	1,957.3	19.61	1,859.8	5.69	1,774.4	8.74	10.31
SAL-49-60	105.98	267.56	0.40	0.13707	0.0018	7.64463	0.07456	0.40463	0.00268	2,190.6	22.67	2,190.1	8.76	2,190.3	12.3	0.01
SAL-49-61	58.52	37.87	1.55	0.1504	0.00301	9.12105	0.16481	0.44001	0.00446	2,350.4	33.85	2,350.2	16.53	2,350.7	19.96	0.01
SAL-49-62	36.86	299.4	0.12	0.11502	0.0015	5.36578	0.05129	0.33847	0.00215	1,880.2	23.3	1,879.4	8.18	1,879.3	10.35	0.05
SAL-49-63	119.43	4,961.86	0.02	0.17761	0.02764	1.60645	0.24197	0.06562	0.00288	2,630.7	237.69	972.7	94.26	409.7	17.41	137.42
SAL-49-64	44.73	676.82	0.07	0.11529	0.00133	5.39238	0.04031	0.33935	0.00198	1,884.4	20.68	1,883.6	6.4	1,883.6	9.52	0.04
SAL-49-65	71.11	312.16	0.23	0.11606	0.00152	5.46396	0.0525	0.34158	0.00218	1,896.4	23.31	1,895	8.25	1,894.2	10.47	0.12
SAL-49-66	140.64	583.72	0.24	0.1203	0.00161	5.88853	0.05928	0.35513	0.00233	1,960.7	23.7	1,959.5	8.74	1,959.1	11.09	0.08
SAL-49-67	66.48	84.26	0.79	0.11496	0.00239	5.36595	0.10017	0.33864	0.00314	1,879.3	36.96	1,879.4	15.98	1,880.1	15.13	0.04
SAL-49-68	29.86	74.24	0.40	0.11454	0.00217	5.32086	0.08844	0.33704	0.00286	1,872.7	33.72	1,872.2	14.21	1,872.4	13.78	0.02
SAL-49-69	200.49	273.25	0.73	0.05002	0.00293	0.21326	0.01212	0.03093	0.0004	196	130.48	196.3	10.14	196.4	2.47	0.05
SAL-49-70	29.32	78.55	0.37	0.05041	0.00517	0.23421	0.02366	0.03371	0.00058	214.1	221.3	213.7	19.46	213.7	3.63	0.00
SAL-49-71	34.32	89.98	0.38	0.06399	0.00398	0.36124	0.02183	0.04096	0.00057	741.3	126.29	313.1	16.28	258.8	3.56	20.98
SAL-49-72	76.81	356.53	0.22	0.12134	0.00151	6.11451	0.05345	0.36559	0.00227	1,976.1	21.95	1,992.3	7.63	2,008.6	10.72	1.62
SAL-49-73	359.38	460.92	0.78	0.15855	0.00184	10.05482	0.0764	0.46011	0.00279	2,440.2	19.51	2,439.8	7.02	2,440.1	12.32	0.00
SAL-49-74	47.86	399.51	0.12	0.11479	0.00144	5.34671	0.04749	0.33794	0.0021	1,876.5	22.4	1,876.4	7.6	1,876.8	10.09	0.02
SAL-49-75	93.27	173.06	0.54	0.05069	0.00312	0.232	0.01389	0.0332	0.00044	226.8	136.13	211.9	11.45	210.6	2.73	0.62
SAL-49-76	148.49	397.06	0.37	0.11557	0.00143	5.42584	0.04713	0.3406	0.0021	1,888.9	22.12	1,888.9	7.45	1,889.6	10.09	0.04
SAL-49-77	91.16	284.44	0.32	0.16411	0.00214	10.70081	0.10357	0.47306	0.00325	2,498.5	21.76	2,497.5	8.99	2497	14.24	0.06
SAL-49-78	61.54	61.55	1.00	0.07543	0.00713	0.31325	0.02892	0.03013	0.00061	1,080.1	178.83	276.7	22.36	191.3	3.83	44.64

Table 1 *(continued)*

Sample and analyses spot number	Th (ppm)	U (ppm)	Th/U	Isopotic ratios $^{207}Pb/^{206}Pb$	1 s	$^{207}Pb/^{235}U$	1 s	$^{206}Pb/^{238}U$	1 s	Ages(Ma) $^{207}Pb/^{206}Pb$	1 s	$^{207}Pb/^{235}U$	1 s	$^{206}Pb/^{238}U$	1 s	Discordance (%)
SAL-49-79	125.05	205.74	0.61	0.1141	0.00223	5.27847	0.09147	0.33562	0.00297	1,865.7	34.88	1,865.4	14.79	1,865.5	14.33	0.01
SAL-49-80	58.63	431.11	0.14	0.13635	0.00178	5.08467	0.04846	0.27054	0.00175	2,181.4	22.52	1,833.6	8.09	1,543.5	8.86	41.33
SAL-49-81	17.13	1,448.37	0.01	0.15615	0.00187	3.03444	0.02431	0.14098	0.00085	2,414.4	20.22	1,416.3	6.12	850.2	4.8	66.58
SAL-49-82	185.83	236.05	0.79	0.13732	0.00193	7.66706	0.08424	0.40507	0.00287	2,193.6	24.24	2,192.7	9.87	2192.3	13.18	0.06
SAL-49-83	159.93	471.83	0.34	0.05124	0.00167	0.2765	0.00852	0.03915	0.00034	251.4	73.29	247.9	6.78	247.6	2.09	0.12
SAL-49-84	306.14	441.79	0.69	0.12461	0.00154	6.34172	0.05496	0.36922	0.0023	2,023.2	21.7	2,024.2	7.6	2,025.7	10.85	0.12
SAL-49-85	140.69	1,609.34	0.09	0.05503	0.00083	0.50334	0.00612	0.06636	0.00041	413.2	33.21	414	4.13	414.2	2.45	0.05
SAL-49-86	82.66	483.58	0.17	0.11621	0.00148	5.49079	0.05075	0.34276	0.00217	1,898.8	22.78	1899.2	7.94	1,899.9	10.43	0.06
SAL-49-87	89.09	107.35	0.83	0.05028	0.0043	0.24166	0.02031	0.03487	0.00054	207.8	187.11	219.8	16.61	221	3.36	0.54
SAL-49-88	459.63	1,565.57	0.29	0.05786	0.00117	0.22961	0.00408	0.02879	0.0002	524.4	43.88	209.9	3.37	183	1.23	14.70
SAL-49-89	41.89	69.54	0.60	0.16188	0.00263	10.69054	0.14741	0.47907	0.00411	2,475.4	27.15	2,496.6	12.8	2,523.2	17.9	1.89
SAL-49-90	716.11	615.33	1.16	0.07339	0.00173	0.38925	0.00829	0.03848	0.0003	1,024.7	46.94	333.8	6.06	243.4	1.87	37.14
SAL-49-91	108.73	356.84	0.30	0.11672	0.00148	5.53414	0.05034	0.34394	0.00217	1,906.6	22.55	1,905.9	7.82	1,905.6	10.42	0.05
SAL-49-92	52.31	370.31	0.14	0.11722	0.00157	5.65674	0.05726	0.35007	0.00231	1,914.3	23.88	1,924.8	8.73	1,934.9	11.05	1.06
SAL-49-93	70.07	184.02	0.38	0.14823	0.00199	8.8817	0.09064	0.43466	0.00302	2,325.6	22.84	2,325.9	9.31	2,326.7	13.58	0.05
SAL-49-94	164.24	149.51	1.10	0.05061	0.0055	0.24658	0.02634	0.03534	0.00071	223.1	233.26	223.8	21.46	223.9	4.44	0.04
SAL-49-95	64.54	246.74	0.26	0.11607	0.00187	5.46912	0.07372	0.34182	0.00257	1,896.5	28.77	1,895.8	11.57	1,895.4	12.34	0.06
SAL-49-96	38.45	237.39	0.16	0.11471	0.00179	5.3383	0.06852	0.3376	0.00249	1,875.3	27.88	1,875	10.98	1,875.1	12.02	0.01
SAL-49-97	693.43	2,466.11	0.28	0.10028	0.00126	1.84495	0.01631	0.13346	0.00081	1,629.2	23.12	1,061.6	5.82	807.6	4.59	31.45
SAL-49-98	73.61	316.48	0.23	0.11724	0.00226	5.36412	0.09129	0.33189	0.00292	1,914.6	34.18	1,879.1	14.57	1,847.5	14.13	3.63
SAL-58-01	0.0308	0.0281	1.10	0.05022	0.00285	0.21267	0.01172	0.03072	0.0004	205	103	196	10	195	3	0.51
SAL-58-02	0.0314	0.0233	1.35	0.04964	0.00176	0.18976	0.00643	0.02773	0.00025	178	62	176	5	176	2	0.00
SAL-58-03	0.0357	0.0187	1.91	0.11314	0.00132	4.33814	0.03443	0.27819	0.00171	136	123	144	9	145	2	0.69
SAL-58-04	0.0356	0.0207	1.72	0.20159	0.00249	15.28375	0.13886	0.55003	0.00388	161	51	156	4	156	1	0.00
SAL-58-05	0.0441	0.0265	1.66	0.04984	0.00205	0.20651	0.00814	0.03006	0.00031	156	67	162	5	163	2	0.61
SAL-58-06	0.0375	0.0303	1.24	0.05095	0.0014	0.26491	0.0068	0.03772	0.0003	175	31	165	3	164	1	0.61
SAL-58-07	1.96	2.77	0.71	0.04997	0.00133	0.20613	0.00511	0.02993	0.00023	166	38	166	3	167	1	0.60
SAL-58-08	0.0341	0.0216	1.58	0.12651	0.00195	6.53423	0.08356	0.37471	0.00289	161	136	166	11	167	3	0.60
SAL-58-09	0.0376	0.0223	1.69	0.15083	0.00229	5.14966	0.06952	0.24762	0.00172	163	101	169	9	170	2	0.59
SAL-58-10	0.0399	0.019	2.10	0.04938	0.00121	0.17818	0.00401	0.02618	0.0002	366	30	185	3	171	1	8.19
SAL-58-11	0.0376	0.0245	1.53	0.10912	0.00125	3.27685	0.02529	0.21787	0.00132	178	58	174	5	174	2	0.00
SAL-58-12	0.315	0.587	0.54	0.11557	0.00152	5.4191	0.05452	0.34017	0.00229	163	64	174	6	175	2	0.57
SAL-58-13	0.889	1.8	0.49	0.11409	0.00152	5.27802	0.05402	0.33563	0.00228	154	27	174	3	176	1	1.14
SAL-58-14	0.0636	0.0288	2.21	0.04913	0.00096	0.18734	0.00322	0.02766	0.00019	179	76	177	7	177	2	0.00
SAL-58-15	0.287	0.516	0.56	0.04993	0.00107	0.1949	0.00376	0.02832	0.0002	174	54	179	5	179	2	0.00
SAL-58-16	0.0374	0.027	1.39	0.04959	0.00197	0.19767	0.00756	0.02892	0.00028	192	32	181	3	180	1	0.56
SAL-58-17	0.0333	0.0149	2.23	0.05003	0.00235	0.21938	0.00995	0.03181	0.00034	184	83	182	7	182	2	0.00
SAL-58-18	0.0544	0.0964	0.56	0.14749	0.00163	8.78608	0.06257	0.43219	0.00263	176	71	183	6	184	2	0.54
SAL-58-19	1.09	1.17	0.93	0.05072	0.00117	0.24277	0.00514	0.03472	0.00026	186	36	186	4	186	1	0.00
SAL-58-20	0.0288	0.0222	1.30	0.16025	0.00183	10.26316	0.07945	0.46462	0.00294	183	46	188	4	189	2	0.53
SAL-58-21	0.0319	0.0259	1.23	0.11337	0.00135	5.20165	0.04359	0.33286	0.0021	194	43	190	4	190	1	0.00
SAL-58-22	0.0304	0.0217	1.40	0.04958	0.00103	0.17638	0.0033	0.02581	0.00018	182	87	189	8	190	2	0.53
SAL-58-23	0.0321	0.0292	1.10	0.04956	0.00156	0.19284	0.00576	0.02823	0.00024	198	60	190	6	190	2	0.00
SAL-58-24	0.0395	0.0232	1.70	0.11534	0.00165	5.41036	0.0621	0.34031	0.00243	188	73	191	7	191	2	0.00
SAL-58-25	0.0328	0.026	1.26	0.11049	0.00175	4.92778	0.06513	0.32355	0.00245	201	46	193	5	192	2	0.52
SAL-58-26	0.0316	0.0197	1.60	0.0498	0.00117	0.20065	0.00433	0.02923	0.00022	-17	116	178	11	193	2	7.77
SAL-58-27	0.03	0.0159	1.89	0.11974	0.00137	5.9532	0.04577	0.36068	0.00223	187	182	194	17	195	4	0.51

Table 1 *(continued)*

Sample and analyses spot number	Th (ppm)	U (ppm)	Th/U	Isopotic ratios						Ages(Ma)						Discordance (%)
				$^{207}Pb/^{206}Pb$	1 s	$^{207}Pb/^{235}U$	1 s	$^{206}Pb/^{238}U$	1 s	$^{207}Pb/^{206}Pb$	1 s	$^{207}Pb/^{235}U$	1 s	$^{206}Pb/^{238}U$	1 s	
SAL-58-28	0.0556	0.0414	1.34	0.05013	0.00141	0.2093	0.0055	0.03029	0.00025	202	54	201	6	201	2	0.00
SAL-58-29	0.0531	0.0331	1.60	0.11234	0.0017	5.10837	0.0636	0.32989	0.00244	196	86	201	8	202	2	0.50
SAL-58-30	0.0311	0.0179	1.74	0.1314	0.00159	7.04338	0.06068	0.38888	0.00252	211	112	203	11	202	3	0.50
SAL-58-31	0.245	0.315	0.78	0.05174	0.00187	0.30537	0.01051	0.04282	0.0004	210	105	204	10	204	2	0.00
SAL-58-32	0.0318	0.0188	1.69	0.11605	0.00145	5.46972	0.0503	0.34193	0.00223	210	174	207	17	206	3	0.49
SAL-58-33	0.0351	0.0193	1.82	0.04964	0.00167	0.18688	0.00599	0.02731	0.00024	204	69	209	7	210	2	0.48
SAL-58-34	0.217	0.28	0.78	0.04965	0.00211	0.19064	0.00778	0.02786	0.00029	224	64	218	7	217	2	0.46
SAL-58-35	0.0304	0.0238	1.28	0.11229	0.00122	4.70741	0.03207	0.30412	0.00181	215	117	217	12	217	3	0.00
SAL-58-36	0.0392	0.0235	1.67	0.05075	0.00148	0.24863	0.00683	0.03554	0.00029	215	208	218	21	218	4	0.00
SAL-58-37	0.0844	0.0407	2.07	0.15166	0.00232	9.26345	0.11838	0.44311	0.00361	227	96	220	8	219	2	0.46
SAL-58-38	0.0293	0.0197	1.49	0.0507	0.0015	0.24759	0.0069	0.03543	0.0003	228	35	221	4	220	2	0.45
SAL-58-39	0.177	0.28	0.63	0.11395	0.00131	5.26867	0.041	0.33545	0.00207	227	49	225	6	224	2	0.45
SAL-58-40	0.0307	0.0237	1.30	0.05092	0.00123	0.25385	0.00565	0.03617	0.00027	221	125	223	13	224	3	0.45
SAL-58-41	0.0785	0.0634	1.24	0.05034	0.00309	0.22112	0.01321	0.03187	0.00043	229	48	225	6	225	2	0.00
SAL-58-42	0.0344	0.0263	1.31	0.11198	0.00127	4.21158	0.03177	0.27285	0.00167	601	78	262	10	226	3	15.93
SAL-58-43	0.083	0.0522	1.59	0.05019	0.00197	0.22881	0.0086	0.03307	0.00032	237	37	230	5	229	2	0.44
SAL-58-44	0.0354	0.0254	1.39	0.11406	0.00144	5.27678	0.04903	0.33564	0.0022	241	119	232	13	231	3	0.43
SAL-58-45	0.036	0.0285	1.26	0.04932	0.00278	0.18125	0.00991	0.02666	0.00035	235	89	237	10	237	3	0.00
SAL-58-46	0.0707	0.042	1.68	0.11559	0.00136	5.41601	0.04427	0.33992	0.00213	245	171	238	19	237	4	0.42
SAL-58-47	0.0329	0.0223	1.48	0.04973	0.00239	0.20472	0.00948	0.02987	0.00034	239	44	239	5	239	2	0.00
SAL-58-48	0.0627	0.0304	2.06	0.1487	0.00164	8.92349	0.06389	0.43535	0.00267	260	63	251	8	250	2	0.40
SAL-58-49	0.0444	0.0258	1.72	0.05064	0.00188	0.2394	0.00852	0.0343	0.00033	256	37	254	5	253	2	0.40
SAL-58-50	0.0373	0.0294	1.27	0.04928	0.00148	0.16592	0.00468	0.02443	0.0002	251	57	259	7	260	2	0.38
SAL-58-51	0.0774	0.0607	1.28	0.11531	0.00269	5.39723	0.11625	0.33956	0.00355	274	62	271	8	270	2	0.37
SAL-58-52	0.0371	0.0247	1.50	0.11419	0.00146	5.29242	0.05072	0.33624	0.00223	2,425	25	673	11	274	3	145.62
SAL-58-53	0.0396	0.0272	1.46	0.11345	0.00146	5.22033	0.05048	0.33381	0.00222	325	37	323	6	323	2	0.00
SAL-58-54	0.0395	0.0181	2.18	0.04875	0.00327	0.1528	0.01003	0.02274	0.0003	1,319	12	541	5	376	2	43.88
SAL-58-55	0.0356	0.0219	1.63	0.04974	0.00139	0.20387	0.00533	0.02973	0.00024	1,785	6	1,476	6	1,271	7	40.44
SAL-58-56	0.0427	0.0211	2.02	0.05993	0.00281	0.29462	0.01335	0.03567	0.00041	2,355	27	1,844	11	1,426	9	65.15
SAL-58-57	0.0518	0.025	2.07	0.11207	0.00172	5.08021	0.06465	0.32885	0.00246	1,624	65	1,568	26	1,527	12	6.35
SAL-58-58	0.0407	0.0287	1.42	0.05032	0.00283	0.22307	0.01223	0.03216	0.00038	1,832	6	1,676	6	1,555	8	17.81
SAL-58-59	0.0379	0.0249	1.52	0.05387	0.00113	0.20007	0.00376	0.02694	0.00019	1,850	7	1,701	7	1,582	9	16.94
SAL-58-60	0.04	0.0292	1.37	0.11702	0.00149	5.00242	0.04739	0.31013	0.00205	1,852	6	1,738	6	1,645	9	12.58
SAL-58-61	0.0402	0.0252	1.60	0.08515	0.00121	0.70428	0.00788	0.06	0.00039	1,837	6	1,769	6	1,712	9	7.30
SAL-58-62	0.624	1.01	0.62	0.04928	0.0037	0.1779	0.01304	0.02619	0.00041	1,911	8	1,820	8	1,741	10	9.76
SAL-58-63	0.0583	0.0377	1.55	0.15738	0.0023	9.9239	0.11937	0.45745	0.00363	1,807	13	1,807	11	1807	12	0.00
SAL-58-64	0.0375	0.027	1.39	0.05123	0.00173	0.29037	0.00933	0.04112	0.00037	1,829	11	1,828	10	1,828	11	0.05
SAL-58-65	0.706	0.991	0.71	0.05133	0.00123	0.28378	0.00628	0.0401	0.0003	1,833	13	1,833	11	1,833	12	0.00
SAL-58-66	0.0342	0.0382	0.90	0.05033	0.00467	0.22562	0.02058	0.03252	0.00056	1,838	12	1,837	11	1,838	12	0.00
SAL-58-67	0.0433	0.0735	0.59	0.11466	0.00173	5.33067	0.06652	0.33727	0.00252	1,854	7	1,853	7	1,852	10	0.11
SAL-58-68	0.0355	0.0246	1.44	0.11677	0.0014	5.54927	0.04762	0.34475	0.00221	1,856	14	1,855	12	1,855	13	0.05
SAL-58-69	0.0356	0.026	1.37	0.14256	0.0017	8.24215	0.06951	0.41944	0.00274	1,855	9	1,856	8	1,857	11	0.11
SAL-58-70	0.0501	0.0254	1.97	0.051	0.00326	0.25663	0.01602	0.0365	0.00048	1,861	9	1,862	8	1,863	11	0.11
SAL-58-71	0.0675	0.0856	0.79	0.11346	0.00188	5.21444	0.07359	0.33342	0.00264	1,863	6	1,864	7	1,865	10	0.11
SAL-58-72	0.0415	0.0289	1.44	0.11544	0.00139	5.40842	0.04638	0.33987	0.00218	1,866	9	1,865	9	1,866	11	0.00
SAL-58-73	0.0396	0.0234	1.69	0.0529	0.00129	0.37419	0.00839	0.05132	0.00039	1,865	8	1,865	8	1,866	11	0.05
SAL-58-74	0.0695	0.0367	1.89	0.04982	0.00489	0.21045	0.02026	0.03065	0.00057	1,867	9	1,868	8	1,869	11	0.11
SAL-58-75	0.0372	0.0202	1.84	0.04572	0.00302	0.19124	0.01238	0.03034	0.00039	1,875	12	1,874	11	1,874	12	0.05

Table 1 *(continued)*

Sample and analyses spot number	Th (ppm)	U (ppm)	Th/U	Isopotic ratios $^{207}Pb/^{206}Pb$	1 s	$^{207}Pb/^{235}U$	1 s	$^{206}Pb/^{238}U$	1 s	Ages(Ma) $^{207}Pb/^{206}Pb$	1 s	$^{207}Pb/^{235}U$	1 s	$^{206}Pb/^{238}U$	1 s	Discordance (%)
SAL-58-76	0.291	0.67	0.43	0.04977	0.00227	0.19611	0.00863	0.02858	0.0003	1,874	7	1,874	7	1,874	10	0.00
SAL-58-77	0.0444	0.0437	1.02	0.15714	0.00406	0.93988	0.02176	0.04339	0.00046	1,885	24	1,884	18	1,885	17	0.00
SAL-58-78	0.302	0.539	0.56	0.05006	0.00171	0.20631	0.00672	0.0299	0.00026	1,889	7	1,887	7	1,886	10	0.16
SAL-58-79	0.0435	0.0387	1.12	0.05016	0.00161	0.21937	0.00665	0.03173	0.00028	1,887	7	1,886	7	1,886	10	0.05
SAL-58-80	0.321	0.582	0.55	0.11178	0.0016	5.05319	0.05803	0.32796	0.00234	1,889	9	1,888	9	1,887	11	0.11
SAL-58-81	0.0339	0.0296	1.15	0.11326	0.00127	4.53737	0.03363	0.29063	0.00178	1,885	11	1,886	10	1,888	12	0.16
SAL-58-82	0.0401	0.035	1.15	0.09997	0.00341	3.68469	0.12113	0.26731	0.0024	1,896	8	1,896	8	1,896	11	0.00
SAL-58-83	0.0547	0.0259	2.11	0.05143	0.00191	0.28036	0.00991	0.03955	0.00039	1,907	7	1,908	7	1,909	11	0.10
SAL-58-84	0.0417	0.0264	1.58	0.12597	0.00161	6.48147	0.06209	0.37326	0.00253	1,938	16	1,937	14	1,936	15	0.10
SAL-58-85	0.0438	0.028	1.56	0.13562	0.00212	7.49507	0.09875	0.40093	0.00323	1,952	6	1,969	7	1,985	11	1.66
SAL-58-86	0.293	0.297	0.99	0.05087	0.00252	0.26304	0.01263	0.03751	0.00044	2,042	8	2,043	8	2,045	12	0.15
SAL-58-87	0.0791	0.0639	1.24	0.05044	0.0032	0.23856	0.01477	0.03431	0.00047	2,050	12	2,051	11	2,052	14	0.10
SAL-58-88	0.0356	0.0267	1.33	0.0511	0.00475	0.2641	0.02407	0.0375	0.0007	2,117	7	2,117	8	2,118	12	0.05
SAL-58-89	0.0384	0.0223	1.72	0.11381	0.00147	5.25815	0.05167	0.33517	0.00226	2,172	12	2,172	12	2,173	15	0.05
SAL-58-90	0.0352	0.0225	1.56	0.05044	0.00557	0.23952	0.02604	0.03445	0.00068	2,259	7	2,258	8	2,258	12	0.04
SAL-58-91	1.57	1.89	0.83	0.04917	0.00185	0.17343	0.00626	0.02559	0.00024	2,317	5	2,316	6	2,316	12	0.04
SAL-58-92	0.0478	0.0297	1.61	0.04931	0.00179	0.18701	0.00648	0.02751	0.00025	2,331	5	2,330	7	2,330	12	0.04
SAL-58-93	0.0407	0.0244	1.67	0.05069	0.00205	0.24188	0.00957	0.03461	0.00029	2,365	11	2,364	12	2,365	16	0.00
SAL-58-94	0.0545	0.0452	1.21	0.05057	0.00343	0.24606	0.01633	0.0353	0.0005	2,428	10	2,428	11	2,428	16	0.00
SAL-58-95	0.1	0.217	0.46	0.11462	0.00137	5.3292	0.04513	0.33731	0.00216	2,458	6	2,459	7	2,460	13	0.08
SAL-58-96	0.353	0.784	0.45	0.11877	0.00216	5.73577	0.09183	0.35034	0.00306	2,839	7	2,833	9	2,825	16	0.50

and Neoproterozoic zircons (Figure 8b): 150–210 Ma (15%), 246–285 Ma (19%), 302–389 Ma (11%), 458–507 Ma (9%), and 599–1,151 Ma (11%). Two age peaks are defined by the Phanerozoic zircons, namely, 205 Ma and 247 Ma. The $\varepsilon_{Hf}(t)$ values of the Phanerozoic zircons (507–150 Ma) are similar to those in sample SAL-19, mostly ranging from −0.7 to 10.7 (Figure 9b), with T_{DM2} model ages from 1,211 to 508 Ma. One zircon with an age of 898 Ma recorded the most positive $\varepsilon_{Hf}(t)$ value of 11.2. The $\varepsilon_{Hf}(t)$ values of 2.4–1.9 Ga zircons range from −2 to 1.6, with T_{DM2} model ages from 2.8 to 2.2 Ga.

5.2. The Sergeevka Nappes

Approximately 100 zircons were obtained from sample SAL-41, and most were too small to analyze (15–40 μm in diameter). Suitable zircons ranged from 40 to 100 μm in diameter and show weak or no zoning (Figure 7), with Th/U ratios of 0.30–1.96. There were 26 concordant U-Pb ages from 49 analyses, with 11 Neoproterozoic zircons (761–1,010 Ma) accounting for 42% of the total, much higher than in other samples (Figure 8c). The late Pan-African and Paleozoic zircons are the second most important population (seven zircons with ages from 301 to 489 Ma), whereas only one Mesozoic zircon was obtained with an age of 178 Ma. Only six zircons were large enough to be analyzed for Lu-Hf isotopes. Two Pan-African zircons show positive $\varepsilon_{Hf}(t)$ values of 0.5 and 10.5 (Figure 9c); two other zircons with ages of ~1.0 Ga have $\varepsilon_{Hf}(t)$ values of −1.3 and 3.7, whereas those of two zircons ~1.8 Ga in age are −0.1 and 1.0 (Figure 9c).

5.3. The Zhuravlevka Turbidite Basin

Zircons from sample SAL-48 can be divided into two groups. One group is characterized by oscillatory zones and the grains are 80–200 μm in length, whereas the other group has weak oscillatory zoning, sector zoning, or no zoning at all and these grains have lengths from 80 to 150 μm (Figure 7). Seventy-nine concordant zircon U-Pb ages were recorded from 99 analyses. The Th/U ratios mostly range from 0.05 to 1.92, although two zircons have Th/U ratios of 0.04 and 0.05 possibly indicating a metamorphic origin. The age populations (Figure 8d) are 129–132 Ma (3%), 175–209 Ma (11%), 216–228 Ma (10%), 240–267 Ma (6%), 337–502 Ma (8%), 752–920 Ma (4%), 1.6–2.1 Ga (43%), and 2.2–2.7 Ga (14%). There are five age peaks in the spectrum: 131 Ma, 189 Ma, 222 Ma, 470 Ma, and 1.9 Ga. Two zircons with ages of 129 and 132 Ma are the youngest recorded in this study. The Hf isotopic features are distinct from the previous samples, with most Phanerozoic zircons (72%) having negative $\varepsilon_{Hf}(t)$ values (−23.5 to −1.3), with T_{DM2} model ages from 2.4 to 1.3 Ga, whereas only six zircons (21%) record positive values (1.6 to 9.4), with T_{DM2} model ages from 636 to 1,029 Ma.

5.4. The Taukha Accretionary Complex

5.4.1. Sample SAL-49

Zircons from sample SAL-49 are 50 to 150 μm in length. Of 98 analyses, 88 were concordant. The Phanerozoic zircons show weak oscillatory zones with small inclusions of opaque material, whereas the Precambrian ones are weakly zoned, sector zoned, or no zoning at all (Figure 7). The Th/U ratios range from 0.22 to 1.55. About 70%

10.1002/2017TC004599

Table 2
Zircon Lu-Hf Isotope Data

No.	Age (Ma)	$^{176}Yb/^{177}Hf$	1σ	$^{176}Lu/^{177}Hf$	1σ	$^{176}Hf/^{177}Hf$	1σ	$\varepsilon_{Hf}(0)$	$\varepsilon_{Hf}(t)$	T_{DM1} (Ma)	T_{DM2} (Ma)	$f_{Lu/Hf}$
SAL-19-03	171	0.025707901	0.001425887	0.001085825	0.000056	0.282032055	0.000022	−26.17	−23.22	1,720.35	2,327.26	−0.967294419
SAL-19-01	169	0.024566698	0.000241839	0.000976706	0.000009	0.282830283	0.000019	2.06	4.99	597.37	766.92	−0.970581144
SAL-19-02	225	0.025435127	0.00089637	0.001000538	0.000029	0.282468713	0.000026	−10.73	−6.59	1,107.40	1,455.85	−0.969863301
SAL-19-04	198	0.052113375	0.000221389	0.002056077	0.000008	0.282966225	0.000030	6.87	10.29	416.59	494.33	−0.938069971
SAL-19-05	202	0.045262733	0.001480546	0.001616357	0.000054	0.282887985	0.000027	4.10	7.66	524.57	644.56	−0.951314555
SAL-19-06	872	0.024741271	0.000170839	0.000955992	0.000006	0.282315507	0.000017	−16.14	2.18	1,320.34	1,498.13	−0.971205055
SAL-19-07	188	0.04531721	0.00030005	0.001712583	0.000012	0.282751974	0.000024	−0.71	2.54	722.20	919.01	−0.948416164
SAL-19-08	263	0.049385998	0.002209208	0.001874439	0.000080	0.282771285	0.000030	−0.03	4.79	697.44	854.88	−0.94354098
SAL-19-09	301	0.018480175	0.000242015	0.000740155	0.000008	0.282749763	0.000027	−0.79	5.06	706.78	870.95	−0.977706187
SAL-19-10	226	0.03224073	0.000807907	0.00117848	0.000028	0.282820496	0.000021	1.72	5.85	614.52	765.37	−0.964503606
SAL-19-11	192	0.071462879	0.000228465	0.002633954	0.000005	0.282957966	0.000026	6.58	9.80	435.56	516.95	−0.920664042
SAL-19-12	730	0.045723872	0.000375494	0.001744173	0.000011	0.282612878	0.000028	−5.63	9.20	922.97	993.84	−0.947464664
SAL-19-13	235	0.014772504	0.000274876	0.000721967	0.000011	0.282625702	0.000025	−5.17	−0.77	880.21	1,141.68	−0.978254011
SAL-19-14	842	0.055368045	0.001989927	0.002004136	0.000071	0.282285194	0.000043	−17.22	−0.14	1,401.36	1,601.37	−0.939634466
SAL-19-15	265	0.026764298	0.000597948	0.001132777	0.000024	0.282798659	0.000023	0.94	5.93	644.79	792.90	−0.965880223
SAL-19-16	282	0.027777704	0.000587971	0.001069808	0.000021	0.282615242	0.000050	−5.54	−0.18	903.10	1,146.77	−0.967776877
SAL-19-18	162	0.024446008	0.000521247	0.001044796	0.000021	0.282129512	0.000026	−22.72	−19.96	1,582.99	2,141.79	−0.968530238
SAL-19-19	187	0.075917503	0.001910681	0.002504289	0.000057	0.282838034	0.000041	2.34	5.47	611.21	755.01	−0.924569615
SAL-19-20	265	0.028647505	0.000490775	0.001204115	0.000016	0.282862198	0.000027	3.19	8.17	555.54	668.08	−0.963731482
SAL-19-22	830	0.019711315	0.000273466	0.000856849	0.000012	0.282404403	0.000030	−13.00	4.46	1,193.01	1,338.30	−0.974191287
SAL-19-25	251	0.026028253	0.000629231	0.00110501	0.000025	0.282806948	0.000025	1.24	5.93	632.55	781.74	−0.966716579
SAL-19-26	1198	0.031102512	0.00078815	0.001081896	0.000028	0.28206689	0.000031	−24.94	0.49	1,671.73	1,857.37	−0.967412774
SAL-19-27	252	0.023435113	0.000198713	0.000959872	0.000008	0.282892461	0.000025	4.26	9.00	509.07	610.97	−0.97108818
SAL-19-28	169	0.027653129	0.000456739	0.001142888	0.000018	0.282854219	0.000021	2.91	5.82	565.98	720.65	−0.965575667
SAL-19-29	209	0.042636415	0.001106275	0.001688185	0.000045	0.282761643	0.000031	−0.37	3.33	707.81	892.03	−0.949151064
SAL-19-30	433	0.02577988	0.000366223	0.000906977	0.000012	0.282543555	0.000024	−8.08	0.62	999.82	1,225.63	−0.972681419
SAL-19-31	277	0.027859627	0.000584484	0.001064727	0.000022	0.282508699	0.000022	9.31	−4.05	1,053.06	1,357.67	−0.967929923
SAL-19-32	180	0.018876437	0.000300569	0.00080194	0.000012	0.282106679	0.000025	−23.53	−20.35	1,604.49	2,177.53	−0.975845183
SAL-19-33	264	0.031391894	0.000494104	0.001207454	0.000019	0.282795272	0.000031	0.82	5.78	650.89	800.70	−0.963630911
SAL-40-01	898	0.053369596	0.00067386	0.001764249	0.000017	0.282555697	0.000036	−7.65	10.78	1,005.58	1,045.01	−0.946859973
SAL-40-02	343	0.017975067	0.000403328	0.000680992	0.000014	0.282121298	0.000029	−23.01	−16.24	1,579.27	2,082.15	−0.979488186
SAL-40-03	710	0.013750789	0.000201489	0.000482137	0.000008	0.282007861	0.000025	−27.02	−12.06	1,726.49	2,147.49	−0.985477815
SAL-40-04	1914	0.009845096	0.000729279	0.000354406	0.000026	0.281620444	0.000026	−40.72	1.57	2,246.37	2,385.61	−0.989325111
SAL-40-10	150	0.115854515	0.00076981	0.003836763	0.000024	0.282933045	0.000042	5.70	7.93	488.94	587.04	−0.884434851
SAL-40-05	2399	0.006651692	0.000195156	0.000259124	0.000006	0.28129982	0.000026	−52.06	1.54	2,670.95	2,785.84	−0.992195047
SAL-40-06	258	0.040521817	0.00152316	0.001544465	0.000061	0.282636634	0.000029	−4.79	−0.02	884.06	1,118.63	−0.953479977
SAL-40-07	498	0.01709931	0.000499595	0.00065141	0.000016	0.28269694	0.000039	−2.65	7.56	779.05	893.68	−0.980379216
SAL-40-08	1983	0.049993386	0.000555206	0.001944797	0.000023	0.281534749	0.000034	−43.75	−2.02	2,462.64	2,635.21	−0.941421774
SAL-40-09	277	0.023626011	0.00024005	0.000819706	0.000008	0.282582201	0.000028	−6.71	−1.41	943.43	1,211.08	−0.975310047
SAL-40-11	210	0.031117228	0.000258806	0.001317125	0.000008	0.282891962	0.000031	4.24	8.02	514.66	631.39	−0.960327556
SAL-40-12	207	0.022630483	0.00078682	0.000923208	0.000031	0.282244829	0.000030	−18.64	−14.89	1,417.66	1,899.23	−0.972192524
SAL-40-13	199	0.032671418	0.000487166	0.001309721	0.000017	0.28295634	0.000027	6.52	10.06	422.40	508.05	−0.960550577
SAL-40-14	201	0.072317763	0.002047223	0.002678847	0.000080	0.282800059	0.000023	0.99	4.39	670.45	826.53	−0.919311825
SAL-40-15	285	0.027999292	0.000226455	0.001097094	0.000007	0.282855331	0.000026	2.95	8.38	563.71	672.78	−0.96695501
SAL-40-16	458	0.031734478	0.000792676	0.001334348	0.000032	0.28264351	0.000031	−4.54	4.58	869.32	1,026.64	−0.959808781
SAL-40-17	159	0.015632023	0.000662827	0.000639535	0.000024	0.282400144	0.000029	−13.15	−10.41	1,192.12	1,613.97	−0.980736898
SAL-40-18	462	0.045466604	0.001655161	0.001616106	0.000059	0.282538825	0.000035	−8.25	0.87	1,025.68	1,235.36	−0.951322117
SAL-40-19	252	0.007689745	9.32793E−05	0.000284549	0.000003	0.282722357	0.000022	−1.76	3.09	736.39	940.56	−0.991429245
SAL-40-20	1151	0.018729603	0.000665582	0.00063829	0.000020	0.282055991	0.000010	−25.32	−0.31	1,667.38	1,878.25	−0.980774394

Table 2 *(continued)*

No.	Age (Ma)	^{176}Yb/^{177}Hf	1σ	^{176}Lu/^{177}Hf	1σ	^{176}Hf/^{177}Hf	1σ	$\varepsilon_{Hf}(0)$	$\varepsilon_{Hf}(t)$	T_{DM1} (Ma)	T_{DM2} (Ma)	$f_{Lu/Hf}$
SAL-40-21	254	0.026902937	0.000382904	0.001012355	0.000012	0.282628625	0.000011	−5.07	0.34	882.87	1,130.93	−0.96950738
SAL-40-23	599	0.010990161	3.58313E−05	0.000405134	0.000001	0.282336583	0.000012	−15.40	−2.36	1,272.42	1,553.26	−0.987797166
SAL-40-24	507	0.019802065	0.000424752	0.000643163	0.000015	0.282450239	0.000014	−11.38	−0.43	1,122.69	1,374.01	−0.980627607
SAL-40-25	259	0.015592144	7.99611E−05	0.00050607	0.000003	0.282494854	0.000014	−9.80	−4.20	1,056.88	1,386.63	−0.984756939
SAL-40-26	204	0.096796479	0.001126081	0.003082008	0.000039	0.282779959	0.000015	0.28	4.35	708.14	868.21	−0.907168427
SAL-40-27	1871	0.000369727	2.17456E−06	1.07864E−05	0.000000	0.281553222	0.000011	−43.10	−1.38	2,316.57	2,508.93	−0.999675108
SAL-40-28	246	0.019733766	0.000165174	0.000736828	0.000005	0.282700583	0.000014	−2.53	2.76	775.70	990.07	−0.977806373
SAL-40-29	264	0.03004936	0.000925276	0.001060766	0.000036	0.282566795	0.000012	−7.26	−1.64	971.18	1,248.85	−0.96804921
SAL-41-06	1010	0.033917498	0.000679902	0.001141079	0.000020	0.282266094	0.000013	−17.89	3.70	1,396.07	1,546.51	−0.965630162
SAL-41-10	1845	0.024053407	0.000155479	0.000831521	0.000005	0.28163511	0.000012	−40.21	−0.09	2,254.26	2,418.45	−0.97495418
SAL-41-13	998	0.016477102	0.000622266	0.00055825	0.000020	0.282121929	0.000013	−22.99	−1.28	1,573.35	1,810.02	−0.983185244
SAL-41-15	1862	0.026117731	0.00047785	0.000871828	0.000015	0.281657113	0.000011	−39.43	1.02	2,226.51	2,372.20	−0.973740108
SAL-41-17	489	0.030676709	0.001654753	0.001081953	0.000048	0.282491747	0.000016	−9.91	0.51	1,077.40	1,307.97	−0.967411047
SAL-41-18	482	0.016114393	0.00027377	0.000658193	0.000011	0.282775131	0.000013	0.11	10.52	669.71	746.23	−0.980174916
SAL-48-1	222	0.023449111	1.61557E−05	0.000599851	0.000000	0.282315361	0.000018	−16.15	−11.37	1,308.25	1,753.39	−0.981932192
SAL-48-2	2358	0.045245166	0.000197363	0.001170828	0.000009	0.281302952	0.000019	−51.95	−0.98	2,730.44	2,875.15	−0.964734087
SAL-48-3	2252	0.03837172	0.000435231	0.001038245	0.000012	0.281414458	0.000021	−48.01	0.84	2,568.84	2,693.51	−0.968727554
SAL-48-4	422	0.034035845	0.000322428	0.000919619	0.000004	0.282415416	0.000016	−12.61	−3.58	1,179.59	1,481.04	−0.972300647
SAL-48-5	131	0.022403961	0.000136557	0.000728049	0.000004	0.282899362	0.000019	4.50	7.32	496.23	644.16	−0.978070806
SAL-48-6	920	0.006797004	1.56976E−05	0.000181224	0.000001	0.281965838	0.000016	−28.51	−8.30	1,770.12	2,131.73	−0.994541454
SAL-48-7	228	0.028628955	8.65815E−05	0.000900892	0.000006	0.282363824	0.000018	−14.43	−9.57	1,251.05	1,658.83	−0.972864707
SAL-48-8	474	0.022758491	4.57594E−05	0.000567374	0.000001	0.282378597	0.000015	−13.91	−3.66	1,219.70	1,526.19	−0.982910407
SAL-48-9	222	0.05806383	0.000224504	0.001398744	0.000003	0.282328723	0.000022	−15.68	−11.01	1,317.28	1,733.58	−0.957869142
SAL-48-11	226	0.035980655	0.000352672	0.000883868	0.000007	0.282363775	0.000023	−14.44	−9.61	1,250.55	1,659.59	−0.97337747
SAL-48-12	190	0.04548052	0.000206281	0.001182842	0.000002	0.281993839	0.000018	−27.52	−23.51	1,777.99	2,394.31	−0.964372215
SAL-48-13	242	0.03268175	3.12201E−05	0.000846882	0.000001	0.282233302	0.000018	−19.05	−13.88	1,430.83	1,907.08	−0.974491494
SAL-48-14	176	0.030980647	0.001089182	0.000851982	0.000026	0.282581171	0.000018	−6.75	−2.98	945.68	1,253.87	−0.974337904
SAL-48-15	217	0.056150995	0.000156964	0.001374976	0.000004	0.282383197	0.000020	−13.75	−9.19	1,239.50	1,629.04	−0.958585047
SAL-48-16	227	0.059076719	0.00057468	0.001444965	0.000010	0.282073672	0.000020	−24.70	−19.94	1,678.37	2,227.52	−0.956476968
SAL-48-17	129	0.031433812	0.000248479	0.000927541	0.000007	0.282573599	0.000016	−7.02	−4.27	958.20	1,287.90	−0.972062033
SAL-48-20	209	0.065952285	0.000162739	0.001623031	0.000002	0.282734613	0.000024	−1.32	3.05	745.40	944.80	−0.951113518
SAL-48-21	220	0.041097093	4.8242E−05	0.001019221	0.000003	0.282034088	0.000017	−26.10	−21.42	1,714.51	2,303.64	−0.969300575
SAL-48-22	268	0.062651525	0.000236601	0.001848679	0.000005	0.282880853	0.000014	3.85	9.42	538.23	636.42	−0.944316911
SAL-48-23	426	0.029402053	0.000189061	0.00087452	0.000002	0.282478923	0.000017	−10.36	−1.24	1,089.44	1,354.53	−0.973659034
SAL-48-24	202	0.043229542	0.000242317	0.001088839	0.000002	0.282336966	0.000017	−15.38	−11.10	1,294.92	1,722.92	−0.967203646
SAL-48-25	192	0.03183049	9.49252E−05	0.000870503	0.000001	0.282829227	0.000016	2.02	6.13	597.18	759.15	−0.973780022
SAL-48-26	176	0.024816139	0.000229575	0.000840483	0.000006	0.282306656	0.000016	−16.46	−12.69	1,328.64	1,790.67	−0.974684241
SAL-48-27	249	0.03032706	3.1335E−05	0.000818901	0.000003	0.282677479	0.000016	−3.34	1.99	809.82	1,035.08	−0.975334304
SAL-48-28	208	0.032436099	0.00017303	0.000927922	0.000007	0.282349766	0.000019	−14.93	−10.50	1,271.56	1,694.43	−0.972050549
SAL-48-29	752	0.032321319	0.000230564	0.000866759	0.000003	0.281957201	0.000022	−28.81	−12.67	1,813.83	2,238.42	−0.973892798
SAL-48-30	260	0.024822144	0.000135785	0.000841479	0.000007	0.282543807	0.000015	−8.07	−2.50	997.74	1,293.44	−0.974654251
SAL-48-31	438	0.02709622	0.00016813	0.00078851	0.000007	0.282549942	0.000017	−7.85	1.56	987.78	1,209.21	−0.976249704
SAL-48-32	216	0.025680255	0.000130956	0.000778793	0.000002	0.282398978	0.000020	−13.19	−8.56	1198.11	1,594.04	−0.976542379
SAL-49-1	327	0.018679477	0.000142439	0.000579491	0.000002	0.28208681	0.000016	−24.23	−17.18	1,622.50	2,154.37	−0.982545444
SAL-49-2	186	0.033735287	0.000174378	0.001029551	0.000003	0.2825533	0.000020	−7.73	−3.78	989.36	1,305.74	−0.968989432
SAL-49-4	1867	0.023194898	0.00062174	0.000657029	0.000016	0.281536533	0.000022	−43.69	−2.88	2,378.04	2,586.37	−0.980209961
SAL-49-5	246	0.027456953	0.000512236	0.000750194	0.000008	0.282503344	0.000021	−9.50	−4.22	1,051.82	1,377.54	−0.977403804
SAL-49-6	2636	0.019189776	0.00018134	0.000516424	0.000003	0.280839625	0.000021	−68.34	−10.09	3,303.89	3,579.66	−0.984445064
SAL-49-7	184	0.031216093	0.000383459	0.000981427	0.000013	0.282630333	0.000017	−5.01	−1.09	879.74	1,154.98	−0.970438932
SAL-49-8	1617	0.021222355	4.32051E−05	0.000576733	0.000003	0.281601542	0.000022	−41.39	−6.05	2,284.96	2,559.26	−0.982628514
SAL-49-9	1922	0.039998705	0.000304819	0.0010323	0.000011	0.281472248	0.000018	−45.96	−4.42	2,489.42	2,712.83	−0.968906636

Table 2 *(continued)*

No.	Age (Ma)	$^{176}Yb/^{177}Hf$	1σ	$^{176}Lu/^{177}Hf$	1σ	$^{176}Hf/^{177}Hf$	1σ	$\varepsilon_{Hf}(0)$	$\varepsilon_{Hf}(t)$	T_{DM1} (Ma)	T_{DM2} (Ma)	$f_{Lu/Hf}$
SAL-49-10	2204	0.063841523	0.00047208	0.001946853	0.000012	0.281400642	0.000022	−48.50	−2.08	2,650.64	2,811.30	−0.941359846
SAL-49-11	277	0.063906159	0.000500165	0.001617153	0.000017	0.282286139	0.000026	−17.18	−11.40	1,385.47	1,797.78	−0.951290583
SAL-49-12	1912	0.024483785	0.000205464	0.000627129	0.000003	0.281413068	0.000018	−48.06	−6.22	2543.41	2,801.52	−0.98111057
SAL-49-13	230	0.039291591	0.00052936	0.001155211	0.000018	0.282741476	0.000019	−1.08	3.80	726.36	919.52	−0.965204479
SAL-49-14	251	0.007756638	0.000106931	0.000298865	0.000008	0.282559776	0.000025	−7.51	−2.04	961.62	1,260.78	−0.990998037
SAL-49-15	262	0.025112519	0.000128327	0.000656756	0.000001	0.282611483	0.000020	−5.68	−0.03	898.55	1,158.05	−0.980218186
SAL-49-16	251	0.021783796	0.000181037	0.000647633	0.000007	0.282842577	0.000021	2.50	7.91	574.94	707.11	−0.98049299
SAL-49-17	189	0.084738809	0.000178734	0.002263551	0.000004	0.282289857	0.000030	−17.05	−13.19	1,404.56	1,827.48	−0.931820748
SAL-49-18	220	0.05123526	0.000450893	0.001425813	0.000008	0.282616908	0.000024	−5.48	−0.86	909.35	1,170.67	−0.95705384
SAL-49-19	196	0.088228471	0.000504067	0.002689564	0.000016	0.282825033	0.000026	1.88	5.83	633.64	778.98	−0.918989044
SAL-49-20	213	0.027883445	5.76113E−05	0.000751448	0.000003	0.28272299	0.000024	−1.73	2.84	744.57	959.40	−0.977366038
SAL-49-21	210	0.038606663	5.73356E−05	0.001006536	0.000002	0.28276087	0.000022	−0.39	4.08	696.08	887.92	−0.969682657
SAL-49-22	247	0.01762994	8.73719E−05	0.000485649	0.000001	0.282473488	0.000017	−10.56	−5.21	1,085.90	1,433.24	−0.98537203
SAL-49-23	414	0.020014871	4.11642E−05	0.000592818	0.000001	0.282199963	0.000015	−20.23	−11.29	1,467.32	1,899.23	−0.98214405
SAL-49-24	223	0.03021058	0.000528125	0.000882594	0.000017	0.282841032	0.000020	2.44	7.21	580.70	723.53	−0.973415832
SAL-58-1	195	0.024625686	4.34599E−05	0.000681749	0.000003	0.282182216	0.000022	−20.86	−16.67	1,495.24	2,024.11	−0.979465378
SAL-58-2	176	0.023367167	3.78543E−05	0.000651944	0.000002	0.282188526	0.000020	−20.63	−16.85	1,485.37	2,019.40	−0.980363144
SAL-58-3	1839	0.015955367	7.61353E−05	0.000493936	0.000003	0.280963327	0.000023	−63.96	−23.66	3,137.40	3,674.59	−0.985122421
SAL-58-4	190	0.039608791	8.97747E−05	0.001090362	0.000004	0.281965998	0.000020	−28.50	−24.48	1,812.31	2,447.53	−0.96715778
SAL-58-5	238	0.017999661	8.24803E−05	0.000519407	0.000001	0.282534179	0.000019	−8.41	−3.27	1,002.70	1,318.36	−0.984355207
SAL-58-6	190	0.033369074	0.000118152	0.001054256	0.000002	0.282596324	0.000023	−6.21	−2.17	929.40	1,219.91	−0.968245313
SAL-58-7	166	0.044866576	0.000311693	0.001190842	0.000005	0.282009218	0.000019	−26.98	−23.47	1,756.95	2,373.94	−0.964131264
SAL-58-8	175	0.017044733	5.40888E−05	0.000528871	0.000000	0.282258683	0.000017	−18.15	−14.38	1,384.00	1,882.63	−0.984070149
SAL-58-9	180	0.035167161	0.000260204	0.001000726	0.000006	0.282141947	0.000019	−22.28	−18.46	1,563.86	2,110.32	−0.969857651
SAL-58-10	183	0.02017681	0.000120955	0.000514239	0.000001	0.282019523	0.000020	−26.61	−22.66	1,711.96	2,343.39	−0.984510861
SAL-58-11	204	0.035447526	3.80943E−05	0.00099026	0.000001	0.282857996	0.000023	3.04	7.39	558.34	698.40	−0.970172884
SAL-58-12	2317	0.033954025	0.000155616	0.000962978	0.000010	0.28131391	0.000021	−51.56	−1.17	2,700.75	2,852.83	−0.970994653
SAL-58-13	220	0.073261906	0.000645652	0.001812569	0.000009	0.282513314	0.000024	−9.15	−4.58	1,067.75	1,376.92	−0.945404556
SAL-58-14	1854	0.033593901	0.000522689	0.000816434	0.000011	0.281512877	0.000019	−44.53	−4.21	2,420.14	2,647.57	−0.975408602
SAL-58-15	164	0.028404029	3.63311E−05	0.000798447	0.000001	0.282061786	0.000019	−25.12	−21.61	1,666.37	2,270.93	−0.975950391
SAL-58-16	179	0.021441617	0.000215186	0.000651206	0.000008	0.282254413	0.000019	−18.30	−14.46	1,394.33	1,890.05	−0.980385375
SAL-58-17	185	0.028998169	0.000403648	0.000915381	0.000010	0.282339757	0.000019	−15.29	−11.34	1,285.11	1,723.02	−0.972428287
SAL-58-18	192	0.033540376	0.000271757	0.001086826	0.000006	0.282394422	0.000018	−13.35	−9.28	1,214.29	1,614.70	−0.967264275
SAL-58-19	270	0.018405609	0.000643667	0.000502069	0.000016	0.282365825	0.000022	−14.36	−8.53	1,235.27	1,634.34	−0.984877437
SAL-58-20	173	0.011520345	3.9087E−05	0.0003539	0.000000	0.282635267	0.000019	−4.84	−1.08	858.51	1145.70	−0.989340369
SAL-58-21	178	0.022341513	5.66464E−05	0.000662303	0.000001	0.282042344	0.000016	−25.80	−21.98	1,687.20	2,302.15	−0.980051129
SAL-58-22	225	0.032149737	6.11985E−05	0.000961859	0.000004	0.282539292	0.000018	−8.23	−3.43	1,007.26	1,317.30	−0.97102834
SAL-58-23	224	0.030748062	0.000290812	0.000897579	0.000004	0.282326063	0.000019	−15.77	−10.99	1,303.60	1,734.05	−0.972964502
SAL-58-24	229	0.045679514	0.000278453	0.001267483	0.000005	0.282490915	0.000019	−9.94	−5.10	1,083.90	1,413.01	−0.961822789
SAL-58-25	202	0.04779911	0.000509935	0.00138193	0.000014	0.282439876	0.000019	−11.75	−7.50	1,159.54	1,524.08	−0.958375587
SAL-58-26	209	0.062325704	0.000146746	0.00169631	0.000012	0.28281271	0.000024	1.44	5.80	634.37	791.34	−0.948906326
SAL-58-27	169	0.020883565	1.0272E−05	0.000662717	0.000001	0.28213085	0.000021	−22.67	−19.04	1,565.35	2,134.30	−0.980038656
SAL-58-28	189	0.034315738	0.000152748	0.001179198	0.000003	0.282642976	0.000020	−4.56	−0.56	866.48	1,129.51	−0.96448198
SAL-58-29	155	0.041241726	0.000540329	0.001163737	0.000009	0.282304475	0.000022	−16.53	−13.25	1,343.09	1,805.05	−0.964947687
SAL-58-30	144	0.026141267	0.000262916	0.000857102	0.000004	0.282269935	0.000021	−17.76	−14.68	1,380.30	1,875.11	−0.974183678
SAL-58-31	188	0.036824382	0.000252912	0.001214388	0.000010	0.282821489	0.000020	1.75	5.73	613.69	778.41	−0.963422049
SAL-58-32	204	0.060211223	0.000448054	0.001682185	0.000010	0.282620315	0.000019	−5.36	−1.11	910.76	1,171.94	−0.949331774
SAL-58-33	259	0.007744696	0.000119661	0.000217076	0.000003	0.282352438	0.000015	−14.84	−9.19	1,244.50	1,662.38	−0.993461569
SAL-58-34	253	0.047441892	0.000143853	0.00150246	0.000006	0.282752691	0.000020	−0.68	4.63	717.09	891.70	−0.954745188
SAL-58-35	166	0.007063732	1.39387E−05	0.000192744	0.000000	0.281982479	0.000018	−27.92	−24.31	1,748.07	2,420.34	−0.994194443

of the zircons are in the range 1.5–2.6 Ga with a peak age at 1.9 Ga (Figure 8e). The other 30% range in age from 414 Ma to 176 Ma, with three age ranges, 176–226 Ma (17%), 239–262 Ma (10%), and 309–414 Ma (3%). Five zircons with ages ranging from 1.5 to 2.6 Ga were selected for Lu-Hf isotope analysis, recording $\varepsilon_{Hf}(t)$ values of −10.1 to −2.1 (Figure 9e). Seventeen Phanerozoic zircons were also analyzed for Lu-Hf isotopes, and their $\varepsilon_{Hf}(t)$ values vary from −17.2 to 7.9. However, ~70% record negative values from −17.2 to −1, with T_{DM2} model ages from 2.1 to 1.1 Ga.

5.4.2. Sample SAL-58

Zircons from sample SAL-58 range from 50 to 200 μm in length/diameter. Most show magmatic oscillatory zones in CL, with some showing sector zones (Figure 7). Eighty-eight concordant ages were obtained from a total of 96 analyses. The Th/U ratios are >0.5, which are the highest of the six samples. The age spectrum is similar to sample SAL-49; however, the proportion of 1.5–2.6 Ga zircons (41%) is smaller (Figure 8f). Phanerozoic zircons account for 59%, with three age ranges: 145–210 Ma (35%), 217–239 Ma (15%), and 250–270 Ma (5%). Two Precambrian zircons and 32 Phanerozoic zircons were analyzed for Lu-Hf isotopes. The $\varepsilon_{Hf}(t)$ of the Phanerozoic zircons is mainly negative (80%), ranging from −24.5 to −0.5, with T_{DM2} model ages from 2.5 to 1.1 Ga, whereas the $\varepsilon_{Hf}(t)$ of the two Precambrian zircons (~1.8 Ga and 2.3 Ga) are −4.2 and −1.2, respectively, with T_{DM2} model ages of 2.6 Ga and 2.8 Ga, respectively (Figure 9f).

6. Discussion

6.1. Depositional Ages of Sandstones in the Southern Sikhote-Alin Orogenic Belt

Detrital zircon data can help determine the maximum depositional age of the analyzed sandstone sample (Dickinson & Gehrels, 2009; Gehrels, 2014). Generally, in the active continental margin, the youngest zircon age is close to the depositional age because the supply of volcanic materials from arc magmatism. However, only one youngest zircon age is not enough to constrain the depositional age. In this study, the youngest peak age in the spectrum (Gehrels, 2014) and previous paleontological research are applied together to solve this issue.

In the Samarka belt, the youngest zircon ages recorded from samples SAL-19 and SAL-40 are 162 Ma and 150 Ma, respectively, implying that they were deposited after the Middle Jurassic. According to Russian paleontological research, sandstone near sample SAL-19 is underlain by the Olenekian-Bathonian chert and the Oxfordian-Tithonian mudstone and siltstone (Kemkin, 2008; Khanchuk, 2001), which means the sandstone was deposited after the Late Jurassic.

In the Sergeevka nappes, a shallow-marine and clastic rock assemblage ranges in age ranging from Devonian to Jurassic (Khanchuk, 2006; Khanchuk et al., 2016). The youngest zircon U-Pb age recorded in this study is 178 Ma in sample SAL-41. However, no fossil data in the outcrop of sample SAL-41 are available to further constrain this, so it is proposed that deposition may occur in or after the Middle Jurassic.

The Zhuravlevka basin is composed mainly of turbidites with depositional ages ranging from the Berriasian to Albian (Malinovsky & Golozubov, 2011). But the youngest zircon in sample SAL-48 has an age of 129 Ma and the youngest peak is ~131 Ma, constraining the depositional age in the late Early Cretaceous. This maximum depositional age is verified by the faunal research in the sandstone and siltstone from the same outcrop, showing an Aptian to Albian age (Golozoubov, 2006).

In the Taukha accretionary complex, the age of turbidite is Berriasian to Valanginian (i.e., Early Cretaceous: 145–133 Ma) according to detailed faunal research (Golozoubov et al., 1992; Kemkin & Kemkina, 2000). The new zircon ages support this result, with the youngest zircon U-Pb age constraining the maximum depositional age of the sandstone at 145 Ma.

6.2. Possible Provenance of the Detrital Zircons

In the Late Jurassic to Early Cretaceous of NE Asia, four geological units had the potential to feed the southern Sikhote-Alin orogenic belt (Figure 1): the Siberia Craton (SC), the eastern CAOB, especially the Bureya-Jiamusi-Khanka Block (BJKB), the North China Craton (NCC), and the South China Craton (SCC).

Although the northern Korean Peninsula is a contiguous part of the eastern NCC (Zhao et al., 2005), the southern Korean Peninsula has tectonic affinities with the SCC because of the similarities in rock assemblages and metamorphic history from the Neoproterozoic to Mesozoic. With respect to the provenance of the Sikhote-Alin area, we will discuss the whole of the Korean Peninsula along with the eastern NCC because they have been a united source area following collision along the Imjingang Belt in the Middle Triassic (Figure 1; Cheong et al., 2013; Kim et al., 2008).

6.2.1. Possible Provenance of the Precambrian Detrital Zircons

The Precambrian zircons in the southern Sikhote-Alin show two major peaks at 2.5 and 1.8 Ga, with a much smaller population at around 0.8 Ga (Figures 8b–8f).

Late Archean and Paleoproterozoic ages (2.5 and 1.8 Ga) are most widespread in the eastern NCC. The oldest units in the eastern NCC are early Archean in age, including ~3.8 Ga, 3.7–3.6 Ga, and 3.3–3.1 Ga rocks (Wu et al., 2008). However, the predominant rocks are 2.7–2.5 Ga in age, including high-grade tonalitic-trondhjemitic-granodioritic (TTG) gneisses and granitoids (Zhao & Zhai, 2013). Paleoproterozoic rocks (1.95–1.85 Ga) mainly crop out in three linear tectonic belts in the western, central, and eastern NCC. One view is that these belts represent continent-continent collisional belts (Wilde et al., 2002; Zhai & Santosh, 2011; Zhao et al., 2012, 2005, 2001; Zhao & Zhai, 2013), whereas other researchers propose that they were generated as continental rifts within a single continent (Li et al., 2005, 2004, 2006; Zhang & Yang, 1988). Minor mafic dykes were emplaced in the NCC from ~1.8 to 0.9 Ga (Peng et al., 2008, 2011). Precambrian granitoids and metamorphic rocks are also found in the Korean Peninsula. In North Korea, the TTG gneisses and granitic rocks have ages ranging from 1.93 to 1.85 Ga (Zhai et al., 2007; Zhao et al., 2006). In the Ryeongnam massif of South Korea, granite gneisses with ages of 1.9–2.1 Ga are likewise reported (Turek & Kim, 1996). The detrital zircons from the river mouths in North Korea are also dominated by Paleoproterozoic populations (~2.2–2.1 Ga and 1.9–1.8 Ga) with minor Archean zircons (~2.5 Ga; Wu, Yang, Lo, et al., 2007).

In the Hida metamorphic complex of Japan, zircons with ages of 1.8 Ga and 1.1 Ga were obtained from meta-sedimentary gneiss and a few Permian to Triassic granites, and the 1.1 Ga peak is less important (Horie et al., 2010; Sano et al., 2000). Thus, there is a possibility that the Hida metamorphic complex contributed Precambrian zircon to the Sikhote-Alin orogenic belt. However, the 2.5–2.0 Ga zircons are absent in both gneiss and granite, indicating that the Hida metamorphic complex cannot be the main source area.

Paleoproterozoic A- and S-type granites formed at 1.9–1.8 Ga are also found in South China (Chen et al., 2015; Qiu et al., 2000; Zheng et al., 2004, 2006). However, the most widespread magmatic and metamorphic rocks in the SCC are from 1.0 to 0.75 Ga, for example, the igneous rocks of 1,000–850 Ma related to the collision between the Yangtze and Cathaysia blocks, and the bimodal magmatism at 850–750 Ma due to rifting of the Rodinia supercontinent (Charvet, 2013; Charvet et al., 2010; Li et al., 1999; Z. X. Li et al., 2002; X. H. Li et al., 2002; Li & Li, 2007). The 1.0–0.75 Ga zircons are always well represented in sandstones from the SCC (Jia et al., 2010; Yang et al., 2012). However, the age population of 1.0 to 0.75 Ga in age is small in the southern Sikhote-Alin orogenic belt, so it is considered that the SCC is unlikely to be the source area. Instead, the 1.0–0.75 Ga zircons in the southern Sikhote-Alin are most likely derived from the Neoproterozoic basement of the BJKB (Kim et al., 2008; Lee et al., 1998, 2003; Luan et al., 2017; Wilde et al., 2015; Wu et al., 2011; Yang et al., 2017).

Zircon age spectra with peak ages at 3.3, 3.0, 2.6, and 1.8 Ga, especially the 1.8 Ga ages, were also reported in the southern Siberia Craton (Rojas-Agramonte et al., 2011), which is consistent with zircon ages from the Zhuravlevka and Taukha belts. However, the eastern segment of the Mongol-Okhotsk Ocean between the Siberia Craton and the eastern CAOB was not closed before the Early Cretaceous, which makes it unlikely that sediments were transported to the Sikhote-Alin, because the transport distance would be too large given that the sedimentary characteristics of sandstones from the Sikhote-Alin indicate that they resulted from near-source deposition (Figure 5; Donskaya et al., 2013; Khanchuk et al., 2016; Kravchinsky et al., 2002). Thus, it is proposed that the Siberia Craton could not be the source area for the southern Sikhote-Alin orogenic belt.

6.2.2. Potential Provenance of Phanerozoic Zircons

In the BJKB, the Pan-African metamorphic and igneous rocks range in age from 540 to 480 Ma with a peak of ~500 Ma (Wilde et al., 2000; Zhou et al., 2011). In the middle Paleozoic, only a few inherited zircons with 390–290 Ma ages are reported in the granitic rocks along the western BJKB (Miao et al., 2015). A magmatic arc belt (290–274 Ma in age) was generated along the eastern margin of the Jiamusi Block (Bi et al., 2015; Meng et al., 2008; Sun, Xu, Wilde, Chen, et al., 2015; Yu et al., 2013), whereas there are 270–244 Ma I-type granodiorites and 220–170 Ma highly fractionated I-type granitoids in the western BJKB and adjacent areas

(Jahn et al., 2015; Liu et al., 2017; Wu et al., 2003a, 2003b, 2011; Xu et al., 2013; Yang et al., 2015b). These granites are mostly the result of reworking of juvenile crust, commonly with weak negative to positive zircon $\varepsilon_{Hf}(t)$ values from −4 to 16 (Cao et al., 2011; Meng et al., 2011; Yang et al., 2006; Yu et al., 2012).

In the Phanerozoic, Mesozoic magmatism, especially the granitoids and relevant volcanic rocks, was generated in the NCC (Griffin et al., 1998; Menzies et al., 2007, 1993; Qi et al., 2015; Wilde et al., 2003; Yang et al., 2008; Zhang et al., 2014; Zhu et al., 2012). Intrusive and volcanic rocks were emplaced in the NCC from the Early Triassic to Late Cretaceous, with the Triassic magmatic rocks mainly located along the western segment of the northern margin of the NCC. Thus, it is unlikely to be the source of the Sikhote-Alin orogenic belt. After the Jurassic, magmatism moved eastward and also increased in volume (Zhang et al., 2014). The most important zircon age populations are 180–150 Ma and 130–110 Ma, usually with negative to weakly positive zircon $\varepsilon_{Hf}(t)$ values of −32 to 5, because of the involvement of basement in the magma source (Yang et al., 2009; Zhang et al., 2007; R. Zhang et al., 2009; S. H. Zhang et al., 2009; Zheng et al., 2004; Zhu et al., 2012). Similar magmatic events also took place in the Korean Peninsula at this time. The northern Korean Peninsula is characterized by middle Cretaceous granites (~110 Ma) and also contains some granites ranging in age from 250 to 170 Ma (Wu, Yang, Lo, et al., 2007). In the southern Korean Peninsula, 190–160 Ma is the most important magmatic episode, with local early Paleozoic arc magmatism at 440–370 Ma and Triassic granites at 260–220 Ma (Cheong et al., 2013, 2014; S. Kim et al., 2011; J. Kim et al., 2011; Kim et al., 2015). In addition, zircon Lu-Hf isotopes of Korean Peninsula rocks imply that Paleoarchean to Paleoproterozoic crust provided important source materials to these granitoids, and thus, the zircon $\varepsilon_{Hf}(t)$ values are negative from −31 to −2 (Cheong et al., 2013, 2014, 2015). However, there are minor granitoids (265–252 Ma) recording positive zircon $\varepsilon_{Hf}(t)$ values of 10 to 15, with T_{DM2} model ages from 600 to 400 Ma (Cheong et al., 2013).

In the eastern Siberia Craton and adjacent coastal areas, the Paleo-Pacific subduction-related magmatism mainly took place in the Late Cretaceous, located along an active continental margin (up to 3,000 km long) and is the most important magmatic event regionally (Kirillova, 2003). However, it is younger than the depositional age of sandstones in the southern Sikhote-Alin, meaning that eastern Siberia and adjacent areas cannot be the source area for these rocks.

6.3. Provenance Analysis in the Southern Sikhote-Alin Orogenic Belt

6.3.1. The Samarka Accretionary Complex

The spectrum of zircon ages in sample SAL-19 is similar to that of the Nadanhada accretionary belt, which is located along the eastern margin of the BJKB, where the sediments were shown to be derived from the eastern CAOB, especially the BJKB, although no Archean zircons were reported from the latter (Sun, Xu, Wilde, & Chen, 2015; Zhou et al., 2014; Figures 8a, 8g, and 10).

In sample SAL-19, zircons with ages of 268–236 Ma and 227–162 Ma were most likely derived from the adjacent magmatic rocks in the western BJKB, whereas the Early Permian ages (275–302 Ma) mostly likely came from the magmatic rocks in the eastern and central BJKB (Bi et al., 2015; Sun, Xu, Wilde, Chen, et al., 2015; Sun, Xu, Wilde, & Chen, 2015; Wu et al., 2011; Yang et al., 2015). The Phanerozoic zircons show weakly negative to positive $\varepsilon_{Hf}(t)$ values from −6 to 11 which are similar to those from the BJKB (Figure 9a). In addition, the age groups of ~502 Ma and 1,000–700 Ma are in accord with the Pan-African and Neoproterozoic basement ages, respectively, in the Jiamusi-Khanka Block (Yang et al., 2017; Zhou et al., 2014). However, there are some zircons with ages of 1.6–2.7 Ga ($<$10%), indicating a possible minor contribution from the eastern NCC, which is consistent with the evidence that three Jurassic zircons have negative $\varepsilon_{Hf}(t)$ values (−20 to −22.5).

Although collected in the same belt, sample SAL-40 shows a different provenance (Figures 8b). Late Pan-African (458–507 Ma) and Neoproterozoic (599–1,151 Ma) zircon ages indicate that the BJKB likewise supplied sediments to the unit hosting sample SAL-40, with most Phanerozoic zircons showing positive $\varepsilon_{Hf}(t)$ values with young T_{DM2} model ages, further supporting this view (Figure 9b). However, ages from 1.8 to 2.6 Ga are more important in sample SAL-40, accounting for 36%, which implies that the eastern NCC and/or Korean Peninsula provided more detritus to this part of the Samarka accretionary complex.

There is an unnamed but significant fault that separates the two sample sites, marking the boundary between different components or thrust sheets/slices within the Samarka accretionary complex, which are called the main Samarka belt (sample SAL-19) and eastern Samarka belt (sample SAL-40), respectively. According to

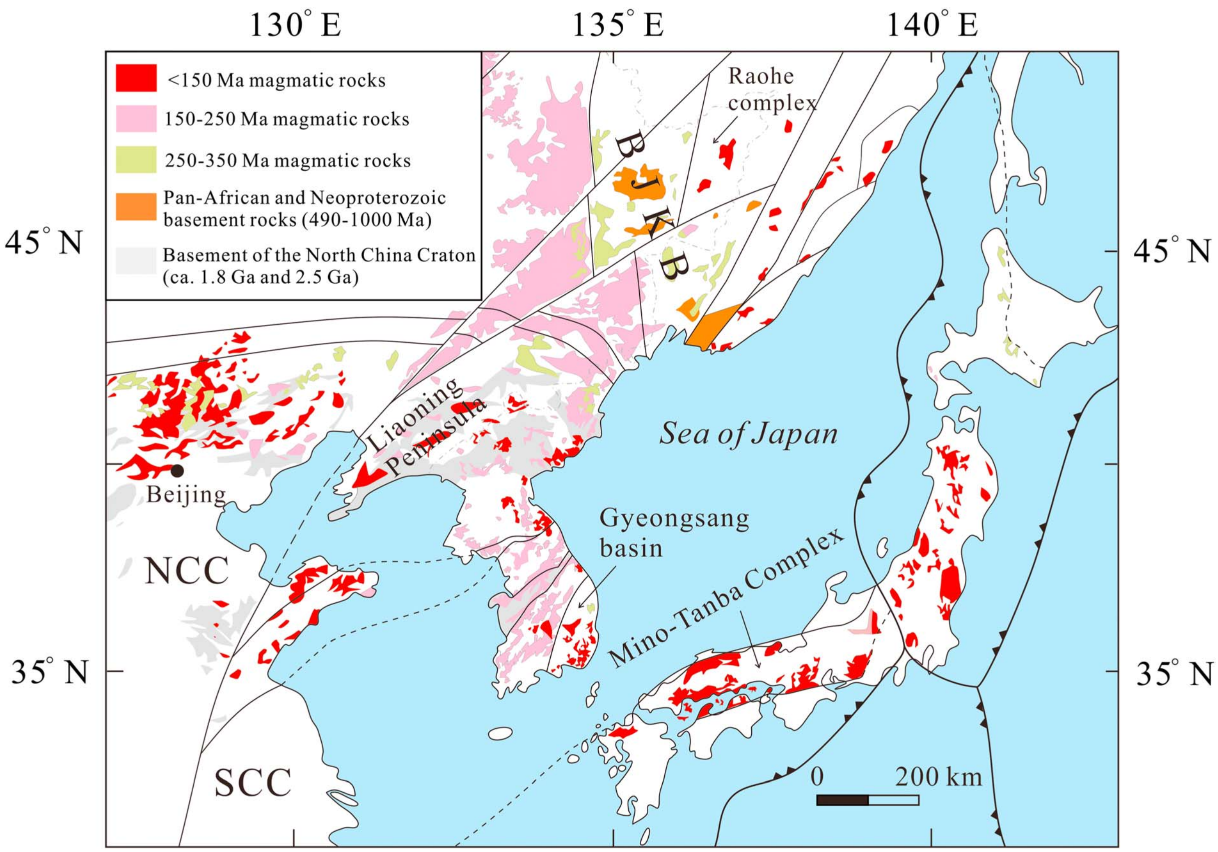

Figure 10. Distribution of Archean to Early Cretaceous magmatism in the possible source areas for the Sikhote-Alin belts (Cheong et al., 2013; Jiang et al., 2013; Kim et al., 2011; Wu, Yang, Wilde, et al., 2007; Zhang et al., 2013; Zhao & Zhai, 2013).

recently published data, detrital zircons from the "coastal Samarka belt" (the southernmost part of the Samarka accretionary complex adjacent to the coast of the Sea of Japan) show an age spectrum with peaks at 189 Ma, 247 Ma, and 1.8 Ga, similar to sample SAL-40 in this study, implying that significant detritus was derived from the NCC and Korean Peninsula (Tsutsumi et al., 2016). Thus, the Samarka accretionary is not a single geological unit and was divided into several thrust slices/sheets according to the structural analysis and geometry (Figure 4). Different components of the Samarka belt show at least two kinds of provenance characteristic, one is the BJKB and the other is the NCC.

6.3.2. The Sergeevka Nappes

The nappes include fragments of the Paleozoic continental margin, and the major rock types are silica-unsaturated mafic rocks containing much fewer zircons than the granitoids (Figure 7). The number of zircons in sample SAL-41 is thus too small for a valid provenance analysis. However, it is inferred that the Neoproterozoic zircons and late Pan-African zircons with positive $\varepsilon_{\mathrm{Hf}}(t)$ values may have originated from the BJKB or the local denudation of mafic and metamorphic rocks (Figures 8c and 9c). The zircons with Paleoproterzoic ages could have been supplied from the NCC or the Korean Peninsula. A source in the SCC is also possible for this sandstone because of the abundance of zircons with ages from 700 to 1,000 Ma. Thus, the provenance of the Sergeevka nappes remains uncertain based on this study and requires further research.

6.3.3. The Zhuravlevka Turbidite Basin

The zircon age spectrum of sample SAL-48 is similar to that of sample SAL-40, suggesting derivation from both the NCC and BJKB (Figure 8d).

Zircons with an age of 420–500 Ma are an important component of the BJKB and the adjacent blocks of the eastern CAOB. However, the abundance of 420–500 Ma zircons is much lower than that of the Neoproterozoic and Archean zircons, suggesting the eastern NCC and Korean Peninsula was also an important source of detritus. Precambrian zircons make up 57% of the population and show major peaks at 1.8 Ga

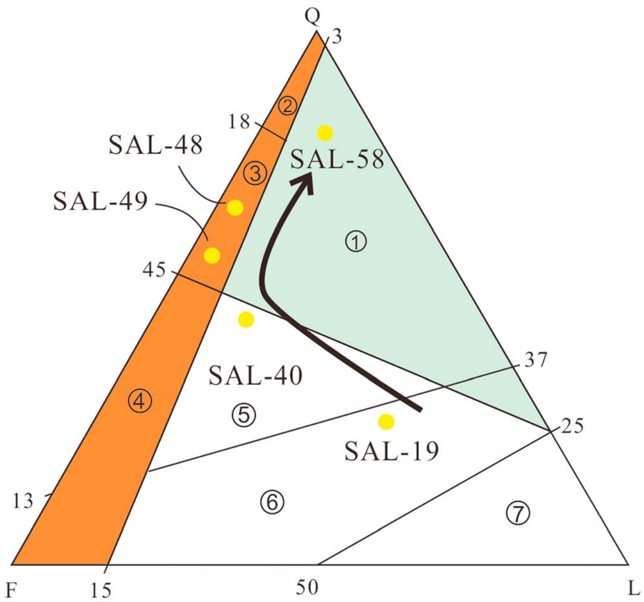

Figure 11. Q-P-L diagram for the sandstones in the Samarka, Zhuravlevka, and Taukha belts (Dickinson, 1985; Dickinson et al., 1983). Numbers in the figure: 1. Recycled orogen; 2. Craton interior; 3. Transitional continent; 4. Basement uplift; 5. Dissected arc; 6. Transitional arc; 7. Undissected arc. The arrow shows the change in trend of the tectonic setting of the provenance area from an arc to a transitional continent and finally to a recycled orogen, during which the contribution from the old craton is increasingly important.

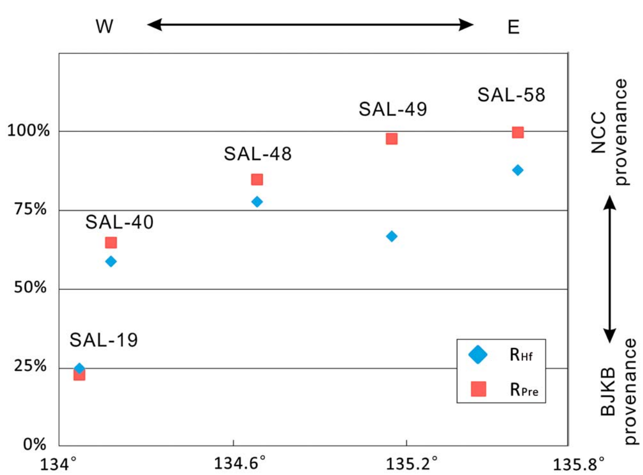

Figure 12. Ratios (R_{Hf} and R_{Pre}) versus the longitude of the sample locations. The two ratios are calculated to show the different provenance of samples investigated in this study. R_{Hf} is the ratio of the number of Phanerozoic zircons with positive $\varepsilon_{Hf}(t)$ values divided the number of the Phanerozoic zircons in each sample. R_{Pre} is the ratio of the number of Archean and Paleoproterozoic zircons in each sample divided the number of Precambrian zircons. Both ratios increase from west to east, meaning that in these samples the contribution from the eastern NCC and/or Korean Peninsula increases from west to east. This is because the Phanerozoic zircons with positive $\varepsilon_{Hf}(t)$ values are mostly from the eastern BJKB, whereas the Archean and Proterozoic zircons are mostly from the eastern NCC. Sample SAL-41 is not shown because the number of analyses is insufficient for a meaningful result.

and 2.5 Ga, which is characteristic of the eastern NCC and Korean Peninsula (Darby & Gehrels, 2006; Li & Huang, 2013; Zhao et al., 2005; Zhu et al., 2012). This is further verified by the Phanerozoic zircon Lu-Hf isotopes, with up to 73% having negative $\varepsilon_{Hf}(t)$ values (Figure 9d). The age population at ~250 Ma is small, whereas zircons with Middle Jurassic to Cretaceous ages are abundant, which correlates with the most important period of Mesozoic magmatism in the eastern NCC and Korean Peninsula (Cheong et al., 2013, 2014; Qi et al., 2015; Zhang et al., 2013; Zhu et al., 2012).

6.3.4. The Taukha Accretionary Complex

Both samples SAL-49 and SAL-58 from the Taukha accretionary complex are characterized by two main age groups; one Paleoproterozoic and the other Phanerozoic (Figures 8e and 8f). The absence of late Pan-African and Neoproterozoic ages indicates that the BJKB did not supply sediments to the Taukha accretionary complex during the Late Jurassic to Early Cretaceous. Thus, the eastern NCC (including the Korean Peninsula) was the most likely source. The zircons with ages of ~2.5 Ga and 1.8 Ga record basement ages of the NCC (Zhao et al., 2005). The zircons with ages of 420–300 Ma could be derived from arc magmatism in the central Korean Peninsula (Kim et al., 2015), and those with ages of 260–230 Ma might be related to arc magmatism and the continent-continent collision belt along the Imjingang Belt (the possible extension of the Sulu-Dabie orogenic belt into the Korean Peninsula; Cheong et al., 2014; J. Kim et al., 2011). Zircons with ages of 220–150 Ma are likely related to collisional magmatism in the eastern NCC and/or Paleo-Pacific subduction-related magmatism in the southern Korean Peninsula (Kusky et al., 2007; Li et al., 2013; S. H. Zhang et al., 2009; Zhang et al., 2013). About 70–80% of the Phanerozoic zircons have negative $\varepsilon_{Hf}(t)$ values in samples SAL-49 and SAL-58, consistent with a NCC source (Figures 9e and 9f; Yang et al., 2006; Sun, Xu, Wilde, & Chen, 2015). However, there are also a few zircons with positive $\varepsilon_{Hf}(t)$ values; for example, five Mesozoic zircons in sample SAL-49 show positive $\varepsilon_{Hf}(t)$ values from 2.8 to 7.9. These values are consistent with the Neoproterozoic juvenile crustal component in South Korea (Cheong et al., 2013).

6.4. Provenance Variation in the Southern Sikhote-Alin Orogenic Belt

According to the composition of sandstones in the southern Sikhote-Alin orogenic belt, different samples show different tectonic settings for the provenance area, changing gradually from an arc to a continental setting (Figure 11).

For sample SAL-19, a transitional arc setting fits the absence of a zircon age peak at 1.8 Ga from the NCC and the abundance of Jurassic zircons most likely derived from the continental arc in the eastern CAOB, which is supported by their negative $\varepsilon_{Hf}(t)$ values. Sample SAL-40 has less lithic fragments and more quartz, illustrating the growing importance of sediments from the Asian continental basement. Samples SAL-48 and SAL-49 plot in the transitional continental area, implying that the deformation belt at the northern margin of the NCC and Korean Peninsula was the main source area. For sample SAL-49, a likely minor contribution from South Korea is indicated by the similar positive $\varepsilon_{(Hf)}$ t values of five Mesozoic zircons (Cheong et al., 2013). Finally, sample SAL-58 was likely fed by a recycled orogen, such as existed

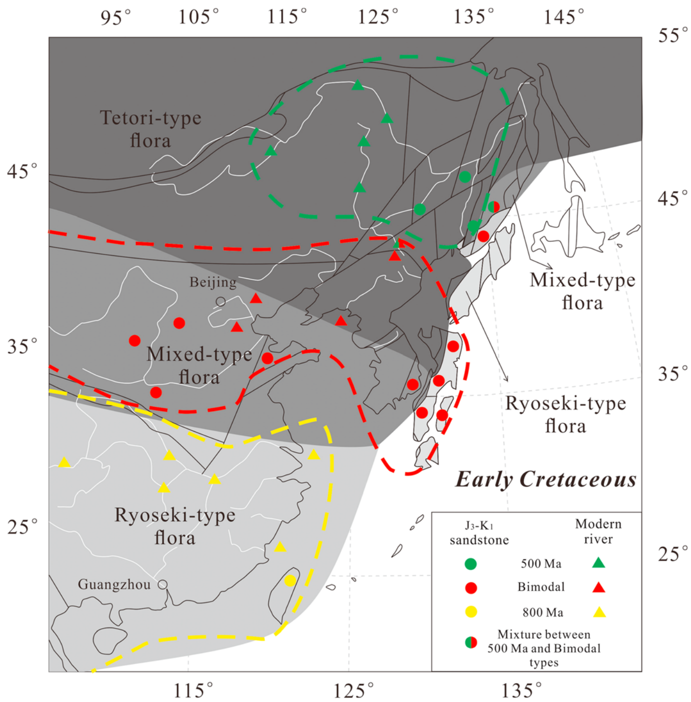

Figure 13. Provinces in the Early Cretaceous East Asia show different types of detrital zircon spectra. The dashed lines show the range of each province. The green dashed line shows the 500 Ma-type province; the red one shows the bimodal-type province; the yellow one shows the 800 Ma-type province. The paleophytogeograhic provinces are also shown, modified after Kimura (1979, 2000) and Golozoubov et al. (1999).

accretionary complex and suture zone/fold-thrust belts of collision orogen (Dickinson et al., 1983). Collision events between mature block/arcs happened in the Japanese Island from Late Paleozoic to Mesozoic and accretionary complexes were built in the gaps of collision (Charvet, 2013; Charvet et al., 1983; Isozaki, 1997; Maruyama, 1997). The highlands associated with the pre-Early Cretaceous subduction and collision events were possible to supply detritus to the Taukha accretionary complex. However, the first-cycle of sediments shows that the eastern NCC and Korean Peninsula were the initial source areas indicated by the bimodal zircon age spectrum.

Along the sample traverse (Figure 2b), the proportion of zircons with 1.8 and 2.5 Ga ages and Phanerozoic zircons with negative zircon $\varepsilon_{Hf}(t)$ values increases from west to east, which likewise indicates the growing importance of the NCC and/or Korean Peninsula as the source (Figure 12). For sample SAL-49, the decoupling of R_{Pre} and R_{Hf} in Figure 10 is attributed to the five Mesozoic zircons with positive $\varepsilon_{Hf}(t)$ values, most likely showing the minor proportion contributed by Neoproterozoic juvenile crust in South Korea (Cheong et al., 2013).

7. Tectonic Implications

Three provinces with different zircon age spectra can be recognized along the eastern Asian continental margin from southeastern Russia to south China (Figure 13), based on the U-Pb age data of detrital zircons collected from the Late Jurassic to Early Cretaceous sandstones and modern river sands. Each zircon age spectrum is generally limited to within a particular area, which helps us better understand the specific geological characteristics in different areas and thus allows to compare that with the southern Sikhote-Alin orogenic belt.

1. Bimodal type: This type of zircon age spectrum shows two important age groups, that is, a Phanerozoic group and a Paleoproterozoic to Archean group (with peaks at ~1.8 and 2.5 Ga; Figure 14a). Very few, if any, zircons with ages between the two major groups have been found. The bimodal-type spectrum appears in the Late Jurassic to Early Cretaceous sandstones from the basins in the interior of the NCC (Li & Huang, 2013; Wang et al., 2016), SW Japan (Aoki et al., 2014; Fujisaki et al., 2014; Isozaki et al., 2010; Nakama et al., 2010) and South Korea (Lee et al., 2015). Modern river sands along the coast of the eastern NCC and Korean Peninsula also have similar spectra (Wu, Yang, Lo, et al., 2007; Yang et al., 2009).
2. 500 Ma type: This type of zircon age spectrum is characterized by important peaks at ~180, 220, 250, and 500 Ma, but ages around ~1.8 or 2.5 Ga are much lesser abundant than in the Bimodal type, or, indeed, sometimes absent (Figure 14b). A minor age group from 0.7 to 1.0 Ga can also be found in the interior of the eastern CAOB, consistent with the Neoproterozoic basement of the BJKB (Khanchuk et al., 2010; Wilde et al., 1997; Yang et al., 2017). The 500 Ma-type spectrum is also found around the BJKB, such as the Heilongjiang Complex and Nadanhada belt (Zhou et al., 2009, 2015; Sun, Xu, Wilde, & Chen, 2015), and the river sands from the middle reach of the Amur River.
3. 800 Ma type: The spectra in the eastern SCC always contain a prominent age peak at ~0.8 Ga, which is the most significant characteristic of this area (Figure 14c; Wang et al., 2014; Yui et al., 2012). Zircon peaks at ~130 Ma, 170 Ma, 1.8 Ga, and 2.5 Ga are also present in this type, derived from Jurassic-Cretaceous magmatism and basement rocks of the SCC. This type of spectrum is dominant in almost all of the modern river sands collected from the Yangtze River and its branches (Yang et al., 2012). However, very few Late Jurassic to Early Cretaceous sandstones can be found in the present SCC, except perhaps the Tananao complex in Taiwan which fits well with the 800 Ma-type spectrum (Li et al., 2012; Yui et al., 2012).

In the southern Sikhote-Alin, sample SAL-19 from the main Samarka accretionary complex shows a 500 Ma-type spectrum. Samples SAL-49 and SAL-58 from the Taukha accretionary complex have typical bimodal-type

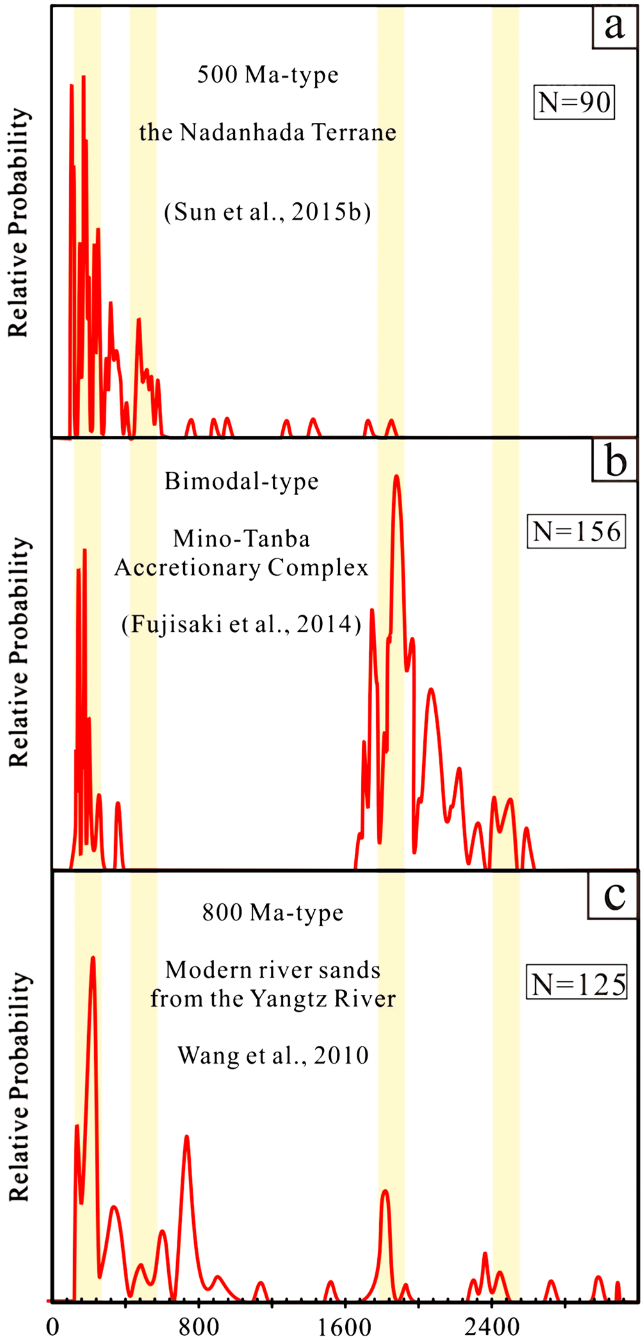

Figure 14. Typical spectra of detrital zircons in the (a) 500 Ma-type, (b) bimodal-type, and (c) 800 Ma-type provinces in the Early Cretaceous of East Asia.

spectra. However, sample SAL-40 from the eastern Samarka belt and sample SAL-48 from the Zhuravlevka basin are a mixture of sediments with the 500 Ma type and bimodal type. The detrital monazite ages in the Samarka belt and Zhuravlevka basin also support this viewpoint (Tsutsumi et al., 2016). In the main Samarka belt, there is a significant peak at ~500 Ma, which is not shown in the monazite data from the Zhuravlevka or Taukha (Figure 15). Thus, the influence from the BJKB to the Zhuravlevka and Taukha was quite weak. Importantly, located in their present geographic positions, it is difficult for the eastern Samarka accretionary complex, the Zhuravlevka turbidite basin, and the Taukha accretionary complex to be fed by sediments from the eastern NCC or Korean Peninsula (Figures 1 and 10). It is also virtually impossible for the Taukha belt to exclude sediments from the BJKB in its present location. This strongly indicates that the belts in the southern Sikhote-Alin area were moved by tectonic movement significantly, such as subduction, collision, and strike slip. Therefore, discussing the tectonic settings will be very necessary in order to explain the abrupt changing of provenance types across the Central Sikhote-Alin Fault.

Many hypotheses have been raised in the past decades in the Pacific tectonic realm to explain the collage of the numerous belts in this region, including the (1) collision orogeny, (2) accretionary orogeny, and (3) strike-slip faulting along a transform margin.

In SW Japan, collision orogeny was identified based on the discovery of large thrust sheet and nappes (Charvet et al., 1985; Faure et al., 1986). These nappe tectonics are explained by the intermittent docking of continental blocks/mature arcs to the hinterland. The Sr-Nd isotopic research of granitoids in SW Japan supports this viewpoint because the participation of old crust can be detected in the felsic magmatism (Jahn, 2010). Structural geological analysis also reveals nappe/thrust tectonics similar to that in the classical collisional orogenic belt (Charvet et al., 1985). Faure et al. (1995) proposed similar model in Sikhote-Alin, underlining the importance of continental blocks in orogeny. Recently, Jahn et al. (2015) studied the Sr-Nd isotopes in the granitoids in Sikhote-Alin. The result also supports the possible existence of an old crust basement. However, the explanation of Sr-Nd isotopes is argued because the remelting of the sedimentary rocks in Sikhote-Alin, including abundant detritus from old continental blocks/cratons, can also explain the isotopic data (Khanchuk et al., 2016; Kruk et al., 2014).

Some other studies suggest that accretionary orogeny, instead of collision, was dominant in the Japanese Island (Isozaki et al., 2010; Maruyama, 1997). In their models, the Japanese Islands are basically a large accretionary prism which was influenced by high-pressure metamorphism, accretion of sea mount/plateau, and ridge subduction. As a result, the Japanese Islands grew continuously eastward due to persistent subduction and underthrusting of the oceanic plate. The age of the thrust sheets, therefore, tends to be younger from hinterland to the ocean side.

According to some Russian geologists, the eastern Asian margin was a transform plate boundary in Early Cretaceous, alike to the modern plate margin in California, alike to the Saint Andreas Fault (Golozoubov, 2006; Golozoubov et al., 1999; Khanchuk, 2001; Khanchuk et al., 2016). Accretionary orogeny associated with subduction took place in the Jurassic and Late Cretaceous in their representative model (Khanchuk et al., 2016). Whereas in the Early Cretaceous (145–100 Ma), the collage of some major units in Sikhote-Alin was

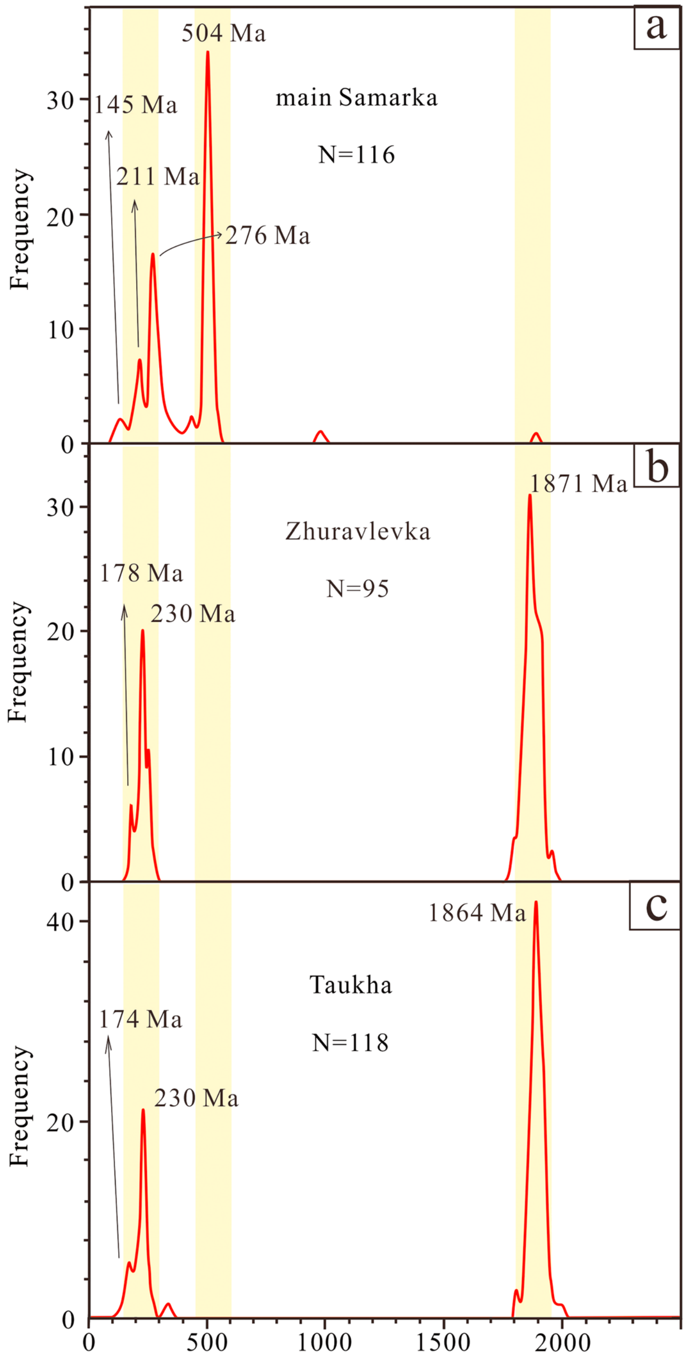

Figure 15. Spectra of detrital monazite collected in (a) the main Samarka, (b) the Zhuravlevka, and (c) the Taukha belts (Tsutsumi et al., 2016).

attributed to the northward displacement by strike-slip faults. It is noted that strike-slip faulting is also emphasized by the "collisional orogeny" and "accretionary orogeny" models, although it is not considered to be the only/major geodynamic mechanism. For example, the post-collision strike-slip faulting was important in reworking of the south Kitakami-Kurosegawa continental block after its collision with the hinterland of Japan (Charvet, 2013; Kato & Saka, 2003, 2006). In the previous models for Sikhote-Alin, the "terranes" were suggested to be built near South China and then moved northward to its present location by sinistral strike-slip faulting (Natal'in, 1993).

In the southern Sikhote-Alin, nappe/thrust tectonics can be identified in the Sergeevka nappes (Figures 2 and 4), in which the two-stage evolution is similar to that of the south Kitakami-Kurosegawa block in Japan, namely, the thrusting at the early stage and reworking by strike-slip faulting at the later stage (Figure 16a). High-pressure metamorphism (blueschist facies) happened when the slab was subducted and then exhumed during the collsion. These nappes were thrust upon the Samarka accretionary complex, suggesting a collisional orogeny (Khanchuk et al., 2016). At the first stage, the subduction and collision between the Sergeevka and Samarka were responsible for the emplacement of the nappes (Figure 16a). At the later stage, the continental block was dismembered into several fragments, which is clearly shown on the regional geological map (Figure 2).

One of the key questions about the tectonics in Sikhote-Alin is that if the collisional orogeny played an important role. In the northern Sikhote-Alin area, Faure et al. (1995) identified a continental block, the Anuy microcontinent, which was proposed to collide with the western belts in the middle Cretaceous. Nd isotopes of granites also indicate that the basement of the Sikhote-Alin orogenic belt may be an old crust, instead of a juvenile one (Jahn et al., 2015). However, this conclusion should be drawn carefully now. In reality, there is no valid geochronological data showing any evidence of "old continental basement" so far. Thus, in addition to the Sergeevka block, the existence of other old crust/continental block is difficult to assure, making it difficult to identify the collisional orogeny in Sikhote-Alin. This issue still needs more detailed research in future.

Anyway, no matter accretion or collision model of the belts from east to west does not fit the new data in this study. The detrital zircon dating and Lu-Hf isotopes reveal that the provenance features of belts separated by the Central Sikhote-Alin Fault are quite different. The affinity of NCC/Korean Peninsula is recognized in the eastern Samarka belt, Zhuravlevka basin, and Taukha accretionary complex, whereas the Nadanhada and main Samarka accretionary complexes were dominated by the BJKB. The provenance of the Nadanhada and main Samarka belts is comprehensible because they are adjacent to the BJKB. But it is very difficult to explain the weak signal of the BJKB and strong influence from the NCC in other belts because they are adjacent to the eastern CAOB as well. In this study, the sinistral strike-slip faulting, represented by the Central Sikhote-Alin Fault, is proposed to be responsible for this issue. It is suggested that the eastern Samarka, Zhuravlevka, and Taukha belts were not located adjacent to the BJKB when deposited, but farther south than their present locations, possibly near the Korean Peninsula to accept the sediments from the NCC (Figure 16b). The sinistral strike-slip faulting system transported the belts to north. This strike-slip faulting system should be active after the collision of the Sergeevka nappes and the initial collage between the Zhuravlevka, Kema, and Taukha belts (Figure 16c) because the

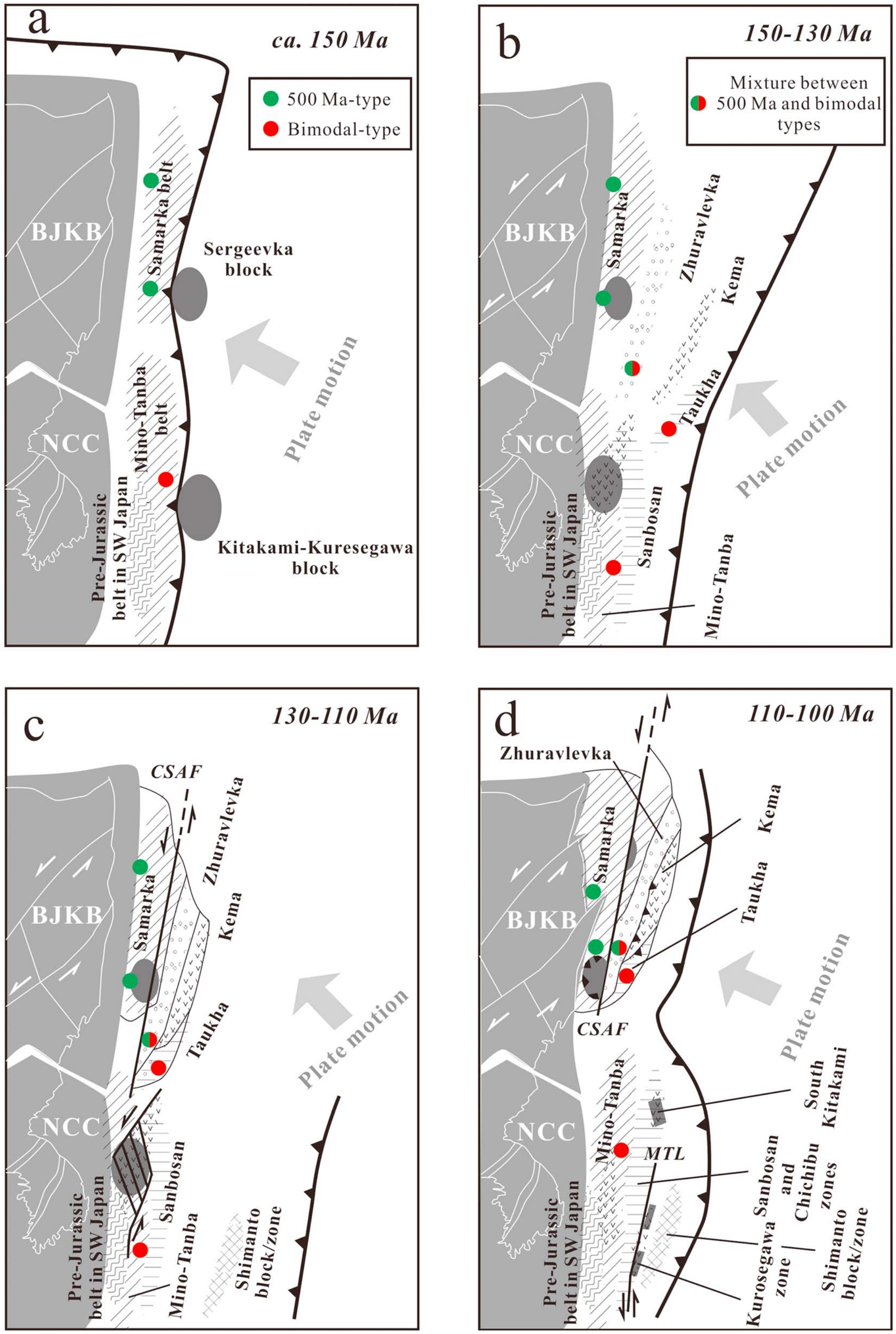

Figure 16. Tectonic reconstruction of the East Asian continental margin at 150 to 100 Ma. Faults: CSAF = the Central Sikhote-Alin Fault; MTL = the Median Tectonic Line in Japan. The reconstruction in SW Japan is modified after Kato and Saka (2003) and Charvet (2013). The plate motion direction is according to Müller et al. (2008).

Central Sikhote-Alin Fault cuts the Samarka belt, Sergeevka nappes, and most boundaries between the major belts (Figure 2). It should be noted that thrusting was the initial contact relationship between most belts in Sikhote-Alin except the Zhruavlevka turbidite basin which was deposited along the Central Sikhote-Alin Fault at the very beginning (Khanchuk et al., 2016; Malinovsky & Golozubov, 2011).

Evidence for northward transport is also recorded by the floral distribution in the sedimentary rocks. Two major paleophytogeographic provinces are recognized in the area, the Tetori-type floral province in the north and the Ryoseki-type floral province in the south (Figure 12; Batten, 1984; Kimura, 1979; Vakhrameev, 1987; Yabe et al., 2003). A mixed-type floral province is further recognized between these two (Kimura et al., 1988; Kimura, 2000). Although the province boundaries are roughly latitudinal, more detailed research shows an irregular flora distribution in the southern Sikhote-Alin (Figure 12). Plants from the southernmost Sikhote-Alin are similar to the Ryoseki-type flora, whereas some areas in the Sikhote-Alin are assigned to the mixed-type flora domain (Golozoubov et al., 1999; Kimura, 2000). Tectonic reconstruction based on the floral assemblages in East Asia indicates that northward movement could be more than 5° of latitude in SW Japan and 15° of latitude in the southern Sikhote-Alin (Golozoubov et al., 1999). However, there remain uncertainties about the affinity of belts as recorded by the detrital zircon, monazite, and flora. The reason is that the floral assemblage is mainly determined by latitude, whereas the provenance of sediments is mainly constrained by their paleogeographic location when deposited. However, in this instance, both pieces of evidence are consistent with northward transport after the initial collision, including the paleomagnetic research published recently, showing that northward movement was important for some belts in Sikhote-Alin (Didenko et al., 2014; Khanchuk, Didenko, Tikhomirova, et al., 2015).

The exact offset is very difficult to evaluate for the Cental Sikhote-Alin Fault because (1) the sinistral displacement may be changed by the complicated deformations in the region, for example, the dextral movement at later stage, faulting and folding due to subduction or collision; (2) the Central Sikhote-Alin Fault has been an inactive fault for dozens of million years, making the direct evidence used to evaluate the offset, such as rivers and ranges, very obscure; and (3) the forest almost cover the whole Sikhote-Alin area and there is even no good outcrop of the fault founded for now. Thus, the offset of the sinistral faults in the Sikhote-Alin area is still an unsolved issue which needs more detailed research and direct evidence.

The timing of this northward transport with parallel-margin left-lateral motion has not been well constrained. However, in the southern Sikhote-Alin it can be inferred that the northward movement occurred in the late Early Cretaceous based on the magmatic and floral evidence. There is also a magmatic gap between 130 and 110 Ma in the Sikhote-Alin, probably due to plate motion parallel to the continental margin, which weakened the effect of subduction beneath the continent and thus reduced arc magmatism (Jahn et al., 2015; Khanchuk, 2001; Khanchuk et al., 2016; Maruyama, 1997). After ~110 Ma, magmatism in the Sikhote-Alin became quasi-continuous from 100 to 56 Ma as a result of westward subduction of the Izanagi and Pacific plates (Jahn et al., 2015; Kruk et al., 2014). The floral assemblages were different in various basins of the southern Sikhote-Alin prior to this magmatic gap (Golozoubov et al., 1999). However, the flora were similar between 110 and 100 Ma (Golozobov et al., 1999), providing some constraint on the timing of sinistral movement on the major strike-slip faults.

8. Conclusions

The southern Sihote-Alin orogenic belt is composed, from west to east, of the Samarka, Zhuravlevka, and Taukha belts, which are separated by thrusts and strike-slip faults. The Sergeevka nappes include Paleozoic continental margin fragments that were covered by late Paleozoic to Mesozoic sedimentary rocks and were thrust over the Samarka accretionary complex.

Detrital zircon U-Pb ages and Lu-Hf isotopes of sandstones in the various belts constrain the provenance as follows: (1) the main Samarka belt mainly received terrigenous sediments from the eastern CAOB (mainly from the BJKB); (2) the Zhuravlevka basin and eastern Samarka belt were fed by both the eastern CAOB and NCC (probably including the Korean Peninsula); (3) the sediments of the Taukha belt were derived from the eastern NCC and Korean Peninsula; and (4) the provenance of the Jurassic sediments in the Sergeevka nappes is largely unconstrained due to insufficient data and needs to be further investigated.

The initial contact relationship between most belts in the Sikhote-Alin orogenic belt is thrust resulted from collisional orogeny and subduction of the Paleo-Pacific Ocean. However, the Zhuravlevka turbidite basin was deposited along the Central Sikhote-Alin Fault.

The Sergeevka nappes were thrust upon the Samarka belt before the Early Cretaceous and then reworked by sinistral strike-slip faults. The Taukha belt and Kema arc collided with the Zhuravlevka basin before the Late Cretaceous. However, sinistral strike-slip faulting was important in the final collage of the Sikhote-Alin orogenic belt after the initial thrusting. The eastern Samarka belt, Zhuravlevka basin, and Taukha belt were transported northward from the margin of the NCC to their present location. The timing of this northward movement is estimated as the late Early Cretaceous.

Acknowledgments
We would like to thank Igor Alexandrov, Victor P. Nechaev, Bei Xu, and Pan Zhao for their help with the fieldwork and their important suggestions for this manuscript. The comments from Editor John Geissman, Associate Editor Andrei Khudoley, Jian-bo Zhou, Jacques Charvet, and an anonymous reviewer are essential to improve the quality of our manuscript, especially for the part of tectonic reconstruction. We acknowledge Tatsuaki Kimura and other geologists from China, Japan, and Korea who contributed to the paleophyto-geography and tectonic reconstruction of East Asia. Y. H. Yue from the Institute of Tibetan Plateau Research, Chinese Academy of Sciences, is thanked for her kind help with LA-ICP-MS dating. In addition, Z.C. Liu, L. Xu and other staff at the State Key Laboratory of Geological Processes and Mineral Resources, China University of Geosciences (Wuhan), gave valuable advice on the analysis of zircon Lu-Hf isotopes. The data presented in this paper are available in Tables 1 and 2. This research was financially supported by the State Key Program of National Natural Science Foundation of China (41730210) and the Major State Basic Research Development Program of China (2013 CB429804) and partly funded by the Fundamental Research Funds for the Central Universities (310827161010).

References

Aoki, K., Isozaki, Y., Kofukuda, D., Sato, T., Yamamoto, A., Maki, K., … Hirata, T. (2014). Provenance diversification within an arc-trench system induced by batholith development: The Cretaceous Japan case. *Terra Nova*, *26*(2), 139–149. https://doi.org/10.1111/ter.12080

Argentov, V., Gnibidenko, G., Popov, A., & Potap'ev, S. (1976). *Deep Structure of Primorye*. Moscow (in Russian): Nauka.

Batten, D. (1984). Palynology, climate and the development of Late Cretaceous floral provinces in the Northern Hemisphere; a review. In *Fossils and Climate*, (pp. 127–164). Chichester, UK: John Wiley.

Berger, W., & Winterer, E. (1974). Plate stratigraphy and the fluctuating carbonate line. In *Pelagic sediments: On land and under the sea* (pp. 11–48). *International Association of Sedimentologists. Special Publication Number 1*, Oxford, UK: Blackwell Scientific Publications.

Bi, J. H., Ge, W. C., Yang, H., Zhao, G. C., Xu, W. L., & Wang, Z. H. (2015). Geochronology, geochemistry and zircon Hf isotopes of the Dongfanghong gabbroic complex at the eastern margin of the Jiamusi Massif, NE China: Petrogensis and tectonic implications. *Lithos*, *234*, 27–46.

Bingen, B., Birkeland, A., Nordgulen, Ø., & Sigmond, E. M. (2001). Correlation of supracrustal sequences and origin of terranes in the Sveconorwegian orogen of SW Scandinavia: SIMS data on zircon in clastic metasediments. *Precambrian Research*, *108*(3-4), 293–318. https://doi.org/10.1016/S0301-9268(01)00133-4

Blichert-Toft, J., & Albarède, F. (1997). The Lu-Hf isotope geochemistry of chondrites and the evolution of the mantle-crust system. *Earth and Planetary Science Letters*, *148*(1-2), 243–258. https://doi.org/10.1016/S0012-821X(97)00040-X

Cao, H., Wenliang, X., Fuping, P., & Xingzhou, Z. (2011). Permian tectonic evolution in southwestern Khanka Massif: Evidence from Zircon U-Pb chronology, Hf isotope and Geochemistry of gabbro and diorite. *Acta Geologica Sinica (English Edition)*, *85*(6), 1390–1402.

Cawood, P. A., Hawkesworth, C., & Dhuime, B. (2012). Detrital zircon record and tectonic setting. *Geology*, *40*(10), 875–878. https://doi.org/10.1130/G32945.1

Charvet, J. (2013). The neoproterozoic–early paleozoic tectonic evolution of the South China Block: An overview. *Journal of Asian Earth Sciences*, *74*, 198–209.

Charvet, J., Shu, L., Faure, M., Choulet, F., Wang, B., Lu, H., & Le Breton, N. (2010). Structural development of the Lower Paleozoic belt of South China: Genesis of an intracontinental orogen. *Journal of Asian Earth Sciences*, *39*(4), 309–330. https://doi.org/10.1016/j.jseaes.2010.03.006

Chen, Z. H., Xing, G. F., & Zhao, X. L. (2015). Palaeoproterozoic A-type magmatism in northern Wuyishan terrane, Southeast China: Petrogenesis and tectonic implications. *International Geology Review*, *1–14*.

Chen, Y., Zhang, Z., Li, K., Yu, H., & Wu, T. (2016). Detrital zircon U–Pb ages and Hf isotopes of Permo-Carboniferous sandstones in central Inner Mongolia, China: Implications for provenance and tectonic evolution of the southeastern Central Asian Orogenic Belt. *Tectonophysics*, *671*, 183–201. https://doi.org/10.1016/j.tecto.2016.01.018

Cheng, R., Wu, F., Ge, W., Sun, D., Liu, X., & Yang, J. (2006). Emplacement age of Raohe Complex in eastern Heilongjiang Province and the tectonic evolution of the eastern part of Northeastern China. *Acta Petrologica Sinica*, *22*(2), 353–376. (in Chinese with English abstract)

Cheong, C. s., Yi, K., Kim, N., Lee, T. H., Lee, S. R., Geng, J. Z., & Li, H. K. (2013). Tracking source materials of Phanerozoic granitoids in South Korea by zircon Hf isotopes. *Terra Nova*, *25*(3), 228–235. https://doi.org/10.1111/ter.12027

Cheong, C. S., Kim, N., Kim, J., Yi, K., Jeong, Y. J., Park, C. S., … Cho, M. (2014). Petrogenesis of Late Permian sodic metagranitoids in southeastern Korea: SHRIMP zircon geochronology and elemental and Nd–Hf isotope geochemistry. *Journal of Asian Earth Sciences*, *95*, 228–242. https://doi.org/10.1016/j.jseaes.2014.06.005

Cheong, C. S., Kim, N., Jo, H. J., Cho, M., Choi, S. H., Zhou, H., & Geng, J. Z. (2015). Lithospheric mantle signatures as revealed by zircon Hf isotopes of Late Triassic post-collisional plutons from the central Korean peninsula, and their tectonic implications. *Terra Nova*, *27*(2), 97–105. https://doi.org/10.1111/ter.12135

Darby, B. J., & Gehrels, G. (2006). Detrital zircon reference for the North China block. *Journal of Asian Earth Sciences*, *26*(6), 637–648. https://doi.org/10.1016/j.jseaes.2004.12.005

Dickinson, W. R. (1985). Interpreting provenance relations from detrital modes of sandstones. In G. G. Zuffa (Eds.), *Provenance of Arenites* (pp. 333–361). Dordrecht, Netherlands: Reidel. https://doi.org/10.1007/978-94-017-2809-6_15

Dickinson, W. R., & Gehrels, G. E. (2009). Use of U–Pb ages of detrital zircons to infer maximum depositional ages of strata: A test against a Colorado Plateau Mesozoic database. *Earth and Planetary Science Letters*, *288*(1-2), 115–125. https://doi.org/10.1016/j.epsl.2009.09.013

Dickinson, W. R., Beard, L. S., Brakenridge, G. R., Erjavec, J. L., Ferguson, R. C., Inman, K. F., … Ryberg, P. T. (1983). Provenance of North American Phanerozoic sandstones in relation to tectonic setting. *Geological Society of America Bulletin*, *94*(2), 222–235. https://doi.org/10.1130/0016-7606(1983)94<222:PONAPS>2.0.CO;2

Didenko, A., Khanchuk, A., Tikhomirova, A., & Voinova, I. (2014). Eastern segment of the Kiselevka-Manoma terrane (Northern Sikhote Alin): Paleomagnetism and geodynamic implications. *Russian Journal of Pacific Geology*, *8*(1), 18–37. https://doi.org/10.1134/S1819714014010023

Donskaya, T., Gladkochub, D., Mazukabzov, A., & Ivanov, A. (2013). Late Paleozoic–Mesozoic subduction-related magmatism at the southern margin of the Siberian continent and the 150 million-year history of the Mongol-Okhotsk Ocean. *Journal of Asian Earth Sciences*, *62*, 79–97. https://doi.org/10.1016/j.jseaes.2012.07.023

Faure, M., Caridroit, M., & Charvet, J. (1986). The late Jurassic oblique collisional orogen of SW Japan—New structural data and synthesis. *Tectonics*, *5*(7), 1089–1114. https://doi.org/10.1029/TC005i007p01089

Faure, M., Natal'In, B. A., Monie, P., Vrublevsky, A. A., Borukaiev, C., & Prikhodko, V. (1995). Tectonic evolution of the Anuy metamorphic rocks (Sikhote Alin, Russia) and their place in the Mesozoic geodynamic framework of East Asia. *Tectonophysics*, *241*(3–4), 279–301. https://doi.org/10.1016/0040-1951(94)00186-D

Fernández, R. D., Catalán, J. R. M., Gerdes, A., Abati, J., Arenas, R., & Fernández-Suárez, J. (2010). U–Pb ages of detrital zircons from the Basal allochthonous units of NW Iberia: Provenance and paleoposition on the northern margin of Gondwana during the Neoproterozoic and Paleozoic. *Gondwana Research*, *18*(2–3), 385–399. https://doi.org/10.1016/j.gr.2009.12.006

Fernandez-Suarez, J., Alonso, G. G., Cox, R., & Jenner, G. A. (2002). Assembly of the Armorica microplate: A strike-slip terrane delivery? Evidence from U-Pb ages of detrital zircons. *The Journal of Geology*, *110*(5), 619–626. https://doi.org/10.1086/341760

Fujisaki, W., Isozaki, Y., Maki, K., Sakata, S., Hirata, T., & Maruyama, S. (2014). Age spectra of detrital zircon of the Jurassic clastic rocks of the Mino-Tanba AC belt in SW Japan: Constraints to the provenance of the mid-Mesozoic trench in East Asia. *Journal of Asian Earth Sciences*, *88*, 62–73. https://doi.org/10.1016/j.jseaes.2014.02.006

Gehrels, G. (2014). Detrital zircon U-Pb geochronology applied to tectonics. *Annual Review of Earth and Planetary Sciences*, *42*(1), 127–149. https://doi.org/10.1146/annurev-earth-050212-124012

Gilder, S. A., Leloup, P. H., Courtillot, V., Chen, Y., Coe, R. S., Zhao, X., … Zhu, R. (1999). Tectonic evolution of the Tancheng-Lujiang (Tan-Lu) fault via middle Triassic to Early Cenozoic paleomagnetic data. *Journal of Geophysical Research*, *104*(B7), 15,365–15,390. https://doi.org/10.1029/1999JB900123

Golozoubov, V. V. (2006). *Tectonics of the Jurassic and Lower Cretaceous Complexes of the North-Western Farming of the Pacific Ocean* (p. 231). Vladivostok: *Dal'nauka*. (in Russian)

Golozoubov, V. V., Khanchuk, A. I., Kemkin, I. V., Panchenko, I. V., & Simanenko, V. P. (1992). *Taukha and Zhuravlevka Terranes (South SikhoteAlin)*, (p. 83). Vladivostok: *Preprint*. (in Russian)

Golozoubov, V. V., Markevich, V. S., & Bugdaeva, E. (1999). Early Cretaceous changes of vegetation and environment in East Asia. *Palaeogeography, Palaeoclimatology, Palaeoecology*, *153*(1–4), 139–146. https://doi.org/10.1016/S0031-0182(99)00074-7

Grasse, S. W., Gehrels, G. E., Lahren, M. M., Schweickert, R. A., & Barth, A. P. (2001). U-Pb geochronology of detrital zircons from the Snow Lake pendant, central Sierra Nevada—Implications for Late Jurassic–Early Cretaceous dextral strike-slip faulting. *Geology*, *29*(4), 307–310. https://doi.org/10.1130/0091-7613(2001)029<0307:UPGODZ>2.0.CO;2

Grebennikov, A. V., Khanchuk, A. I., Gonevchuk, V. G., & Kovalenko, S. V. (2016). Cretaceous and Paleogene granitoid suites of the Sikhote-Alin area (Far East Russia): Geochemistry and tectonic implications. *Lithos*, *261*, 250–261. https://doi.org/10.1016/j.lithos.2015.12.020

Griffin, W. L., Zhang, A., O'Reilly, S. Y., Ryan, C. G., Flower, M., Chung, S. L., … Lee, T. Y. (1998). Phanerozoic evolution of the lithosphere beneath the Sino-Korean Craton. In *Mantle dynamics and plate interactions in East Asia, Geographical Series* (Vol. 27, pp. 107–126). Washington, DC: American Geophysical Union.

Griffin, W., Belousova, E., Shee, S., Pearson, N., & O'reilly, S. (2004). Archean crustal evolution in the northern Yilgarn Craton: U–Pb and Hf-isotope evidence from detrital zircons. *Precambrian Research*, *131*(3–4), 231–282. https://doi.org/10.1016/j.precamres.2003.12.011

Gutiérrez-Alonso, G., Fernández-Suárez, J., Jeffries, T., Jenner, G., Tubrett, M., Cox, R., & Jackson, S. (2003). Terrane accretion and dispersal in the northern Gondwana margin. An Early Paleozoic analogue of a long-lived active margin. *Tectonophysics*, *365*(1–4), 221–232. https://doi.org/10.1016/S0040-1951(03)00023-4

Horie, K., Yamashita, M., Hayasaka, Y., Katoh, Y., Tsutsumi, Y., Katsube, A., … Cho, M. (2010). Eoarchean–Paleoproterozoic zircon inheritance in Japanese Permo-Triassic granites (Unazuki area, Hida Metamorphic Complex): Unearthing more old crust and identifying source terranes. *Precambrian Research*, *183*(1), 145–157. https://doi.org/10.1016/j.precamres.2010.06.014

Howell, D. G., Jones, D. L., & Schermer, E. R. (1985). Tectonostratigraphic Terranes of the Circum-Pacific Region. In D. G. Howell (Ed.), *Tectonostratigraphic terranes of the Circum-Pacific region. Circum-Pacific Council for Energy and Mineral Resources*, *Earth Science Series 1* (pp. 3–30). Houston, TX: AAPG.

Hu, Z., Liu, Y., Gao, S., Liu, W., Zhang, W., Tong, X., … Chen, H. (2012). Improved in situ Hf isotope ratio analysis of zircon using newly designed X skimmer cone and jet sample cone in combination with the addition of nitrogen by laser ablation multiple collector ICP-MS. *Journal of Analytical Atomic Spectrometry*, *27*(9), 1391–1399. https://doi.org/10.1039/c2ja30078h

Iizuka, T., Yamaguchi, T., Hibiya, Y., & Amelin, Y. (2015). Meteorite zircon constraints on the bulk Lu−Hf isotope composition and early differentiation of the Earth. *Proceedings of the National Academy of Sciences*, *112*(17), 5331–5336. https://doi.org/10.1073/pnas.1501658112

Isozaki, Y. (1997). Contrasting two types of orogen in Permo-Triassic Japan: Accretionary versus collisional. *Island Arc*, *6*(1), 2–24. https://doi.org/10.1111/j.1440-1738.1997.tb00038.x

Isozaki, Y., Maruyama, S., & Furuoka, F. (1990). Accreted oceanic materials in Japan. *Tectonophysics*, *181*(1–4), 179–205. https://doi.org/10.1016/0040-1951(90)90016-2

Isozaki, Y., Aoki, K., Nakama, T., & Yanai, S. (2010). New insight into a subduction-related orogen: A reappraisal of the geotectonic framework and evolution of the Japanese Islands. *Gondwana Research*, *18*(1), 82–105. https://doi.org/10.1016/j.gr.2010.02.015

Jahn, B. M. (2010). Accretionary orogen and evolution of the Japanese Islands: Implications from a Sr-Nd isotopic study of the Phanerozoic granitoids from SW Japan. *American Journal of Science*, *310*(10), 1210–1249.

Jahn, B. M., Valui, G., Kruk, N., Gonevchuk, V., Usuki, M., & Wu, J. T. (2015). Emplacement ages, geochemical and Sr–Nd–Hf isotopic characterization of Mesozoic to early Cenozoic granitoids of the Sikhote-Alin Orogenic Belt, Russian Far East: Crustal growth and regional tectonic evolution. *Journal of Asian Earth Sciences*, *111*, 872–918. https://doi.org/10.1016/j.jseaes.2015.08.012

Jia, J., Zheng, H., Huang, X., Wu, F., Yang, S., Wang, K., & He, M. (2010). Detrital zircon U-Pb ages of Late Cenozoic sediments from the Yangtze delta: Implication for the evolution of the Yangtze River. *Chinese Science Bulletin*, *55*(15), 1520–1528. https://doi.org/10.1007/s11434-010-3091-x

Kato, K., & Saka, Y. (2003). Kurosegawa terrane as a transform fault zone in southwest Japan. *Gondwana Research*, *6*(4), 669–686. https://doi.org/10.1016/S1342-937X(05)71016-9

Kato, K., & Saka, Y. (2006). New model for the Early Cretaceous development of SW Japan based on basic rocks of the Chichibu Composite Terrane. *Geosciences Journal*, *10*(3), 275–289. https://doi.org/10.1007/BF02910370

Kemkin, I. (2008). Structure of terranes in a Jurassic accretionary prism in the Sikhote-Alin-Amur area: Implications for the Jurassic geodynamic history of the Asian eastern margin. *Russian Geology and Geophysics*, *49*(10), 759–770. https://doi.org/10.1016/j.rgg.2007.12.014

Kemkin, I., & Kemkina, R. (2000). Jurassic-Early Cretaceous biostratigraphic cherty and terrigenous deposits of the Dalnegorsk Ore region (Southern Sikhote-Alin). *Geology of the Pacific Ocean*, *15*(1), 85–106.

Kemkin, I. V., & Kemkina, R. A. (2015). Geochemistry of chert rocks from the Sikhote-Alin Taukha terrane, Russia far east: Significance for determination of their depositional environment. *Environmental Earth Sciences*, *73*(5), 2253–2268. https://doi.org/10.1007/s12665-014-3574-1

Kemkin, I., Filippov, A., & Khanchuk, A. (2006). New data on the structure of the Khabarovsk Terrane of the Jurassic accretionary prism (Sikhote-Alin). *Doklady Earth Sciences*, *406*(1), 28–31. https://doi.org/10.1134/S1028334X06010089

Kemkin, I., Khanchuk, A., & Kemkina, R. (2016). Accretionary prisms of the Sikhote-Alin Orogenic Belt: Composition, structure and significance for reconstruction of the geodynamic evolution of the eastern Asian margin. *Journal of Geodynamics*, *102*, 202–230. https://doi.org/10.1016/j.jog.2016.10.002

Khanchuk, A. I. (2001). Pre-Neogene tectonics of the Sea-of-Japan region: A view from the Russian side. *Earth Science*, *55*(5), 275–291.

Khanchuk, A. I. (Ed.) (2006). *Geodynamics, Magmatism and Metallogeny of the Russian East, Book1* (p. 572). Vladivostok: *Dal'nauka*. (in Russian)

Khanchuk, A. I., Didenko, A. N., Popeko, L. I., Sorokin, A. A., & Shevchenko, B. F. (2015). Structure and evolution of the Mongol-Okhotsk Orogenic Belt. In A. Kroner (Ed.), *The Central Asian Orogenic Belt. Contributions to the Regional Geology of the Earth* (pp. 211–234). Stuttgart, Germany: E. Schweitzerbart Science Publishers.

Khanchuk, A. I., Didenko, A. N., Tikhomirova, A. I., & Voinova, I. P. (2015). Paleomagnetism and geochemistry of the Kiselevka block of the Kiselevka-Manoma terrane (northern Sikhote-Alin): Geodynamic significance. *Geological Society of America Special Papers*, *513*, 513–514.

Khanchuk, A. I., Kemkin, I. V., & Kruk, N. N. (2016). The Sikhote-Alin orogenic belt, Russian South East: Terranes and the formation of continental lithosphere based on geological and isotopic data. *Journal of Asian Earth Sciences*, *120*, 117–138. https://doi.org/10.1016/j.jseaes.2015.10.023

Khanchuk, A. I., Ratkin, V. V., Ryazantseva, M. D., Golozubov, V. V., & Gonokhova, N. G. (1996). *Geology and Mineral Deposits of Primorskiy Krai*, (p. 61). Dalnauka: Vladivostok.

Khanchuk, A. I., & Vysotskiy, S. (2016). Different-depth gabbro–ultrabasite associations in the Sikhote-Alin ophiolites (Russian Far East). *Russian Geology and Geophysics*, *57*(1), 141–154. https://doi.org/10.1016/j.rgg.2016.01.010

Kim, S. W., Williams, I. S., Kwon, S., & Oh, C. W. (2008). SHRIMP zircon geochronology, and geochemical characteristics of metaplutonic rocks from the south-western Gyeonggi Block, Korea: Implications for Paleoproterozoic to Mesozoic tectonic links between the Korean Peninsula and eastern China. *Precambrian Research*, *162*(3–4), 475–497. https://doi.org/10.1016/j.precamres.2007.10.006

Kim, J., Yi, K., Jeong, Y. J., & Cheong, C. S. (2011). Geochronological and geochemical constraints on the petrogenesis of Mesozoic high-K granitoids in the central Korean peninsula. *Gondwana Research*, *20*(2–3), 608–620. https://doi.org/10.1016/j.gr.2010.12.005

Kim, S. W., Kwon, S., Koh, H. J., Yi, K., Jeong, Y. J., & Santosh, M. (2011). Geotectonic framework of Permo–Triassic magmatism within the Korean Peninsula. *Gondwana Research*, *20*(4), 865–889. https://doi.org/10.1016/j.gr.2011.05.005

Kim, S. W., Kwon, S., Park, S. I., Yi, K., Santosh, M., & Ryu, I. C. (2015). Early to Middle Paleozoic arc magmatism in the Korean Peninsula: Constraints from zircon geochronology and geochemistry. *Journal of Asian Earth Sciences*, *113*, 866–882. https://doi.org/10.1016/j.jseaes.2015.09.017

Kimura, T. (1979). Late Mesozoic palaeofloristic provinces in east Asia. *Proceedings of the Japan Academy, Series B Physical and Biological Sciences*, *55*(9), 425–430. https://doi.org/10.2183/pjab.55.425

Kimura, T., Ohana, T., & Mimoto, K. (1988). Discovery of a podocarpaceous plant from the Lower Cretaceous of Kochi Prefecture, in the Outer Zone of southwest Japan. *Proceedings of the Japan Academy, Series B*, *64*(8), 213–216.

Kimura, T. (2000). Early Cretaceous climatic provinces in Japan and adjacent regions on the basis. *Cretaceous Environments of Asia*, *17*, 155. https://doi.org/10.1016/S0920-5446(00)80029-1

Kirillova, G. L. (2003). Cretaceous tectonics and geological environments in East Russia. *Journal of Asian Earth Sciences*, *21*(8), 967–977. https://doi.org/10.1016/S1367-9120(02)00093-7

Kojima, S. (1989). Mesozoic terrane accretion in northeast China, Sikhote-Alin and Japan regions. *Palaeogeography, Palaeoclimatology, Palaeoecology*, *69*, 213–232. https://doi.org/10.1016/0031-0182(89)90165-X

Kojima, S., Igor'V, K., Kametaka, M., & Ando, A. (2000). A correlation of accretionary complexes of southern Sikhote-Alin of Russia and the Inner Zone of Southwest Japan. *Geosciences Journal*, *4*(3), 175–185. https://doi.org/10.1007/BF02910136

Kojima, S., Tsukada, K., Otoh, S., Yamakita, S., Ehiro, M., Dia, C., … Eichwald, L. P. (2008). Geological relationship between Anyui metamorphic complex and Samarka terrane, Far East Russia. *Island Arc*, *17*(4), 502–516. https://doi.org/10.1111/j.1440-1738.2008.00644.x

Kravchinsky, V. A., Cogné, J.-P., Harbert, W. P., & Kuzmin, M. I. (2002). Evolution of the Mongol-Okhotsk Ocean as constrained by new palaeomagnetic data from the Mongol-Okhotsk suture zone, Siberia. *Geophysical Journal International*, *148*(1), 34–57. https://doi.org/10.1046/j.1365-246x.2002.01557.x

Kruk, N. N., Simanenko, V. P., Golozubov, V. V., Kovach, V. P., Vladimirov, V. G., & Kasatkin, S. A. (2014). Geochemistry of rocks in the Anuy metamorphic dome, Sikhote-Alin: Composition of the protoliths and the possible nature of metamorphism. *Geochemistry International*, *52*(3), 229–246. https://doi.org/10.1134/S0016702914010030

Kusky, T., Windley, B., & Zhai, M. G. (2007). Tectonic evolution of the North China Block: From orogen to craton to orogen. *Geological Society, London, Special Publications*, *280*(1), 1–34. https://doi.org/10.1144/SP280.1

Lee, D. W. (1999). Strike–slip fault tectonics and basin formation during the Cretaceous in the Korean Peninsula. *Island Arc*, *8*(2), 218–231. https://doi.org/10.1046/j.1440-1738.1999.00233.x

Lee, K. S., Chang, H. W., & Park, K. H. (1998). Neoproterozoic bimodal volcanism in the central Ogcheon belt, Korea: Age and tectonic implication. *Precambrian Research*, *89*(1–2), 47–57. https://doi.org/10.1016/S0301-9268(97)00077-6

Lee, S. R., Cho, M., Cheong, C. S., Kim, H., & Wingate, M. T. (2003). Age, geochemistry, and tectonic significance of Neoproterozoic alkaline granitoids in the northwestern margin of the Gyeonggi massif, South Korea. *Precambrian Research*, *122*(1–4), 297–310. https://doi.org/10.1016/S0301-9268(02)00216-4

Lee, T. H., Park, K. H., Yi, K., Geng, J. Z., & Li, H. K. (2015). SHRIMP U-Pb ages and Hf isotopic composition of the detrital zircons from the Myogok Formation, SE Korea: Development of terrestrial basin and igneous activity during the early Cretaceous. *Geosciences Journal*, *19*(2), 189–203. https://doi.org/10.1007/s12303-014-0042-6

Li, H. Y., & Huang, X. L. (2013). Constraints on the paleogeographic evolution of the North China Craton during the Late Triassic–Jurassic. *Journal of Asian Earth Sciences*, *70*, 308–320.

Li, Z. X., & Li, X. H. (2007). Formation of the 1300-km-wide intracontinental orogen and postorogenic magmatic province in Mesozoic South China: A flat-slab subduction model. *Geology*, *35*(2), 179–182. https://doi.org/10.1130/G23193A.1

Li, Z., Li, X., Kinny, P., & Wang, J. (1999). The breakup of Rodinia: Did it start with a mantle plume beneath South China? *Earth and Planetary Science Letters*, *173*(3), 171–181. https://doi.org/10.1016/S0012-821X(99)00240-X

Li, Z. X., Li, X. H., Zhou, H., & Kinny, P. D. (2002). Grenvillian continental collision in south China: New SHRIMP U-Pb zircon results and implications for the configuration of Rodinia. *Geology*, *30*(2), 163–166.

Li, X. H., Li, Z. X., Zhou, H., Liu, Y., & Kinny, P. D. (2002). U–Pb zircon geochronology, geochemistry and Nd isotopic study of Neoproterozoic bimodal volcanic rocks in the Kangdian Rift of South China: Implications for the initial rifting of Rodinia. *Precambrian Research*, *113*(1–2), 135–154. https://doi.org/10.1016/S0301-9268(01)00207-8

Li, S. Z., Zhao, G. C., Sun, M., Wu, F. Y., Liu, J. Z., Hao, D. F., … Luo, Y. (2004). Mesozoic, not Paleoproterozoic SHRIMP U–Pb zircon ages of two Liaoji granites, Eastern Block, North China Craton. *International Geology Review*, *46*(2), 162–176. https://doi.org/10.2747/0020-6814.46.2.162

Li, S. Z., Zhao, G. C., Sun, M., Wu, F. Y., Hao, D. F., Han, Z. Z., … Xia, X. P. (2005). Deformational history of the Paleoproterozoic Liaohe Group in the Eastern Block of the North China Craton. *Journal of Asian Earth Sciences*, *24*, 654–669.

Li, S. Z., Zhao, G. C., Sun, M., Zhao, G. T., & Hao, D. F. (2006). Are the South and North Liaohe Groups of the North China Craton different exotic terranes? Nd isotope constraints. *Gondwana Research*, *9*(1–2), 198–208. https://doi.org/10.1016/j.gr.2005.06.011

Li, Z. X., Li, X. H., Chung, S. L., Lo, C. H., Xu, X., & Li, W. X. (2012). Magmatic switch-on and switch-off along the South China continental margin since the Permian: Transition from an Andean-type to a Western Pacific-type plate boundary. *Tectonophysics*, *532*, 271–290.

Liu, F., & Liou, J. (2011). Zircon as the best mineral for P–T–time history of UHP metamorphism: A review on mineral inclusions and U–Pb SHRIMP ages of zircons from the Dabie–Sulu UHP rocks. *Journal of Asian Earth Sciences*, *40*(1), 1–39. https://doi.org/10.1016/j.jseaes.2010.08.007

Liu, Y., Hu, Z., Zong, K., Gao, C., Gao, S., Xu, J., & Chen, H. (2010). Reappraisement and refinement of zircon U-Pb isotope and trace element analyses by LA-ICP-MS. *Chinese Science Bulletin*, *55*(15), 1535–1546. https://doi.org/10.1007/s11434-010-3052-4

Liu, K., Zhang, J., Wilde, S. A., Zhou, J., Wang, M., Ge, M., … Ling, Y. (2017). Initial subduction of the Paleo-Pacific Oceanic plate in NE China: Constraints from whole-rock geochemistry and zircon U–Pb and Lu–Hf isotopes of the Khanka Lake granitoids. *Lithos*, *274–275*, 254–270. https://doi.org/10.1016/j.lithos.2016.12.022

Luan, J. P., Wang, F., Xu, W. L., Ge, W. C., Sorokin, A. A., Wang, Z. W., & Guo, P. (2017). Provenance, age, and tectonic implications of Neoproterozoic strata in the Jiamusi Massif: evidence from U–Pb ages and Hf isotope compositions of detrital and magmatic zircons. *Precambrian Research*, *297*, 19–32.

Ludwig, K. (2001). Isoplot 3.0—A geochronological toolkit for Microsoft Excel, Special Publication No. 4, *Berkeley Geochronology Center, Berkeley, Calif*.

Malinovsky, A., & Golozubov, V. (2011). Lithology and depositional settings of the terrigenous sediments along transform plate boundaries: Evidence from the early cretaceous Zhuravlevka terrane in Southern Sikhote Alin. *Russian Journal of Pacific Geology*, *5*(5), 400–417. https://doi.org/10.1134/S1819714011050058

Maruyama, S. (1997). Pacific-type orogeny revisited: Miyashiro-type orogeny proposed. *Island Arc*, *6*(1), 91–120. https://doi.org/10.1111/j.1440-1738.1997.tb00042.x

Meng, E., Xu, W., Yang, D., Pei, F., Yu, Y., & Zhang, X. (2008). Permian volcanisms in eastern and southeastern margins of the Jiamusi Massif, northeastern China: Zircon U-Pb chronology, geochemistry and its tectonic implications. *Chinese Science Bulletin*, *53*(8), 1231–1245.

Meng, E., Xu, W., Pei, F., Yang, D., Wang, F., & Zhang, X. (2011). Permian bimodal volcanism in the Zhangguangcai Range of eastern Heilongjiang Province, NE China: Zircon U–Pb–Hf isotopes and geochemical evidence. *Journal of Asian Earth Sciences*, *41*(2), 119–132. https://doi.org/10.1016/j.jseaes.2011.01.005

Menzies, M. A., Fan, W., & Zhang, M. (1993). Palaeozoic and Cenozoic lithoprobes and the loss of >120 km of Archaean lithosphere, Sino-Korean craton, China. *Geological Society, London, Special Publications*, *76*(1), 71–81. https://doi.org/10.1144/GSL.SP.1993.076.01.04

Menzies, M., Xu, Y., Zhang, H., & Fan, W. (2007). Integration of geology, geophysics and geochemistry: A key to understanding the North China Craton. *Lithos*, *96*(1–2), 1–21. https://doi.org/10.1016/j.lithos.2006.09.008

Miao, L., Zhang, F., Zhu, M., & Liu, D. (2015). Zircon SHRIMP U–Pb dating of metamorphic complexes in the conjunction of the Greater and Lesser Xing'an ranges, NE China: Timing of formation and metamorphism and tectonic implications. *Journal of Asian Earth Sciences*, *114*, 634–648. https://doi.org/10.1016/j.jseaes.2014.09.035

Mizutani, S. (1987). Mesozoic terranes in the Japanese Islands and neighbouring East Asia. In E. Scheibner (Eds). *Terrane accretion and orogenic belts*, *American Geophysical Union, Geodynamic Series 19*, (pp. 263–273). https://doi.org/10.1029/GD019p0263

Müller, R. D., Sdrolias, M., Gaina, C., Steinberger, B., & Heine, C. (2008). Long-term sea-level fluctuations driven by ocean basin dynamics. *Science*, *319*(5868), 1357–1362. https://doi.org/10.1126/science.1151540

Nakama, T., Hirata, T., Otoh, S., Aoki, K., Yanai, S., & Maruyama, S. (2010). Paleogeography of the Japanese Islands: Age spectra of detrital zircon and provenance history of the orogen. *Journal of Geography*, *119*(6), 1161–1172. https://doi.org/10.5026/jgeography.119.1161

Natal'in, B. (1993). History and modes of Mesozoic accretion in southeastern Russia. *Island Arc*, *2*(1), 15–34. https://doi.org/10.1111/j.1440-1738.1993.tb00072.x

Peng, P., Zhai, M., Ernst, R. E., Guo, J., Liu, F., & Hu, B. (2008). A 1.78 Ga large igneous province in the North China craton: The Xiong'er Volcanic Province and the North China dyke swarm. *Lithos*, *101*(3–4), 260–280. https://doi.org/10.1016/j.lithos.2007.07.006

Peng, P., Bleeker, W., Ernst, R. E., Söderlund, U., & McNicoll, V. (2011). U–Pb baddeleyite ages, distribution and geochemistry of 925Ma mafic dykes and 900Ma sills in the North China craton: Evidence for a Neoproterozoic mantle plume. *Lithos*, *127*(1–2), 210–221. https://doi.org/10.1016/j.lithos.2011.08.018

Qi, G., Zhang, J., & Wang, M. (2015). Mesozoic tectonic setting of rift basins in eastern North China and implications for destruction of the North China Craton. *Journal of Asian Earth Sciences*, *111*, 414–427. https://doi.org/10.1016/j.jseaes.2015.06.022

Qiu, Y. M., Gao, S., McNaughton, N. J., Groves, D. I., & Ling, W. (2000). First evidence of> 3.2 Ga continental crust in the Yangtze craton of south China and its implications for Archean crustal evolution and Phanerozoic tectonics. *Geology*, *28*(1), 11–14. https://doi.org/10.1130/0091-7613(2000)028<0011:FEOGCC>2.0.CO;2

Rojas-Agramonte, Y., Kröner, A., Demoux, A., Xia, X., Wang, W., Donskaya, T., … Sun, M. (2011). Detrital and xenocrystic zircon ages from Neoproterozoic to Palaeozoic arc terranesof Mongolia: Significance for the origin of crustal fragments in the Central Asian Orogenic Belt. *Gondwana Research*, *19*(3), 751–763. https://doi.org/10.1016/j.gr.2010.10.004

Rowley, D. B., Raymond, A., Parrish, J. T., Lottes, A. L., Scotese, C. R., & Ziegler, A. M. (1985). Carboniferous paleogeographic, phytogeographic, and paleoclimatic reconstructions. *International Journal of Coal Geology*, *5*(1–2), 7–42. https://doi.org/10.1016/0166-5162(85)90009-6

Sano, Y., Hidaka, H., Terada, K., Shimizu, H., & Suzuki, M. (2000). Ion microprobe U-Pb zircon geochronology of the Hida gneiss: Finding of the oldest minerals in Japan. *Geochemical Journal*, *34*(2), 135–153. https://doi.org/10.2343/geochemj.34.135

Segal, I., Halicz, L., & Platzner, I. T. (2003). Accurate isotope ratio measurements of ytterbium by multiple collection inductively coupled plasma mass spectrometry applying erbium and hafnium in an improved double external normalization procedure. *Journal of Analytical Atomic Spectrometry*, *18*(10), 1217–1223. https://doi.org/10.1039/b307016f

Sengör, A. C., & Natal'In, B. A. (1996). Turkic-type orogeny and its role in the making of the continental crust. *Annual Review of Earth and Planetary Sciences*, *24*(1), 263–337. https://doi.org/10.1146/annurev.earth.24.1.263

Şengör, A., Natal'In, B., & Burtman, V. (1993). Evolution of the Altaid tectonic collage and Palaeozoic crustal growth in Eurasia. *Nature*, *364*, 22.

Shao, J., & Tang, K. (1995). *Terranes in Northeast China and Evolution of Northeast Asia Continental Margin*, edited, Seismic Press, Beijing.

Söderlund, U., Patchett, P. J., Vervoort, J. D., & Isachsen, C. E. (2004). The 176 Lu decay constant determined by Lu–Hf and U–Pb isotope systematics of Precambrian mafic intrusions. *Earth and Planetary Science Letters*, *219*(3–4), 311–324. https://doi.org/10.1016/S0012-821X(04)00012-3

Song, S., Wang, M. M., Xu, X., Wang, C., Niu, Y., Allen, M. B., & Su, L. (2015). Ophiolites in the Xing'an-Inner Mongolia accretionary belt of the CAOB: Implications for two cycles of seafloor spreading and accretionary orogenic events. *Tectonics*, *34*, 2221–2248. https://doi.org/10.1002/2015TC003948

Sun, M. D., Xu, Y. G., Wilde, S. A., & Chen, H. L. (2015). Provenance of Cretaceous trench slope sediments from the Mesozoic Wandashan Orogen, NE China: Implications for determining ancient drainage systems and tectonics of the Paleo-Pacific. *Tectonics*, *34*, 1269–1289. https://doi.org/10.1002/2015TC003870

Sun, M. D., Xu, Y. G., Wilde, S. A., Chen, H. L., & Yang, S. F. (2015). The Permian Dongfanghong island-arc gabbro of the Wandashan Orogen, NE China: Implications for Paleo-Pacific subduction. *Tectonophysics*, *659*, 122–136. https://doi.org/10.1016/j.tecto.2015.07.034

Taira, A. (2001). Tectonic evolution of the Japanese island arc system. *Annual Review of Earth and Planetary Sciences*, *29*(1), 109–134. https://doi.org/10.1146/annurev.earth.29.1.109

Tang, J., Xu, W., Niu, Y., Wang, F., Ge, W., Sorokin, A. A., & Chekryzhov, I. Y. (2016). Geochronology and geochemistry of Late Cretaceous–Paleocene granitoids in the Sikhote-Alin Orogenic Belt: Petrogenesis and implications for the oblique subduction of the paleo-Pacific plate. *Lithos*, *266*, 202–212.

Tsutsumi, Y., Yokoyama, K., Kasatkin, S. A., & Golozubov, V. V. (2016). Provenance study of accretionary complexes in Primorye, Far East Russia, using ages and compositions of detrital minerals. *Memoirs of the National Museum of Nature and Science*, *51*, 79–87.

Turek, A., & Kim, C.-B. (1996). U-Pb zircon ages for Precambrian rocks in southwestern Ryeongnam and southwestern Gyeonggi massifs, Korea. *Geochemical Journal*, *30*(4), 231–249. https://doi.org/10.2343/geochemj.30.231

Utkin, V. (1993). Wrench faults of Sikhote-Alin and accretionary and destructive types of fault dislocation in the Asia-Pacific transition zone. *The Tancheng-Lujiang wrench fault system*, *225–237*.

Utkin, V. (2013). Shear structural paragenesis and its role in continental rifting of the East Asian margin. *Russian Journal of Pacific Geology*, *7*(3), 167–188. https://doi.org/10.1134/S181971401303007X

Vakhrameev, V. (1987). Climates and the distribution of some gymsosperms in Asia during the Jurassic and Cretaceous. *Review of Palaeobotany and Palynology*, *51*(1–3), 205–212. https://doi.org/10.1016/0034-6667(87)90030-3

Van Achterbergh, E., Ryan, C., & Griffin, W. (2001). *GLITTER On-Line Interactive Data Reduction for the LA-ICPMS Microprobe*. Sydney: *Macquarie Research Ltd*.

Wang, Q., Deng, J., Li, C., Li, G., Yu, L., & Qiao, L. (2014). The boundary between the Simao and Yangtze blocks and their locations in Gondwana and Rodinia: Constraints from detrital and inherited zircons. *Gondwana Research*, *26*(2), 438–448. https://doi.org/10.1016/j.gr.2013.10.002

Wang, J., Chang, S.-C., Lu, H.-B., & Zhang, H.-C. (2016). Detrital zircon provenance of the Wangshi and Laiyang groups of the Jiaolai basin: Evidence for Early Cretaceous uplift of the Sulu orogen, Eastern China. *International Geology Review*, *58*(6), 719–736. https://doi.org/10.1080/00206814.2015.1105728

Wilde, S. A. (2015). Final amalgamation of the Central Asian Orogenic Belt in NE China: Paleo-Asian Ocean closure versus Paleo-Pacific plate subduction—A review of the evidence. *Tectonophysics*, *662*, 345–362. https://doi.org/10.1016/j.tecto.2015.05.006

Wilde, S., Dorsett-Bain, H., & Liu, J. (1997). The identification of a Late Pan-African granulite facies event in northeastern China: SHRIMP U–Pb zircon dating of the Mashan Group at Liu Mao, Heilongjiang Province, China. *Proceedings of the 30th IGC: Precambrian Geology and Metamorphic Petrology*, *17*, 59–74.

Wilde, S. A., Dorsett-Bain, H. L., & Lennon, R. G. (1999). Geological setting and controls on the development of graphite, sillimanite and phosphate mineralization within the Jiamusi Massif: An exotic fragment of Gondwanaland located in north-eastern China? *Gondwana Research*, *2*(1), 21–46. https://doi.org/10.1016/S1342-937X(05)70125-8

Wilde, S. A., Zhang, X., & Wu, F. (2000). Extension of a newly identified 500Ma metamorphic terrane in North East China: Further U–Pb SHRIMP dating of the Mashan Complex, Heilongjiang Province, China. *Tectonophysics*, *328*(1–2), 115–130. https://doi.org/10.1016/S0040-1951(00)00180-3

Wilde, S. A., Zhao, G., & Sun, M. (2002). Development of the North China Craton during the late Archaean and its final amalgamation at 1.8 Ga: Some speculations on its position within a global Palaeoproterozoic supercontinent. *Gondwana Research*, *5*(1), 85–94. https://doi.org/10.1016/S1342-937X(05)70892-3

Wilde, S. A., Wu, F., & Zhang, X. (2003). Late Pan-African magmatism in northeastern China: SHRIMP U–Pb zircon evidence from granitoids in the Jiamusi Massif. *Precambrian Research*, *122*(1–4), 311–327. https://doi.org/10.1016/S0301-9268(02)00217-6

Windley, B. F., Alexeiev, D., Xiao, W., Kröner, A., & Badarch, G. (2007). Tectonic models for accretion of the Central Asian Orogenic Belt. *Journal of the Geological Society*, *164*(1), 31–47. https://doi.org/10.1144/0016-76492006-022

Wu, Y. B., & Zheng, Y. F. (2013). Tectonic evolution of a composite collision orogen: An overview on the Qinling–Tongbai–Hong'an–Dabie–Sulu orogenic belt in central China. *Gondwana Research*, *23*(4), 1402–1428. https://doi.org/10.1016/j.gr.2012.09.007

Wu, F. Y., Jahn, B. M., Wilde, S. A., Lo, C. H., Yui, T. F., Lin, Q., … Sun, D. Y. (2003a). Highly fractionated I-type granites in NE China (I): Geochronology and petrogenesis. *Lithos*, *66*(3–4), 241–273. https://doi.org/10.1016/S0024-4937(02)00222-0

Wu, F. Y., Jahn, B. M., Wilde, S. A., Lo, C. H., Yui, T. F., Lin, Q., … Sun, D. Y. (2003b). Highly fractionated I-type granites in NE China (II): Isotopic geochemistry and implications for crustal growth in the Phanerozoic. *Lithos*, *67*(3–4), 191–204. https://doi.org/10.1016/S0024-4937(03)00015-X

Wu, F. Y., Han, R. H., Yang, J. H., Wilde, S. A., Zhai, M. G., & Park, S. C. (2007). Initial constraints on the timing of granitic magmatism in North Korea using U–Pb zircon geochronology. *Chemical Geology*, *238*(3–4), 232–248. https://doi.org/10.1016/j.chemgeo.2006.11.012

Wu, F. Y., Yang, J. H., Lo, C. H., Wilde, S. A., Sun, D. Y., & Jahn, B. M. (2007). The Heilongjiang Group: A Jurassic accretionary complex in the Jiamusi Massif at the western Pacific margin of northeastern China. *Island Arc*, *16*(1), 156–172. https://doi.org/10.1111/j.1440-1738.2007.00564.x

Wu, F. Y., Yang, J. H., Wilde, S. A., Liu, X. M., Guo, J. H., & Zhai, M. G. (2007). Detrital zircon U–Pb and Hf isotopic constraints on the crustal evolution of North Korea. *Precambrian Research*, *159*(3–4), 155–177. https://doi.org/10.1016/j.precamres.2007.06.007

Wu, F. Y., Zhang, Y. B., Yang, J. H., Xie, L. W., & Yang, Y. H. (2008). Zircon U–Pb and Hf isotopic constraints on the Early Archean crustal evolution in Anshan of the North China Craton. *Precambrian Research*, *167*(3–4), 339–362. https://doi.org/10.1016/j.precamres.2008.10.002

Wu, F. Y., Sun, D. Y., Ge, W. C., Zhang, Y. B., Grant, M. L., Wilde, S. A., & Jahn, B. M. (2011). Geochronology of the Phanerozoic granitoids in northeastern China. *Journal of Asian Earth Sciences*, *41*(1), 1–30. https://doi.org/10.1016/j.jseaes.2010.11.014

Wyld, S. J., & Wright, J. E. (2001). New evidence for Cretaceous strike-slip faulting in the United States Cordillera and implications for terrane-displacement, deformation patterns, and plutonism. *American Journal of Science*, *301*(2), 150–181. https://doi.org/10.2475/ajs.301.2.150

Xiao, W., Windley, B. F., Hao, J., & Zhai, M. (2003). Accretion leading to collision and the Permian Solonker suture, Inner Mongolia, China: termination of the central Asian orogenic belt. *Tectonics*, *22*(6), 1069. https://doi.org/10.1029/2002TC001484

Xu, J. W., & Zhu, G. (1994). Tectonic models of the Tan-Lu fault zone, eastern China. *International Geology Review*, *36*(8), 771–784.

Xu, J., Zhu, G., Tong, W., Cui, K., & Liu, Q. (1987). Formation and evolution of the Tancheng-Lujiang wrench fault system: A major shear system to the northwest of the Pacific Ocean. *Tectonophysics*, *134*(4), 273–310. https://doi.org/10.1016/0040-1951(87)90342-8

Xu, W. L., Pei, F. P., Wang, F., Meng, E., Ji, W. Q., Yang, D. B., & Wang, W. (2013). Spatial–temporal relationships of Mesozoic volcanic rocks in NE China: Constraints on tectonic overprinting and transformations between multiple tectonic regimes. *Journal of Asian Earth Sciences*, *74*, 167–193. https://doi.org/10.1016/j.jseaes.2013.04.003

Xu, B., Zhao, P., Wang, Y., Liao, W., Luo, Z., Bao, Q., & Zhou, Y. (2015). The pre-Devonian tectonic framework of Xing'an–Mongolia orogenic belt (XMOB) in north China. *Journal of Asian Earth Sciences*, *97*, 183–196. https://doi.org/10.1016/j.jseaes.2014.07.020

Yabe, A., Terada, K., & Sekido, S. (2003). The Tetori-type flora, revised: A review. *Memoir of the Fukui Prefectural Dinosaur Museum*, *2*, 23–42.

Yang, J. H., Wu, F. Y., Shao, J. A., Wilde, S. A., Xie, L. W., & Liu, X. M. (2006). Constraints on the timing of uplift of the Yanshan Fold and Thrust Belt, North China. *Earth and Planetary Science Letters*, *246*(3–4), 336–352. https://doi.org/10.1016/j.epsl.2006.04.029

Yang, J. H., Wu, F. Y., Wilde, S. A., Belousova, E., & Griffin, W. L. (2008). Mesozoic decratonization of the North China block. *Geology*, *36*(6), 467–470. https://doi.org/10.1130/G24518A.1

Yang, J., Gao, S., Chen, C., Tang, Y., Yuan, H., Gong, H., … Wang, J. (2009). Episodic crustal growth of North China as revealed by U–Pb age and Hf isotopes of detrital zircons from modern rivers. *Geochimica et Cosmochimica Acta*, *73*(9), 2660–2673. https://doi.org/10.1016/j.gca.2009.02.007

Yang, S., Zhang, F., & Wang, Z. (2012). Grain size distribution and age population of detrital zircons from the Changjiang (Yangtze) River system, China. *Chemical Geology*, *296*, 26–38.

Yang, H., Ge, W., Zhao, G., Yu, J., & Zhang, Y. (2015). Early Permian–Late Triassic granitic magmatism in the Jiamusi–Khanka Massif, eastern segment of the Central Asian Orogenic Belt and its implications. *Gondwana Research*, *27*(4), 1509–1533. https://doi.org/10.1016/j.gr.2014.01.011

Yang, H., Ge, W., Zhao, G., Bi, J., Wang, Z., Dong, Y., & Xu, W. (2017). Zircon U–Pb ages and geochemistry of newly discovered Neoproterozoic orthogneisses in the Mishan region, NE China: Constraints on the high-grade metamorphism and tectonic affinity of the Jiamusi–Khanka Block. *Lithos*, *268*, 16–31.

Yin, A., & Nie, S. (1993). An indentation model for the North and South China collision and the development of the Tan-Lu and Honam fault systems, eastern Asia. *Tectonics*, *12*(4), 801–813. https://doi.org/10.1029/93TC00313

Yu, J., Wang, F., Xu, W., Gao, F., & Pei, F. (2012). Early Jurassic mafic magmatism in the Lesser Xing'an–Zhangguangcai Range, NE China, and its tectonic implications: Constraints from zircon U–Pb chronology and geochemistry. *Lithos*, *142*, 256–266.

Yu, J., Hou, X., Zhang, Y., & Liu, J. (2013). Magma mixing genesis of the Early Permian Liulian pluton at the northeastern margin of the Jiamusi massif in NE China: Evidence from petrology, geochronology and geochemistry. *Acta Petrologica Sinica*, *29*(9), 2971–2986.

Yui, T., Maki, K., Lan, C., Hirata, T., Chu, H., Kon, Y., … Ernst, W. (2012). Detrital zircons from the Tananao metamorphic complex of Taiwan: Implications for sediment provenance and Mesozoic tectonics. *Tectonophysics*, *541*, 31–42.

Zhai, M. G., & Santosh, M. (2011). The early Precambrian odyssey of the North China Craton: A synoptic overview. *Gondwana Research*, *20*(1), 6–25. https://doi.org/10.1016/j.gr.2011.02.005

Zhai, M. G., Guo, J. H., Peng, P., & Hu, B. (2007). U-Pb zircon age dating of a rapakivi granite batholith in Rangnim massif, North Korea. *Geological Magazine*, *114*, 547–552.

Zhang, Q. S., & Yang, Z. S. (1988). *Early Crust and Mineral Deposits of Liaodong Peninsula, China*. Beijing: *Geological Publishing House*.

Zhang, S. H., Zhao, Y., Song, B., Yang, Z. Y., Hu, J. M., & Wu, H. (2007). Carboniferous granitic plutons from the northern margin of the North China block: Implications for a late Palaeozoic active continental margin. *Journal of the Geological Society*, *164*(2), 451–463. https://doi.org/10.1144/0016-76492005-190

Zhang, R., Liou, J., & Ernst, W. (2009). The Dabie–Sulu continental collision zone: A comprehensive review. *Gondwana Research*, *16*(1), 1–26. https://doi.org/10.1016/j.gr.2009.03.008

Zhang, S. H., Zhao, Y., Song, B., Hu, J. M., Liu, S. W., Yang, Y. H., … Liu, J. (2009). Contrasting Late Carboniferous and Late Permian–Middle Triassic intrusive suites from the northern margin of the North China craton: Geochronology, petrogenesis, and tectonic implications. *Geological Society of America Bulletin*, *121*(1–2), 181–200.

Zhang, H. F., Zhu, R. X., Santosh, M., Ying, J. F., Su, B. X., & Hu, Y. (2013). Episodic widespread magma underplating beneath the North China Craton in the Phanerozoic: Implications for craton destruction. *Gondwana Research*, *23*(1), 95–107. https://doi.org/10.1016/j.gr.2011.12.006

Zhang, S. H., Zhao, Y., Davis, G. A., Ye, H., & Wu, F. (2014). Temporal and spatial variations of Mesozoic magmatism and deformation in the North China Craton: Implications for lithospheric thinning and decratonization. *Earth-Science Reviews*, *131*, 49–87. https://doi.org/10.1016/j.earscirev.2013.12.004

Zhao, G., & Zhai, M. (2013). Lithotectonic elements of Precambrian basement in the North China Craton: Review and tectonic implications. *Gondwana Research*, *23*(4), 1207–1240. https://doi.org/10.1016/j.gr.2012.08.016

Zhao, G., Wilde, S. A., Cawood, P. A., & Sun, M. (2001). Archean blocks and their boundaries in the North China Craton: Lithological, geochemical, structural and P–T path constraints and tectonic evolution. *Precambrian Research*, *107*(1–2), 45–73. https://doi.org/10.1016/S0301-9268(00)00154-6

Zhao, G., Sun, M., Wilde, S. A., & Sanzhong, L. (2005). Late Archean to Paleoproterozoic evolution of the North China Craton: Key issues revisited. *Precambrian Research*, *136*(2), 177–202. https://doi.org/10.1016/j.precamres.2004.10.002

Zhao, G. C., Cao, L., Wilde, S. A., Sun, M., Choe, W. J., & Li, S. Z. (2006). Implications based on the first SHRIMP U-Pb zircon dating on Precambrian granitoid rocks in North Korea. *Earth and Planetary Science Letters*, *251*(3–4), 365–379. https://doi.org/10.1016/j.epsl.2006.09.021

Zhao, G., Cawood, P. A., Li, S., Wilde, S. A., Sun, M., Zhang, J., … Yin, C. (2012). Amalgamation of the North China Craton: Key issues and discussion. *Precambrian Research*, *222*, 55–76.

Zhao, P., Chen, Y., Xu, B., Faure, M., Shi, G., & Choulet, F. (2013). Did the Paleo-Asian Ocean between North China Block and Mongolia Block exist during the late Paleozoic? First paleomagnetic evidence from central-eastern Inner Mongolia, China. *Journal of Geophysical Research: Solid Earth*, *118*, 1873–1894.

Zheng, J., Griffin, W., O'Reilly, S. Y., Lu, F., Yu, C., Zhang, M., & Li, H. (2004). U–Pb and Hf-isotope analysis of zircons in mafic xenoliths from Fuxian kimberlites: Evolution of the lower crust beneath the North China Craton. *Contributions to Mineralogy and Petrology*, *148*(1), 79–103. https://doi.org/10.1007/s00410-004-0587-x

Zheng, J., Griffin, W., O'Reilly, S. Y., Zhang, M., Pearson, N., & Pan, Y. (2006). Widespread Archean basement beneath the Yangtze craton. *Geology*, *34*(6), 417–420. https://doi.org/10.1130/G22282.1

Zhou, J. B., & Li, L. (2017). The Mesozoic accretionary complex in Northeast China: Evidence for the accretion history of Paleo-Pacific subduction. *Journal of Asian Earth Sciences*, *145*, 91–100. https://doi.org/10.1016/j.jseaes.2017.04.013

Zhou, J. B., Wilde, S. A., Zhang, X. Z., Zhao, G. C., Zheng, C. Q., Wang, Y. J., & Zhang, X. H. (2009). The onset of Pacific margin accretion in NE China: Evidence from the Heilongjiang high-pressure metamorphic belt. *Tectonophysics*, *478*(3–4), 230–246. https://doi.org/10.1016/j.tecto.2009.08.009

Zhou, J. B., Wilde, S. A., Zhang, X. Z., Zhao, G. C., Liu, F. L., Qiao, D. W., … Liu, J. H. (2011). A> 1300km late Pan-African metamorphic belt in NE China: New evidence from the Xing'an block and its tectonic implications. *Tectonophysics*, *509*(3–4), 280–292. https://doi.org/10.1016/j.tecto.2011.06.018

Zhou, J. B., Cao, J. L., Wilde, S. A., Zhao, G. C., Zhang, J. J., & Wang, B. (2014). Paleo-Pacific subduction-accretion: Evidence from Geochemical and U-Pb zircon dating of the Nadanhada accretionary complex, NE China. *Tectonics*, *33*, 2444–2466. https://doi.org/10.1002/2014TC003637

Zhu, R. X., Yang, J. H., & Wu, F. Y. (2012). Timing of destruction of the North China Craton. *Lithos*, *149*, 51–60. https://doi.org/10.1016/j.lithos.2012.05.013

Zonenshain, L. (1973). The evolution of Central Asiatic geosynclines through sea-floor spreading. *Tectonophysics*, *19*(3), 213–232. https://doi.org/10.1016/0040-1951(73)90020-6